NASA Contractor Report 195424

Investigation of Natural and Man-Made Radiation Effects on Crews on Long Duration Space Missions

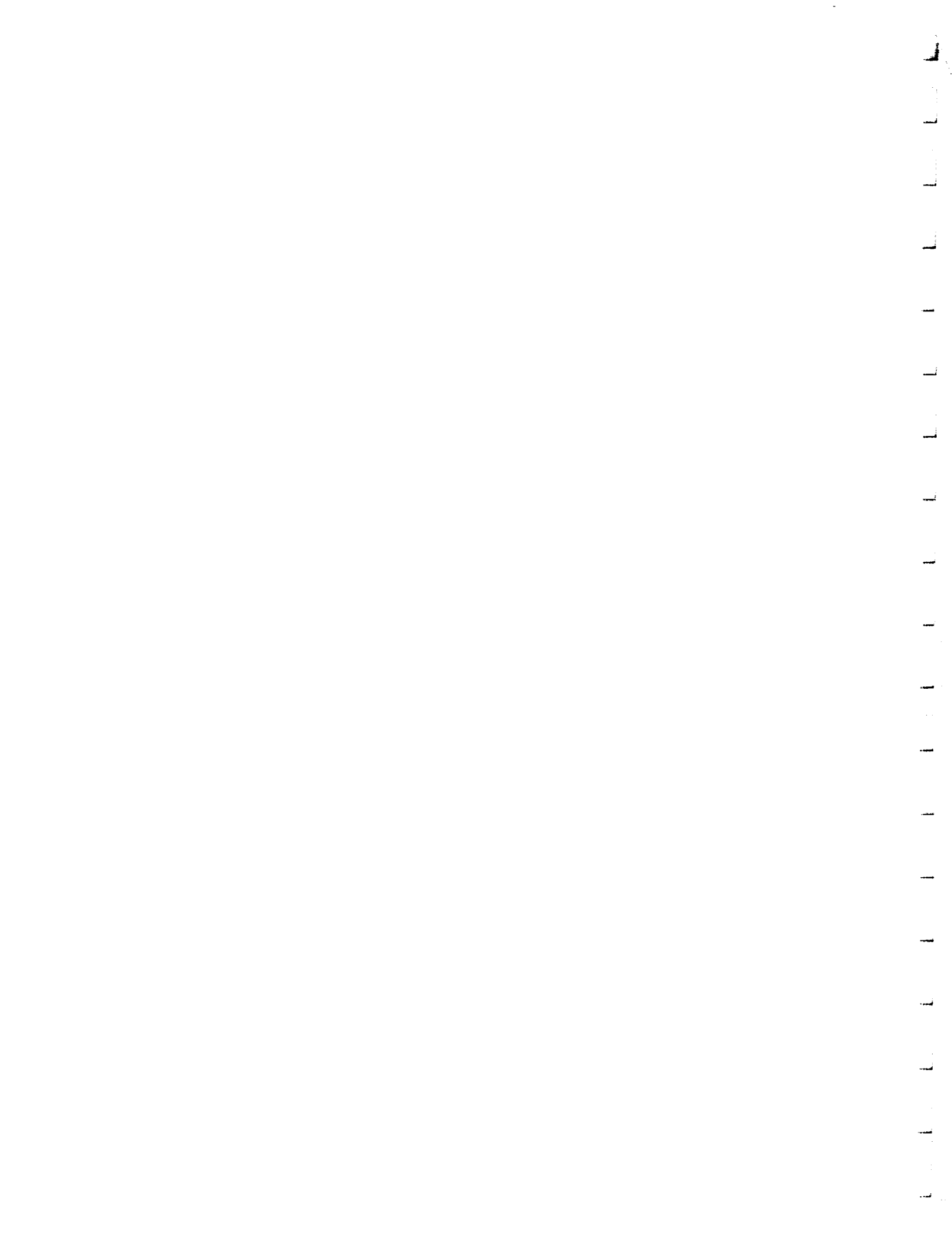Wesley E. Bolch and Alexander Parlos
Texas A&M University
College Station, Texas

February 1996

National Aeronautics and
Space Administration

Investigation of Natural and Man-Made Radiation Effects on Crews on Long Duration Space Missions

Wesley E. Bolch and Alexander Parlos
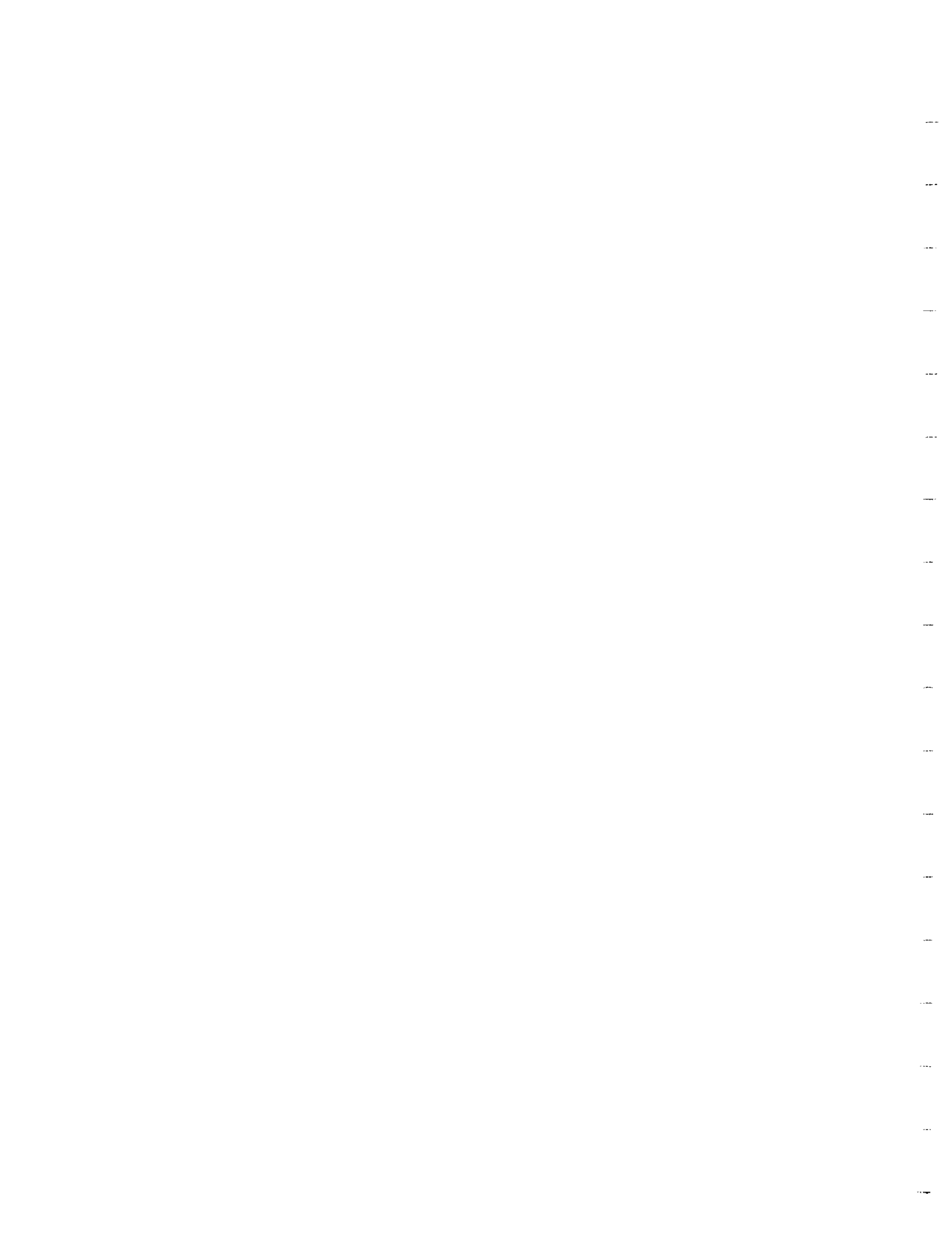*Texas A&M University*
College Station, Texas

February 1996

ACKNOWLEDGMENTS

ABSTRACT

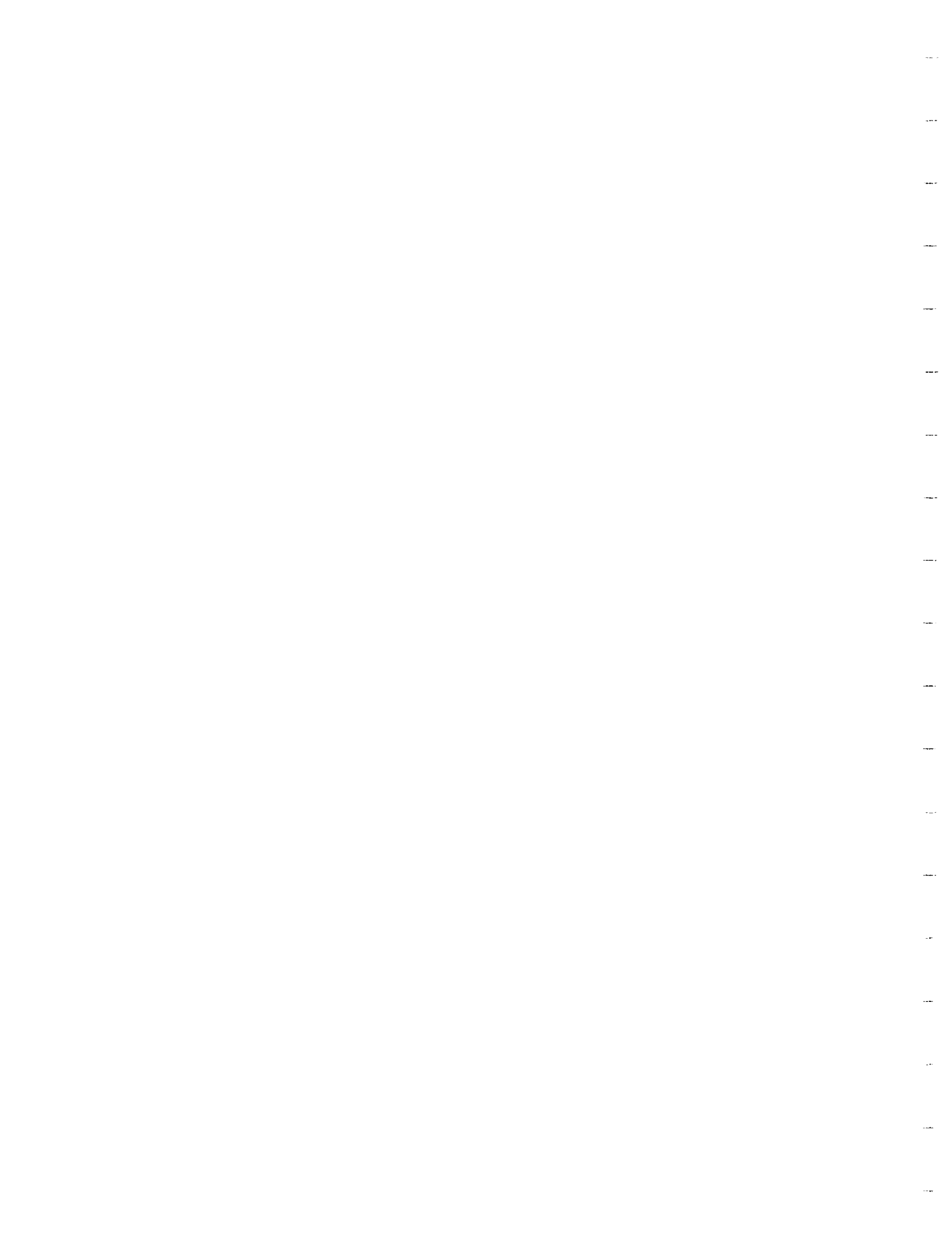Over the past several years, the National Aeronautics and Space Administration (NASA) has studied a variety of mission scenarios designed to establish a permanent human presence on the surface of Mars. Nuclear Electric Propulsion (NEP) is one of the possible elements in this program. During the initial stages of vehicle design work, careful consideration must be given to, not only the shielding requirements of natural space radiation, but to the shielding and configuration requirements of the on-board reactors.

In this work, the radiation transport code MCNP has been used to make initial estimates of crew exposures to reactor radiation fields for a specific manned NEP vehicle design. In this design, three 25 MW_{th}, scaled SP-100-class reactors are shielded by three identical shields. Each shield has layers of beryllium, tungsten, and lithium hydride between the reactor and the crew compartment. Separate calculations are made of both the exiting neutron and gamma fluxes from the reactors during beginning-of-life, full-power operation. This data is then used as the source terms for particle transport in MCNP. The total gamma and neutron fluxes exiting the reactor shields are recorded and separate transport calculations are then performed for a 10 g cm^{-2} crew compartment aluminum thickness. Estimates of crew exposures have been assessed for various thicknesses of the shield tungsten and lithium hydride layers.

A minimal tungsten thickness of 20 cm is required to shield the reactor photons below the 0.05 Sv y^{-1} man-made radiation limit. In addition to a 20-cm thick tungsten layer, a 40-cm thick lithium hydride layer is required to shield the reactor neutrons below the annual limit. If the tungsten layer is 30-cm thick, the lithium hydride layer should be at least 30-cm thick. These estimates do not take into account the photons generated by neutron interactions inside the shield because the MCNP neutron cross sections did not allow reliable estimates of photon production in these materials. These results, along with natural space radiation shielding estimates calculated by NASA Langley Research Center, have been used to provide preliminary input data into a new Macintosh-based software tool developed at Texas A&M. A skeletal version of this tool being developed will allow rapid radiation exposure and risk analyses to be performed on a variety of Lunar and Mars missions utilizing nuclear-powered vehicles.

TABLE OF CONTENTS

CHAPTER I

INTRODUCTION

INTRODUCTION

Manned space flight began more than 30 years ago with single crew-member vehicles like the Mercury capsule. Today, the National Aeronautics and Space Administration (NASA)[†] is making plans for a manned space station scheduled to be launched later this decade. During the late 1980s, a lunar base was being planned for the following decade, and a manned mission to the planet Mars for the decade after that. These latter activities would have required individuals to remain in space for years at a time. An open question is what kind of radiation protection must be provided for humans during such long exposures to space radiation hazards. As a consequence, the resources devoted to the space program must include the protection of the astronauts and an understanding of the space radiation environment.

Former President George Bush addressed the nation on the 20th anniversary of the Apollo lunar landing on July 20, 1989 and had committed the nation to a human-based journey to Mars and the Earth's Moon by the year 2019. This address prompted the formation of a special task force which in 90 days studied and reported the feasibility, the needs, and the alternatives for manned missions to the Moon and to Mars. Within the 90-Day Study, the task force concluded that the realization of the President's directive was feasible (NASA 1990). One of the most significant outcomes of the 90-Day Study had been the identification of seven critical technologies, two of them determining the part of the program treated in this thesis. Namely, it was recommended, among others, to actively pursue: (1) radiation protection, which is part of the strategic goal for a Mars mission, and (2) nuclear electric propulsion (NEP) and nuclear thermal propulsion (NTP), which will potentially reduce a round-trip to Mars to 200 days and will enable mass savings of over 300 metric tons (MT). The trip time for chemically powered vehicles depends on the vehicle's initial mass at low Earth's orbit (IMLEO). Chemical propulsion requires exorbitant IMLEO for a round-trip duration comparable to that for a nuclear-powered

---

[†] A list of acronyms is presented in Appendix A.

vehicle. Consequently, NASA had been studying a variety of mission scenarios under its Space Exploration Initiative (SEI) to establish a permanent human presence on the surface of Mars. In these studies, nuclear propulsion had played a key role in the majority of the designs considered.

INTEGRATED ASSESSMENT OF NATURAL AND MAN-MADE RADIATION SOURCES

Some requirements of the SEI have demonstrated the need for rapid transit times for manned Mars missions. The main reason is to minimize the time astronauts spend in the zero-gravity, high-background radiation environment of space. Nuclear propulsion vehicles offer a reduced transit time as compared to conventional chemically powered vehicles due to their higher levels of specific impulse. The planning of a nuclear-powered manned Mars mission requires an estimate of the total crew exposure, from both man-made and natural sources, in order to verify that this exposure would be low enough to enable the mission. Currently, estimates of the natural space radiation dose can be obtained from previously reported work, with some assumptions regarding the specific mission. As the man-made contributions to the radiation dose to NEP vehicle crew members have not as yet been thoroughly estimated, it is important to provide an assessment of reactor dose rates inside the crew compartment.

From the aforementioned arguments it should be clear that the main motivation for using nuclear propulsion as a means for interplanetary transportation is the reduced trip time it offers, as compared to chemical propulsion. However, in an attempt to reduce the total trip time without significantly increasing the initial mass in low earth orbit (IMLEO), it is necessary to pursue nuclear reactor designs with the lowest possible specific mass. A major component in overall power system sizing, particularly in systems involving manned missions, is the natural and man-made radiation shields. The shields could require significantly different design approaches. For a given reactor technology and at a specific power output, an appropriate choice of both shield designs can indeed effect the overall power system specific mass; this in turn can effect the total radiation dose received by the crew. Therefore, attempts to reduce trip times may result in a reduction of a natural radiation source, but at the same time they may increase the man-made sources leading to an eventual increase in crew cancer risk. On the contrary, overshielding will certainly

reduce such a risk, but may increase trip times as a result of increased power system specific mass; this will in turn increase crew exposure to natural radiation.

RADIATION DOSE LIMITS

During interplanetary missions, astronauts will be confronted with nontrivial background radiation. On Earth, the background radiation is well below any level of concern. Occupational radiation dose limits are set to ensure the safety of radiation workers and do not include the radiation doses from natural sources. During space travel, however, the background radiation is much higher and it can reach lethal levels. Consequently, dose estimates to crew members during space missions must include both contributions from natural and man-made radiation sources.

The space radiation environment consists of several types of energetic charged particles: electrons, protons, helium ions, and heavier particles. The relative importance of each of these components to the radiation burden of members of a given space mission depends strongly on many details of the mission itself. These include the spacecraft trajectory, the time the mission occurs during the solar cycle, the orbital altitude, the mission duration, and the available shielding within the spacecraft. Some more poorly known physical factors are also important, such as the chance of large emissions of particles from the sun and the broad temporal and spatial fluctuations of several of the trapped radiation components. The National Council on Radiation Protection and Measurements (NCRP) in its Report No. 98 recommends astronaut dose limits (NCRP 1989). The risk estimates will influence spacecraft design and mission planning in order to comply with the NCRP dose limits from natural radiation sources.

It is an accepted fact that natural space radiation provides a more hostile environment than that found on Earth. For this reason, space radiation dose limits for "routine missions" and guidelines for "exploratory missions" have been recommended (NCRP 1989) and accepted by NASA. Specific limits were set for the skin, lens of the eye, and the hematopoietic system (Blood Forming Organs or BFO). In addition, the "As Low As Reasonably Achievable" (ALARA) principle was adopted. Radiation doses to the BFO are restricted because they are the most sensitive target sites for radiation-induced carcinogenesis. Table 1.1 gives radiation dose limits for NASA's space workers as currently recommended by the NCRP (NCRP 1989). These career limits correspond to a

3% lifetime excess risk of fatal cancer where a career is assumed to be approximately 10 years. For the blood forming organs, the career limits range from 1 Sv for females 25 years-of-age at first exposure to 4 Sv for males 55 years-of-age at first exposure. Annual and 30-day limits are also specified so as to prevent the occurrence of nonstochastic radiation effects such as cataracts or skin damage. An individual may receive 0.5 Sv to the BFO in a given year of space activity, yet cannot receive more than one-half the annual limit within any one 30-day period.

These dose limits are for total radiation exposures regardless of source. The Occupational Safety and Health Administration (OSHA) of the U.S. Department of Labor, the organization with regulatory authority over radiation exposures to NASA personnel, has adopted these limits for the total exposure to all radiation sources. In addition, however, current limits specified by OSHA limit exposures from man-made radiation sources to only 0.05 Sv per year (OSHA 1987).

Table 1.1 Limits for protection against nonstochastic effects (30-day) and stochastic effects (Annual and Career) in Sv. Reference (NCRP 1989).

Time Period	BFO	Lens of the Eye	Skin
30-day	0.25	1	1.5
Annual	0.5	2	3
Career	1.0 to 4.0	4	6

SUMMARY

The research described in this report comprises a preliminary attempt to address the combined Radiological Health and the Nuclear Reactor Engineering aspects of NEP vehicles, in an integrated and systematic manner. Total dose estimates resulting from both natural and man-made radiation sources are reported for a selected vehicle configuration.

The study of man-made radiation dose to the crew of a nuclear-powered space vehicle is performed utilizing the MCNP radiation transport code. In addition, natural radiation dose is incorporated using estimates previously made at the NASA Langley Research Center. Background information on previous dose estimates for natural space radiation, a description of the NEP vehicle, and estimates of radiation doses for man-made sources in space missions is initially presented. Thereafter, an overview of the methods used to assess the man-made radiation source term used in this project is described. In particular, brief descriptions of TWODANT and ORIGEN2 codes are presented, followed by the operating and post-shutdown fluxes of the SP-100 reactor scaled to 25 MW$_{th}$. Additionally, the computational methods used in modeling the NEP vehicle, that is the MCNP code, are described. The results of the radiation transport modeling of the NEP vehicle are reported, and both man-made and natural radiation source induced crew doses are presented.

The literature review indicated the advantage of nuclear propulsion for deep space missions, such as a Mars mission. It emphasized that space natural radiation sources create a hostile environment. Consequently, the time spent in space should be minimized and this can be done by shortening the travel time. There is currently no comprehensive dose estimate for the NEP vehicle in the literature. In this work, the dose variations as a function of two parameters, namely the tungsten and the lithium hydride layer thicknesses of the shadow shield, were assessed.

CONCLUSIONS

The shield thickness required to reduce the reactor dose to the crew below the 0.05 Sv y^{-1} limit is summarized in Table 1.2. The data indicate that a 30-cm thick tungsten layer followed by a 30-cm thick lithium hydride layer would serve as an adequate shield considering only the photon and neutron source terms from the reactor and its shield. Photon production by neutron interactions in the shield have not been considered, yet the LiH layer would probably have to be increased to further attenuate this photon component of the crew dose.

Because of MCNP deep penetration limitations, the dosimetry results had to be interpolated. The study identified that photons generated by the reactor neutrons

interacting with the shield material were the main dosimetric concern. In general, the neutron source is the major shield design concern for the SP-100 reactor. Photons from the reactor are easily shielded and contribute in a negligible way to the total dose as long as the tungsten layer exceeds 15 cm in thickness.

Table 1.2 Summary of tungsten and lithium hydride thickness requirements to lower the dose rate inside the crew compartment for the source particles below the 0.05 Sv y^{-1} limit.

W Thickness (cm)	LiH Thickness (cm)		
	Neutron Component	Photon Component	Total
10	52	140	140
20	40	No requirement	40
30	30	No requirement	30

REPORT OUTLINE

The previous estimates of radiation doses from natural sources, the NEP vehicle design, and the estimates of radiation doses from man-made sources in space are reviewed in Chapter II. Chapter III describes the relevant tools used in the calculations of the man-made source term. The results of the calculations with the general Monte Carlo Code for Neutron and Photon Transport (MCNP), detailed in Chapters IV and V, give the neutron and photon reactor flux incident upon the astronauts within the crew compartments during full-power operation. Radiation doses to the bone marrow is estimated through the use of fluence-to-dose equivalent conversion factors (DCF). The most recent compilation of these factors is given in the Publication 51 of the International Commission on Radiological Protection (ICRP) (ICRP 1987). The DCF values are given over a range of energies and for four irradiation geometries. A brief user's guide is provided in Chapter

VI for the Macintosh-based computational tool developed in this project. Finally, Chapter VII provides the conclusions and recommendations of this report.

CHAPTER II

BACKGROUND INFORMATION

INTRODUCTION

This chapter presents the relevant background information regarding the nature and design of nuclear electric propulsion (NEP) vehicles. Furthermore, some background material is presented regarding estimates of radiation dose from natural and man-made sources. The presentation of radiation dose estimates from natural sources includes previous work performed at the NASA Langley Research Center.

NUCLEAR ELECTRIC PROPULSION (NEP) VEHICLE DESIGN

The Nuclear Electric Propulsion (NEP) design is one of the possible solutions for a manned Mars mission selected by NASA. The high specific impulse provided by this type of vehicle will enable short trip times to Mars, thus reducing crew exposures to galactic cosmic rays and solar particle emissions. During the initial stages of vehicle design work, careful consideration must be given to, not only the shielding requirements of natural space radiation, but to the shielding and configuration requirements of the on-board reactors.

The NEP technology includes an SP-100-class nuclear reactor and power conversion subsystem coupled with electrically powered ion thrusters using argon as a possible propellant. The reference vehicle analyzed in this report consists of a multi-reactor NEP vehicle concept utilizing a cluster of three 5 MW_e power modules (George 1992b). Each reactor is located at the end of a 120 m truss. The three reactor trusses radiate outward in a triangular fashion from a central hub consisting of three cylindrical crew habitation modules, the Earth Crew Capture Vehicle (ECCV), six argon propellant tanks, and three ion thrusters. Separate calculations have been made of both the exiting neutron and gamma-ray fluxes from the reactors during full-power beginning-of-life operation. These data form the source terms for particle transport in the computer simulations.

Multi-reactor NEP systems present many advantages for space missions. The redundancy of three 5 MW_e reactors offer a greater potential reliability and their failure modes are less catastrophic because of the partial power possibility. The modularity of multi-reactor NEP systems allows the selection of the power level (15 MW_e) to suit both payload and mission. In the case of an accident, it is easier to repair or refurbish a smaller reactor. The launch packages are also smaller. NEP missions will use standard reactor and power conversion elements. This leads to reduced development and production costs. These advantages are at the expense of the vehicle complexity and mass which are both increased.

ESTIMATES OF RADIATION DOSE FROM NATURAL SOURCES

A major concern to interplanetary mission planners is crew exposures to highly penetrating and damaging space radiation. Space radiation can conveniently be organized into three main categories according to its source: (1) trapped particle radiation, (2) galactic cosmic rays, and (3) solar particle events. The trapped particle radiation consists mostly of electrons and protons trapped in closed orbits by the earth's magnetic field. The galactic radiation consists mostly of protons, with a small admixture of helium ions and an even smaller component of heavier ions. The solar particle radiation consists mostly of protons, with a small contribution from helium ions and heavier particles. The differences between the last two categories are mainly in the vastly different distributions of particle energies involved and in the sporadic nature of the solar disturbances producing the solar particles as compared with the more slowly varying nature of the galactic particle intensities (NCRP 1989).

Whenever radiation fields traverse bulk matter, the physical characteristics (fluxes, energies, and particle types) of the propagating fields are altered through nuclear and electromagnetic interactions with the constituent particles (nucleons and high atomic number (Z) and energy (HZE) particles). These modifications include energy losses resulting from collisions and composition changes resulting from nuclear and electromagnetic breakup (fragmentation) processes. The net result is that radiation environment inside equipment or the human body may differ from the environment interior to the spacecraft. The latter, in turn, will differ from the external space environment.

The space radiation environment consists of several types of energetic charged particles: electrons, protons, helium, and heavier ions. The relative importance of each of these components to the radiation burden of members of a given space mission depends strongly on many details of the mission itself, such as the spacecraft trajectory, the time the mission occurs during the solar cycle, the altitude, the mission duration, and the available shielding within the spacecraft. Some more poorly known physical factors are also important, for example, the chance of large emissions of particles from the sun and the broad temporal and spatial fluctuations of several of the trapped radiation components. Their relative contributions to radiation hazards are most easily understood when considered separately.

The trapped particles consist of both electrons and protons which are held within the earth's magnetic field. Both particles spiral around the geomagnetic field lines, bouncing between mirror points in the Northern and Southern hemispheres. They are trapped in what is called the Van Allen belts. Since they are of opposite charge, the trapped electrons drift eastward and the protons drift westward. The trapped electrons can be found in two partially distinct regions designated the "inner zone" (< 11,500 km) and "the outer zone" (between 11,500 and 70,200 km). The electron intensities in the outer zone are approximately 10 times those in the inner zone. Both zones experience a 10-fold diurnal variation in intensity with a smaller variation corresponding to the 11-year solar cycle. The trapped protons occupy a more limited volume of space and are more dosimetrically important than the electrons for low earth-orbiting missions such as the space station. The most intense region of trapped protons is found between Africa and South America where the proton belt dips to lower altitudes. This region is called the South Atlantic Anomaly (SAA) and is caused by a slight off-center displacement of the earth's magnetic dipole. Radiation belts are not important outside the Earth's magnetosphere.

Galactic cosmic rays (GCR) are typically charged particles such as protons, electrons, or other heavy, energetic particles, which are present isotropically in space and arise from sources outside our solar system. They are the relatively constant component of the natural radiation environment in space. Due to their interactions with the "solar wind", their intensity decreases during the active part of the solar cycle (solar maximum). During solar maximum, when the interplanetary magnetic field strength is greatest, cosmic ray particles are scattered away from our solar system producing a relative minimum in the

GCR flux. Conversely, the GCR flux is largest during minimum solar activity. The maximum total particle flux of GCR at solar minimum is estimated to be about 4 $cm^{-2}s^{-1}$. Their distribution within the energy range of greatest flux is 87% protons, 12% helium ions, and 1% heavier ions (NCRP 1989). This latter group has been given the generic term HZE (High Z and Energy). Although HZE particles are found in low abundance with respect to protons and helium ions, they are much more densely ionizing and thus their contribution to the total GCR dose can be substantial. Due to their high energy, GCRs are very penetrating. Fortunately, the GCR flux is comparatively low, and thus does not pose a serious threat to humans for short duration missions. The risk of long-term stochastic effects such as cancer induction is, however, uncertain at present.

Radiation dose estimates for the GCR-component of the space radiation environment have been made by researchers at NASA's Langley Research Center. Fig. 2.1 displays the GCR annual dose equivalent as a function of water shield thickness both at solar minima and solar maxima as estimated by the Langley researchers (Townsend et al. 1990). For all thickness considered, the dose equivalent during solar maximum is less than half of the dose equivalent during solar minimum. Because the GCR dose is more limiting at solar minimum, most of the studies are restricted to solar minimum periods. This is not meant to imply that exposures during solar maximum periods are not important. On the contrary, the cumulative exposures resulting from combined GCR and increased solar flare activity during solar maximum could potentially be significant.

Fig. 2.2 displays the annual BFO dose equivalent as a function of various shielding material, namely, liquid hydrogen, water, and aluminum, all at solar minima (Townsend et al. 1990). This Fig. indicates that shielding effectiveness per unit mass increases as the composition of the shield changes from heavier to lighter mass elements. For liquid hydrogen, an added advantage is the reduced neutron fluence due to the absence of neutrons in the target composition and the lack of target fragment contributions because of the elementary nature of hydrogen.

In 1992, Townsend et al. corrected the estimates displayed on Figs. 2.1 and 2.2. Using the Langley Research Center galactic cosmic-ray transport computer code and the Computerized Anatomical Man (CAM) model, estimates of interplanetary exposure of astronauts to GCR during periods of solar minimum activity were published for a realistic human geometry shielded by various thicknesses of spacecraft aluminum shielding

(Townsend et al. 1992). Fig. 2.3 displays the resulting BFO dose equivalent as function of aluminum shield thickness from GCR at solar minimum. The equivalent sphere approximation yielded conservative overestimates for the actual organ exposures. This article presented the most recent estimates of GCR shielding when the calculations presented in this thesis were performed. The aluminum thickness of the crew
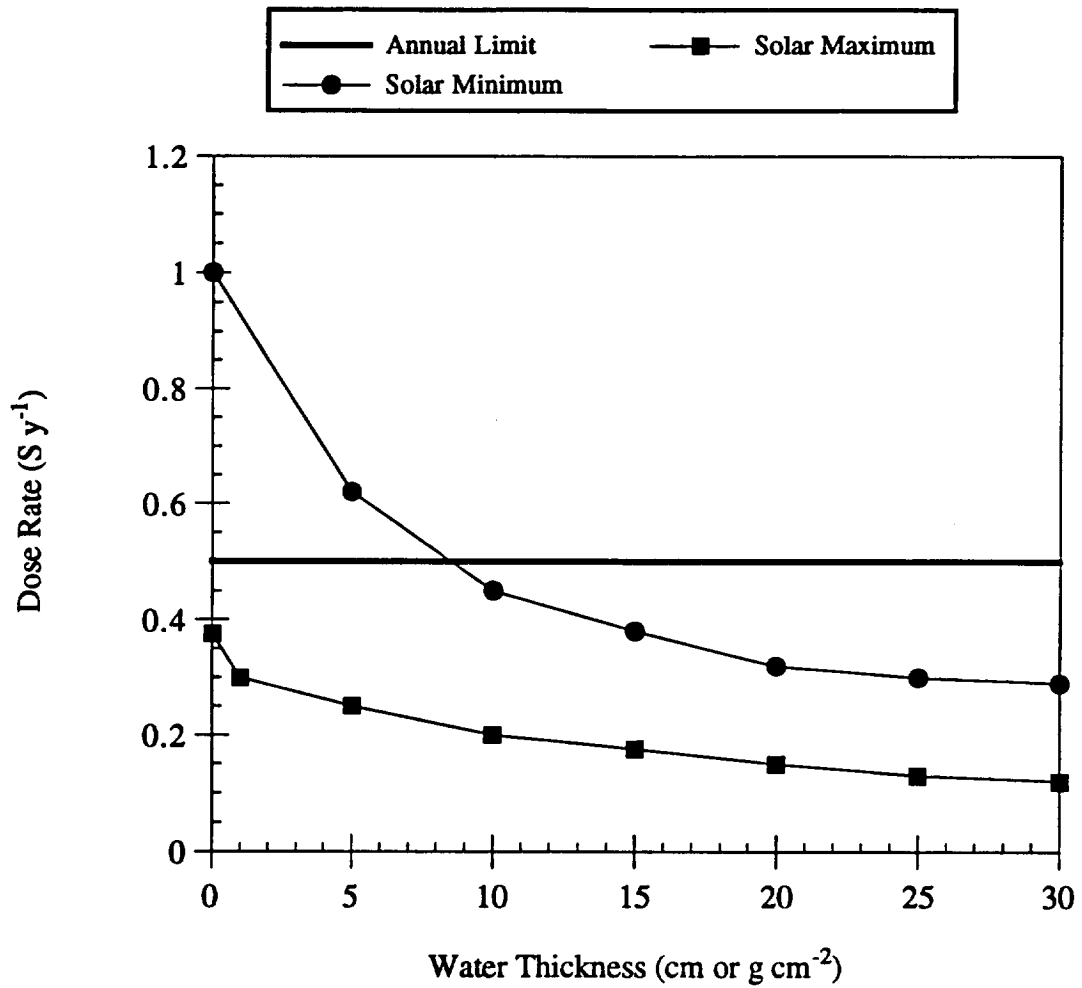
Figure 2.1 Dose equivalent as a function of water shield thickness, resulting from galactic cosmic rays for solar minima and solar maxima. The transport calculations include linear energy transfer (LET) dependent quality factors from ICRP Publication 26 (ICRP 26 1977).

Reference: Townsend et al. (1990).
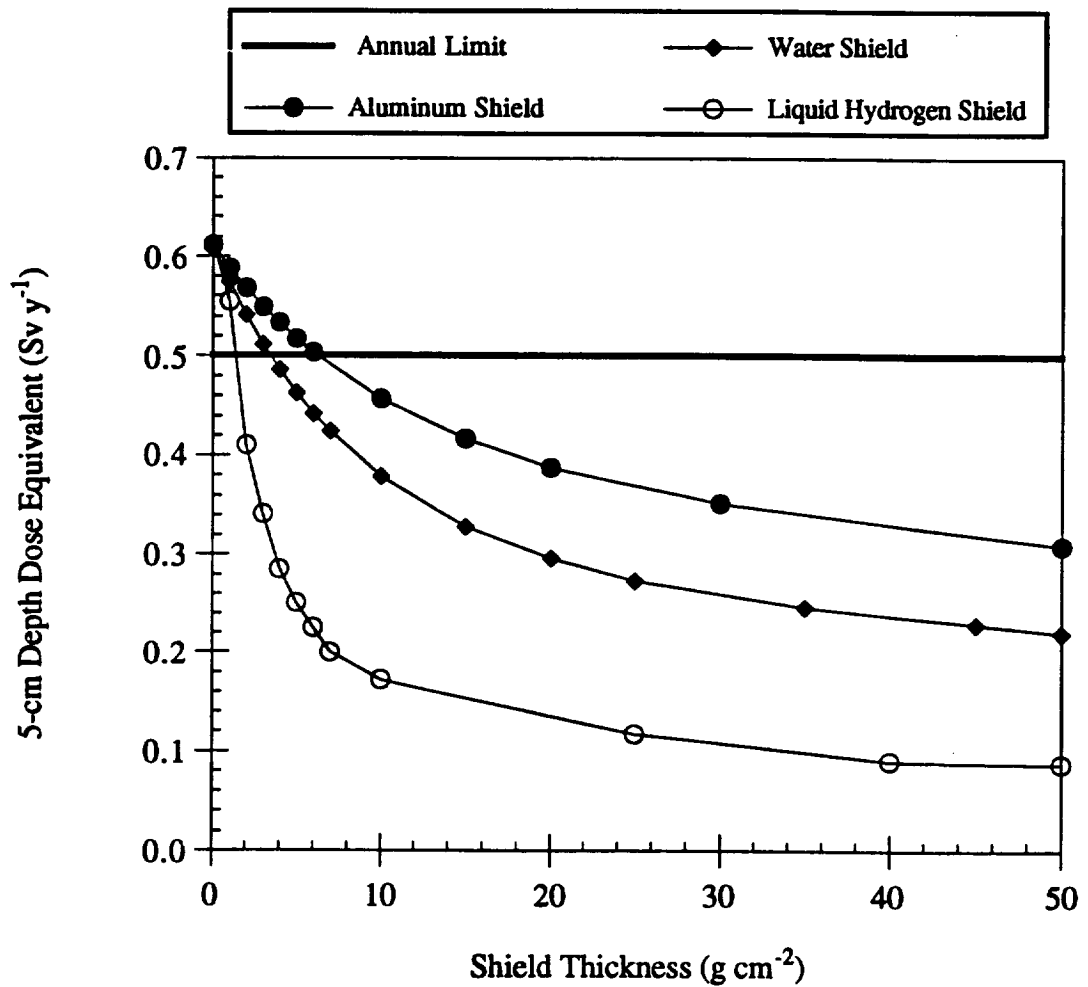
Figure 2.2 BFO dose equivalent as a function of shield type and thickness, resulting from galactic cosmic rays at solar minima. The transport calculations include linear energy transfer (LET) dependent quality factors from ICRP Publication 26 (ICRP 26 1977).

Reference: Townsend et al. (1990).
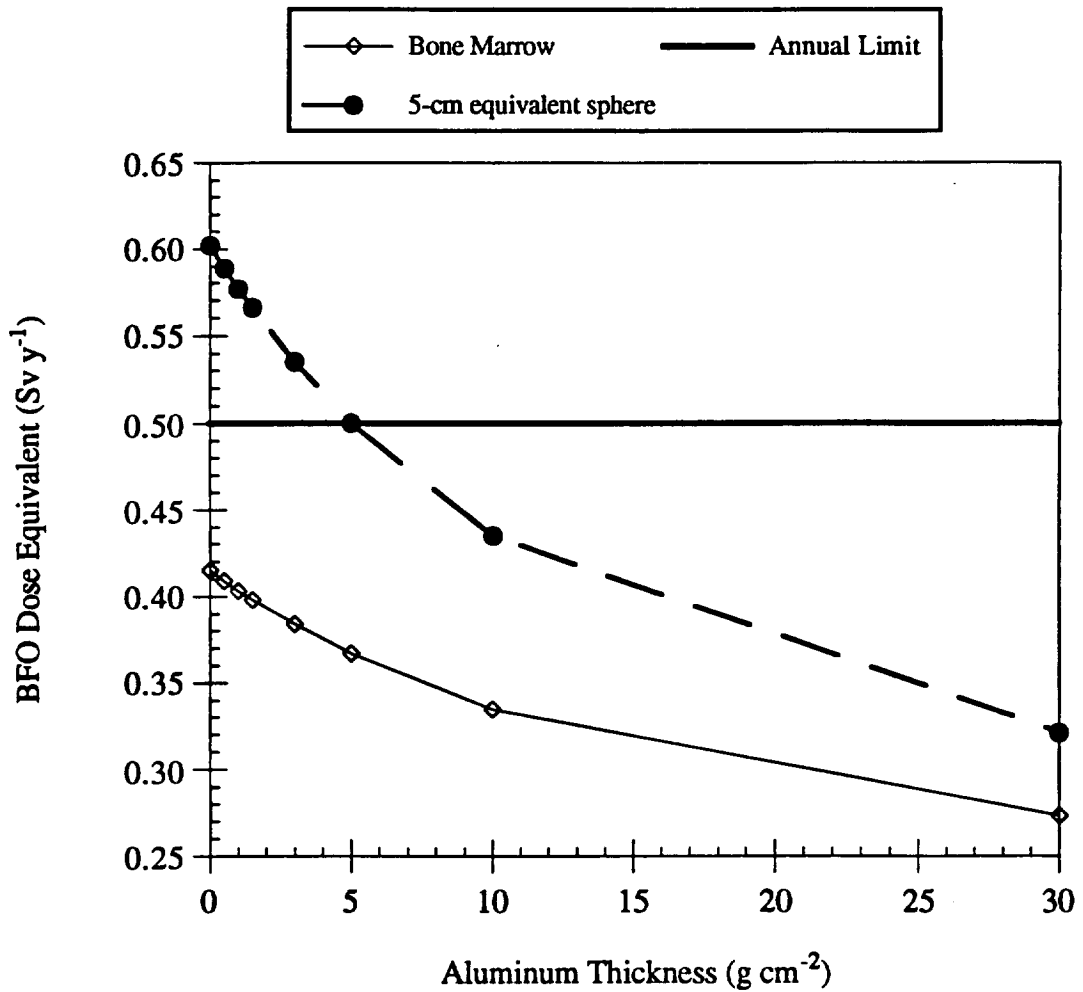
Figure 2.3 BFO dose equivalent from GCR as a function of aluminum shield thickness at solar minimum. Calculations performed using the Langley Research Center GCR transport computer code and the computerized anatomical man (CAM) model. Comparison of the realistic human geometry (CAM model) and the 5-cm-radius tissue equivalent sphere. Reference: Townsend et al. (1992).

compartment was selected from Fig. 2.3 for use in this research and the conservative value of 10 g cm^{-2} was used in the computer input file. This value corresponds to an annual BFO dose equivalent of approximately 0.35 Sv as estimated with the CAM anatomical model.

Recently, Badhwar et al. published new GCR shielding requirement estimates displayed in Fig 2.4 (Badhwar et al. 1993). Using the spherically symmetric diffusion theory of the solar modulation of GCR, and data on the differential energy spectra of hydrogen, helium, oxygen, and iron from 1965 to 1989, they showed that the GCR flux is determined by the diffusion parameter which is a function of the time in the solar cycle. Their analysis also showed that the fluxes in the 1954 and 1976-1977 solar minima were similar and higher than those of 1965. They concluded that the solar cycle for cosmic-ray intensity is approximately 22 years. Using this theory they have obtained the GCR spectra for all nuclei and calculated the depth dose as a function of aluminum thickness. Using ICRP Pub. 26 value for the quality factor and the 1976-1977 spectra, they showed that the shielding required to stay below 0.5 Sv is approximately 17.5 g cm^{-2} of aluminum. The calculated dose equivalent using the ICRP Pub. 60 values for quality factors is about 15% higher than that calculated using ICRP Pub. 26 values. The new GCR shielding estimates reported by Badhwar et al. have not been used in this study, and they are not included in the computational tool that accompanies this report.

Solar particle events (SPE) are large emissions of charged particles from the sun during solar flare activity. They consist mostly of protons, with a small contribution of helium ions and HZE particles, and occur sporadically during the active phase of the nominal 11-year solar cycle. SPEs fall into two general categories according to their intensities: ordinary and anomalously large (AL). Due to the shielding of the earth's magnetic field, ordinary SPEs do not contribute substantially to radiation doses in low earth orbits. Although they occur infrequently, anomalously large SPE can contribute to radiation doses in low earth orbits (LEO) at high inclinations.

Figs. 2.5 and 2.6 give preliminary estimates of total dose equivalent (Sv) exposures in tissue (5-cm depth) behind various thicknesses of water and aluminum shielding for three solar flare events (Townsend et al. 1988). For computational purpose, three major events were selected: February 1956, November 1960, and August 1972. The 1956 event provided the most penetrating radiations. The 1972, the largest ever
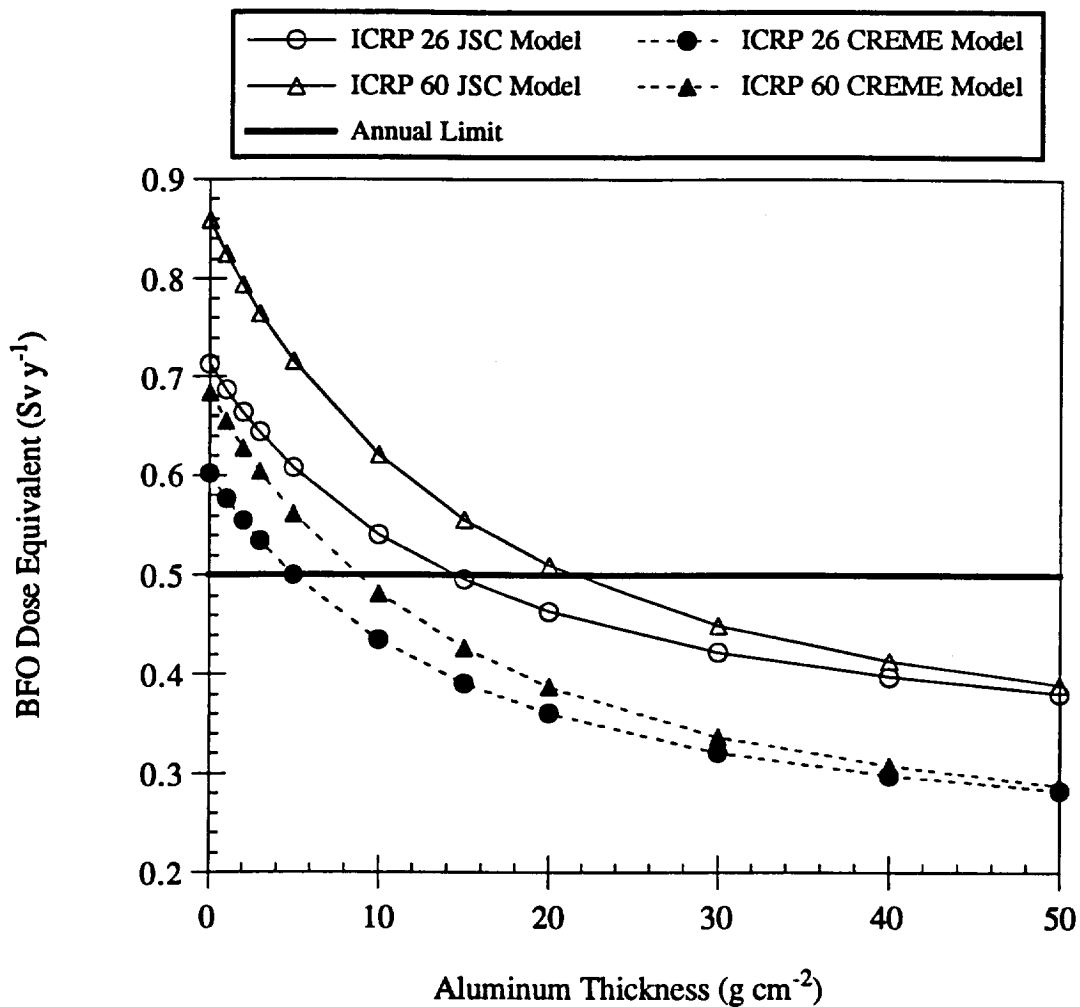
Figure 2.4 Influence of the quality factor variations between ICRP Publication 26 and ICRP Publication 60 on the BFO dose equivalent from GCR as a function of shielding thickness for solar minimum. Calculations performed using the 1976-1977 GCR spectra of Badhwar and O'Neill (1992) and the CREME model.

Reference: Badhwar et al. (1993).
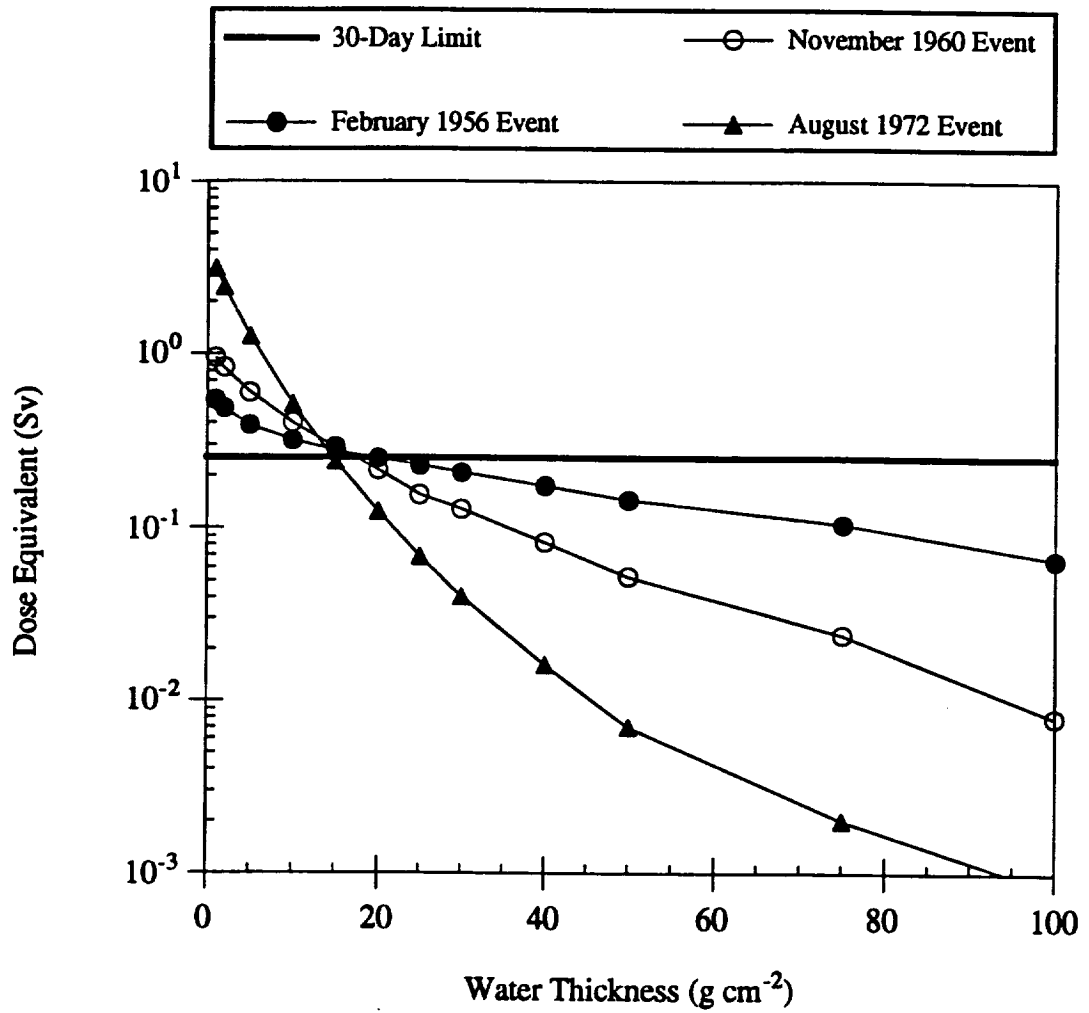
Figure 2.5 Depth-dose equivalent (Sv) in tissue (5 cm depth) as a function of water shield thickness for three Anomalously Large Solar Particle Events. (1 g cm-2 of water is equivalent to a thickness of 1 cm of aluminum).

Reference: Townsend, Nealy, Wilson (1988).
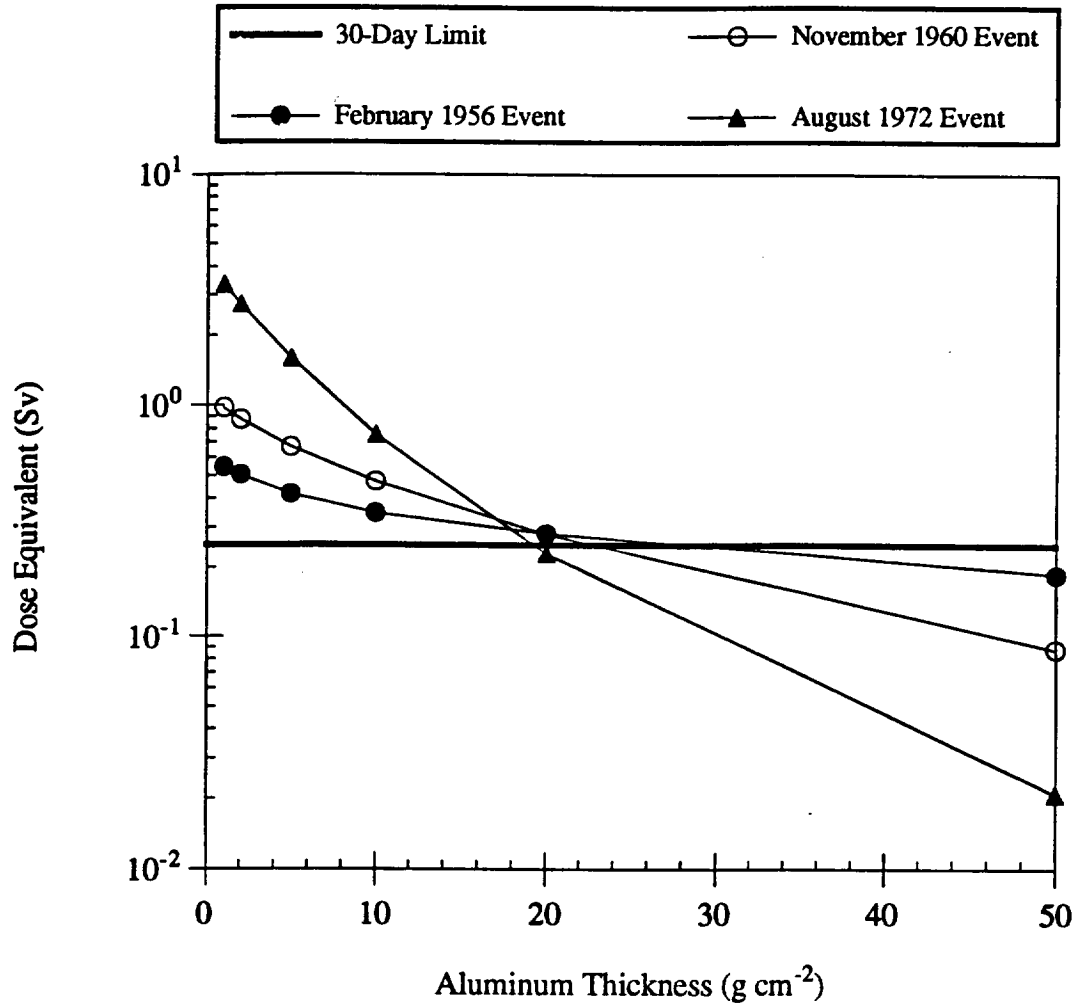
Figure 2.6 Depth-dose equivalent (Sv) in tissue (5 cm depth) as a function of aluminum shield thickness for three Anomalously Large Solar Particle Events. (1 g cm-2 of aluminum is equivalent to a thickness of 0.37 cm of aluminum).

Reference: Townsend, Nealy, Wilson (1988).

recorded at that time, could have been mission-threatening for thinly shielded spacecraft (less than 2 g cm^{-2}). The calculations used integral particle fluences for the events as inputs to the Langley Research Center nucleon transport code BRYNTRN. This deterministic code transports primary and secondary nucleons (protons and neutrons) through any number of layers of target material for arbitrary thickness and composition. Contributions from target nucleus fragmentation and recoil are also included. Both these figures show that SPEs are unpredictable not only on the date of the event but also on the particle fluxes that will be emitted.

Fig. 2.7 presents estimates of the BFO dose equivalent behind various thicknesses of aluminum shielding for the large solar proton events of August 1972 and October 1989 calculated using the coupled neutron proton space radiation transport computer code, BRYNTRN (Townsend et al. 1991). These estimates show that both events could be life-threatening if adequate shielding is not provided.

Fig. 2.8 displays the cumulative BFO dose equivalent as a function of water shield thickness (Simonsen et al. 1993). The GOES-7 satellite time history data of hourly averaged integral proton fluxes at various particle kinetic energies were analyzed for the solar proton event that occurred between October 19 and 29, 1989. By analyzing the time history data, the dose rates which may vary over many orders of magnitude in the early phases of the flare could be estimated as well as the cumulative dose as a function of time.

For deep space missions, such as a Lunar base or Mars mission, the main sources of natural radiation are solar particle events and galactic cosmic rays. The aluminum spacecraft thickness for the crew compartment must provide for adequate shielding from both sources. The worst-case (at solar minimum) GCR radiation absorbed dose and dose equivalent as a function of aluminum thickness have been estimated for various organs (Townsend et al. 1990; Townsend et al. 1992). Aluminum is typically used in spacecraft design. It was concluded that shielding effectiveness per unit mass increases as the composition of the shield changes from heavier to lighter elements. For liquid hydrogen, an added advantage is the reduced neutron fluence due to the absence of neutrons in the target composition and the lack of target-fragment contributions because of the elementary nature of hydrogen. For GCR shielding the materials of choice are those composed of low atomic-mass-number constituents with significant hydrogen content.
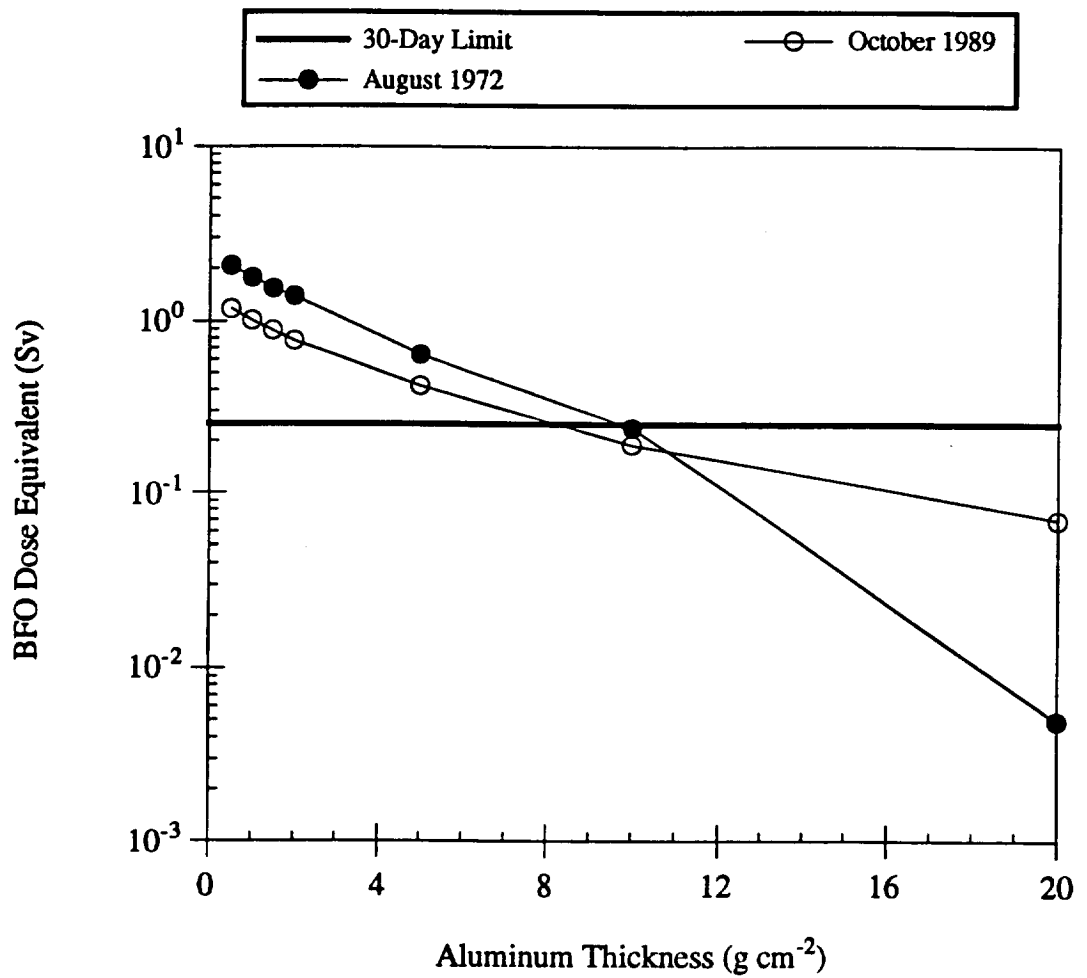
Figure 2.7 BFO dose equivalent as a function of aluminum shield thickness for the August 1972 and October 1989 Solar Particle Events.

Reference: Townsend, Shinn, Wilson (1991).
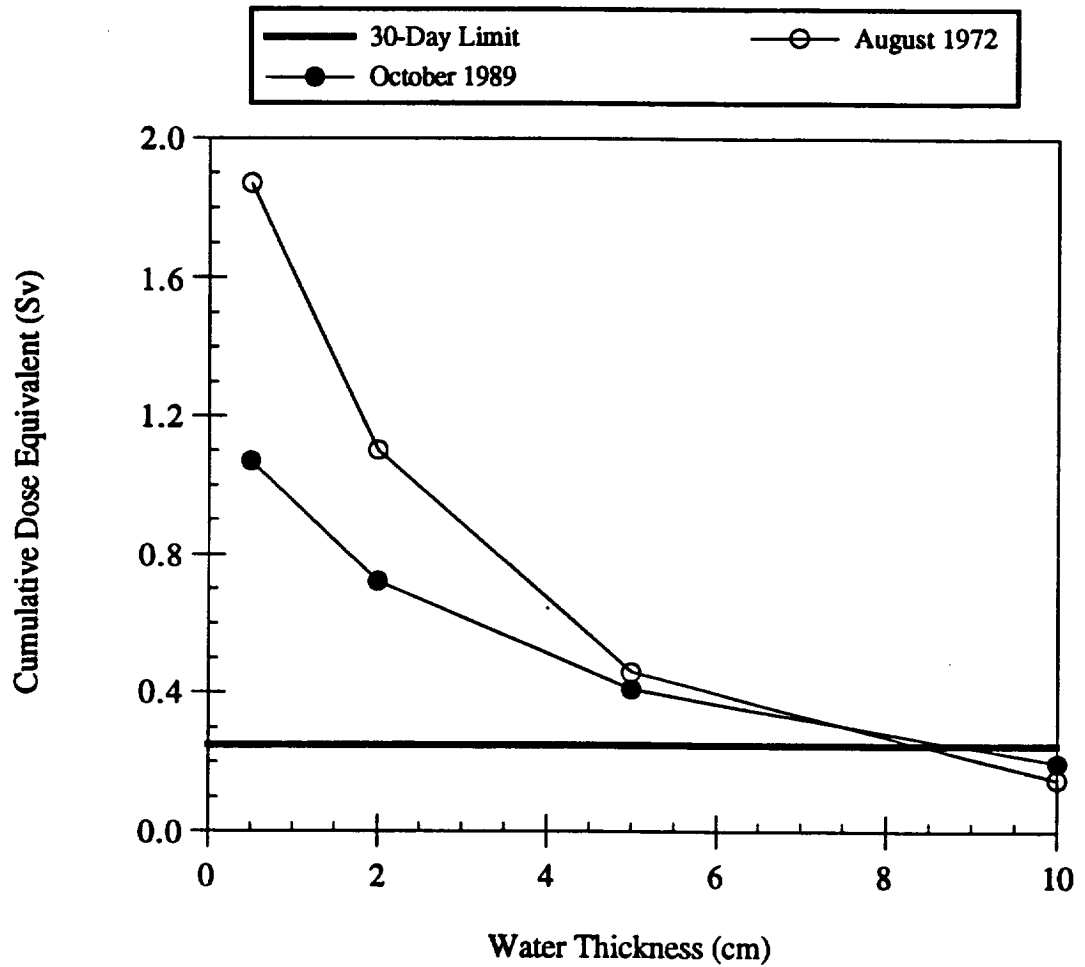
Figure 2.8 BFO dose equivalent from the October 1989 and August 1972 proton flares as a function of water shielding thickness. Calculations performed using the Langley Research Center nucleon transport computer code (BRYNTRN), and the computerized anatomical man (CAM) model.

Reference: Simonsen et al. (1993).

ESTIMATES OF RADIATION DOSE FROM MAN-MADE SOURCES

This section summarizes the results of previous studies investigating radiation doses to the crew for exploratory class mission from on-board reactor sources. In a NASA report from Bolch et al. (1990), scenarios involving the use of nuclear power systems in the vicinity of the Space Station Freedom (SSF) were identified and their radiological impact on the SSF crew was quantified. Several of the scenarios developed related to the use of SSF as an evolutionary transport node for lunar and Mars missions. The use of nuclear power on co-orbiting platforms and the storage and handling issues associated with radioisotopic power systems were also explored as they related to SSF.

On one hand, the analysis methods employed to perform this task were simplified and the results were intended to aid mission planners and identify operational and design constraints on SSF associated with the use of nuclear power sources. The report noted that the analysis procedure developed in this work could be extended to provide more rigorous results.

A central philosophy in these analyses was the utilization of a dose budget concept. The radiation source and resulting dose from the natural space environment at SSF were first analyzed and determined. The difference between the total dose limit (from NCRP guidelines) and the dose from natural sources defined the dose budget for the SSF crew. Given the radiation source terms associated with the nuclear power system in any given scenario, the dose budget was then employed to identify and quantify constraints on the interaction of the system with SSF and its crew.

Both nuclear thermal rockets (NTR) and nuclear electric propulsion (NEP) vehicles were studied. The SP-100 class reactor was assumed for the NEP missions and most of the assumptions made were used in the present research. Nevertheless, the approach and concern are different from the research project (SSF crew dose versus NEP crew dose) and a comparison of the results is not appropriate.

In a conference paper, Schnitzler and Borowski (1991) summarized qualitatively the natural and man-made radiation environment to be encountered during interplanetary missions. Mission profiles and vehicle configurations were presented for typical all-propulsive lunar or Mars missions. Estimates of crew-location biological doses were

developed for all propulsive maneuvers of the nuclear thermal rocket (NTR). The computational methods available to characterize the radiation environment produced by an operating nuclear propulsion system are discussed. They specified that estimations of the dose rate at the crew locations represented a classic "deep penetration" problem and was thus poorly suited to Monte Carlo analysis. Nevertheless, they did not provide any alternative computational method. They used previous results and summarized the natural and man-made doses in a total, budget-like dose estimate.

In a latter paper, Sager (1992) completed the calculations of Schnitzler and found the NTR reactor dose to be 0.05 Sv for a 434-day mission (Sager 1992). No specific description of the reactor shield or the reactor dose calculations were given.

In 1992, J. A. George presented the impact of radiation protection considerations on vehicle design and mission performance during a manned Mars mission (George 1992a). The total interplanetary environment was considered and its radiation protection requirements were investigated in a systems approach. The purpose of this research was to determine the minimum integrated shielding system masses using radiation budgets. Worst-case natural radiation doses and a 10-MW_e NEP reactor dose were studied. For the reactor, shield masses as a function of shielded dose equivalent for a five-layered tungsten/lithium hydride shield were generated using the Lewis Research Center SHIELD code, written by McKissock and Bloomfield in 1989 (McKissock and Bloomfield 1989). In that study, an 11.3° shadow shield was used to shield a dose plane slightly over 40 m in diameter at a payload separation distance of 100 m. The shielding of the reactor is only described as a five-layered tungsten/lithium hydride (the intent of the study was to investigate and size a three-layered beryllium/tungsten/lithium hydride shield) and no dimensions were specified. The study concluded that optimized shielding systems tended to drive allowed reactor doses to 1 rem y^{-1}. It should be noted that most of the article dealt with natural radiation shielding.

CHAPTER III

MAN-MADE RADIATION SOURCE TERM

INTRODUCTION

In this chapter the space nuclear reactor SP-100, used as the basis for the Nuclear Electric Propulsion (NEP) vehicle under consideration, is briefly described. Furthermore, the computational tools used in the man-made radiation source term calculations are briefly outlined, along with the results obtained from the source term calculations of the SP-100 reactor scaled-up to 25 MW_{th}. The radiation source term of the scaled-up SP-100 reactor is reported during steady-state operation as well as following reactor shutdown.

DESCRIPTION OF THE SP-100 SPACE NUCLEAR REACTOR

Until very recently, the SP-100 reactor was under development as part of the U. S. space program during the 1980s. It has a baseline thermal power of 2.4 MW_{th} and employs a static thermoelectric power conversion subsystem to produce 100 kW_e of power. The basic design goals of the SP-100, however, call for scalability up to an order of magnitude higher power. For the purposes of this project, it was assumed that the reactor would generate 25 MW_{th} and utilize an active conversion system (Rankine cycle) in order to provide 5 MW_e of electrical power. The SP-100 is a small, compact, fast-spectrum reactor. It utilizes highly enriched uranium mononitride fuel, niobium -1% zirconium (Nb-1Zr) cladding, and liquid lithium (Li) coolant. The core vessel and structure are composed primarily of Nb-1Zr and the other materials employed in the core are also refractory alloys. Beryllium oxide (BeO) hinged reflector panels located on the outside periphery of the core are employed as the primary control mechanism. The entire core and reflector structure is enclosed in a conical carbon-carbon reentry shield. A layered tungsten (W), lithium-hydride (LiH) shadow shield is employed to decrease the radiation field at the user interface. A schematic of the SP-100 reactor is shown in Fig. 3.1.

FORWARD COOLANT PLENUM
FORWARD ATTACHMENT REGION
FISSION GAS PLENUM (SPACERS)

FISSION GAS PLENUM (SPRINGS)

DUCT
COOLANT BYPASS
VESSEL
REACTOR CORE
RADIAL REFLECTOR

21cm
29cm

AFT GRID PLATE
COOLANT I/O REGION

Be
DEPLETED LiH
TUNGSTEN

NATURAL LiH

241 cm
178cm
71cm
92cm
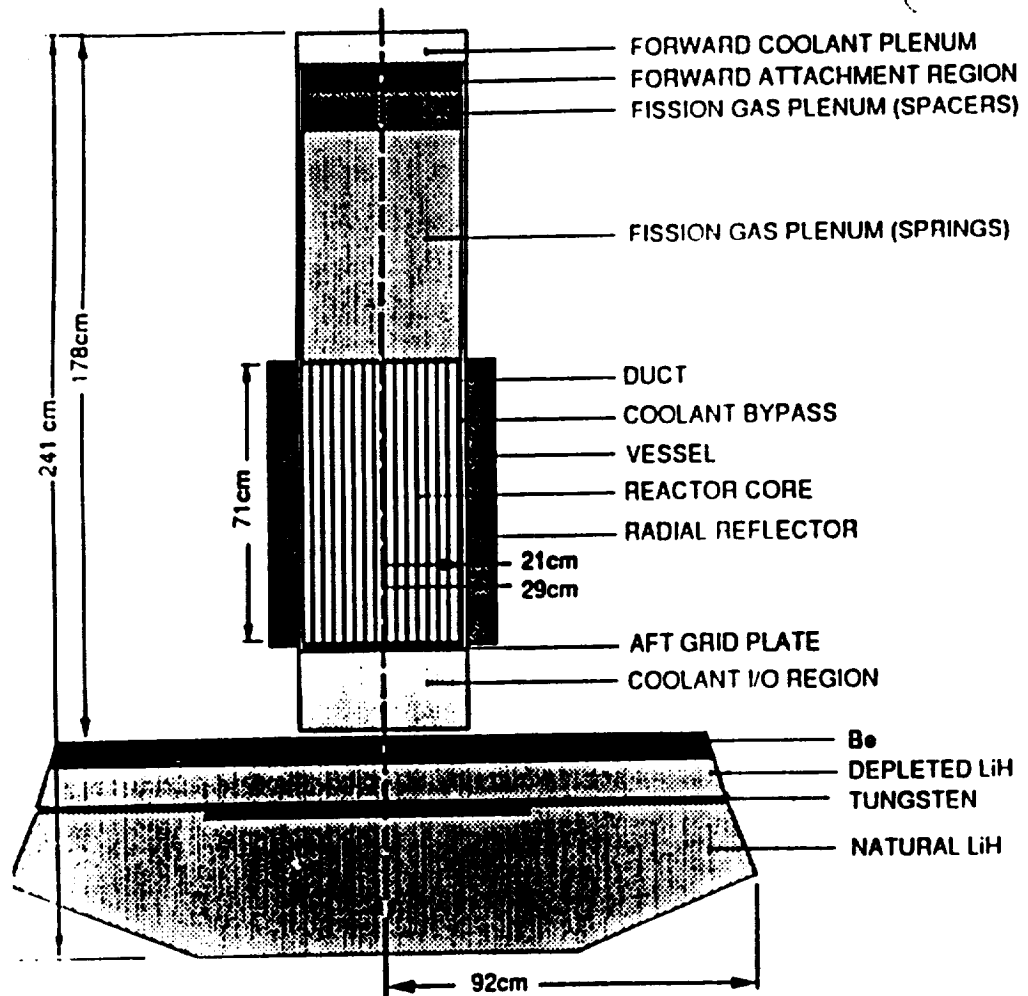
1/20 SCALE

Figure 3.1 SP-100 Space Nuclear Reactor Diagram.

3-2

TWODANT: TWO-DIMENSIONAL, MULTIGROUP, DISCRETE-ORDINATE TRANSPORT CODE

TWODANT solves the two-dimensional multigroup transport equation in plane, cylindrical, spherical, and two-angle plane geometries. Both regular and adjoint, inhomogenous and homogenous (k-eff and eigenvalue search) problems subject to vacuum, reflective, periodic, white, albedo, or inhomogenous boundary flux conditions are solved. General asymptotic scattering is allowed and anisotropic inhomogenous sources are permitted (O'Dell et al. 1989).

TWODANT numerically solves the two-dimensional, multigroup form of the neutral-particle, steady-state form of the Boltzmann transport equation. The discrete-ordinates approximation is used for treating the angular variation of the particle distribution and the diamond-difference scheme is used for phase space discretization. Negative fluxes are eliminated by a local set-to-zero-and-correct algorithm. A standard inner (within-group) iteration, outer (energy-group-dependent source) iteration technique is used. Both inner and outer iterations are accelerated using the diffusion synthetic acceleration method.

The TWODANT code is part of a modular computer program package designed to solve the time-independent, multigroup discrete ordinates form of the Boltzmann transport equation in several different geometries. The modular construction of the package separates the input processing, the transport equation solving, and the post processing (or edit) functions into distinct, independently executable code modules: the Input Module, one or more Solver Modules, and the Edit Module, respectively. The Input and Edit Modules are general in nature and are common to any of the Solver Modules that may be provided in the overall package. The TWODANT Solver Module contains a two-dimensional (slab, cylinder, and sphere), time-dependent transport equation solver using the standard diamond-differencing method for space/angle discretization. Also in existence is a Solver Module named TWOHEX. The TWODANT Solver Module solves the time-dependent transport equation using the diamond-differencing method for space/angle discretization in (r,z), (x,y), and (r, q) geometries. The TWOHEX Solver Module solves the time-independent transport equation on an equilateral triangle spatial mesh.

Some of the major features included in the TWODANT code package are:
(1) a free-field format card-image input capability designed with the user in mind;

(2) highly sophisticated, standardized, data- and file-management techniques; both sequential file and random-access file handling techniques are used;

(3) the use of diffusion synthetic acceleration scheme to accelerate the iterative process in the Solve Module;

(4) direct (forward) or adjoint calculational capability;

(5) standard plane, two-angle plane, cylindrical or spherical geometry options;

(6) arbitrary anisotropic scattering order;

(7) vacuum, reflective, periodic, white, albedo, or surface source boundary condition options;

(8) inhomogeneous (fixed) source or k-eff calculation options as well as time-absorption, nuclide concentration, or dimensional search options;

(9) "diamond-differencing" for solution of the transport equation;

(10) user flexibility in using both card-image or sequence file input;

(11) user flexibility in controlling the execution of both modules and submodules; and,

(12) extensive, user-oriented error diagnostics.

TWODANT INPUT OVERVIEW

The full TWODANT input consists of a title card section, followed by six blocks of free field input. The title card section is not free field. Any input referred to as a block uses the free field input form.

Block-I consists of basic control and dimensional information that allows efficient packing of the array data. This information also allows checking of the lengths of arrays supplied by interface files.

Block-II consists of geometric information.

Block-III consists of the nuclear data specifications.

Block-IV contains mixing information.

Block-V contains the rest of the input needed for specifying the flux calculation.

And lastly, Block-VI contains the edit (i.e. report writing) specifications.

A cross-section library may optionally be placed between Blocks III and IV, if it is in card image form. TWODANT supports many library formats and so the library may or may not be in free format depending upon the option chosen.

ORIGEN2: A COMPUTER CODE FOR CALCULATING THE NUCLIDE COMPOSITION AND CHARACTERISTICS OF NUCLEAR MATERIALS

A wide variety of computer codes are available for calculating the nuclide composition of nuclear reactor fuels during irradiation. Many of these codes are complex and highly developed, involving the use of multiple-energy-group neutron spectra and cross sections to calculate the composition of the nuclear fuel as a function of both space and time. Nevertheless, these codes are incomplete in that they only calculate the amounts of a limited number of nuclides known to be significant in the cases of interest (Croff 1983).

However, there is an entirely different class of problems for which these reactor physics codes are inappropriate because they are cumbersome, expensive to use, and provide too little detail concerning the composition of the material of interest.

ORIGEN2 is a flexible reactor physics code that provides various nuclear material characteristics in easily comprehensible form, and in a variety of useful engineering units, while employing a relatively unsophisticated neutronics calculation. The output is capable of displaying great detail concerning the contribution of each individual nuclide to the overall totals for each engineering unit. The nuclides contained in the ORIGEN2 data bases have been divided into three segments: 130 actinides, 850 fission products, and 720 activation products (a total of 1700 nuclides). These segments are formed by aggregating the 1300 unique nuclides (300 stable) in the data bases since some nuclides appear in more than one segment.

The principal use of ORIGEN2 is to calculate the radionuclide composition and other related properties of nuclear materials. The characteristics that can be computed by ORIGEN2 include, mass, fractional isotopic composition, radioactivity, thermal power,

radioactive and chemical ingestion toxicity, radioactive inhalation toxicity, neutron absorption rate, neutron fission rate, spontaneous fission emission rate, and photon emission. Most of these can be represented on a fractional basis so that the total characteristic for all nuclides in a given segment is 1.0. The materials most commonly characterized include spent reactor fuels, radioactive wastes, recovered elements, uranium ore and mill tailings, and gaseous effluent streams.

DESCRIPTION OF ORIGEN2 CALCULATIONAL METHODS

Most of the calculations carried out by ORIGEN2 are relatively trivial, involving reading and storing data bases, converting units from g-atoms to other characteristic units, and writing the results to output devices. There are, however, two unique features of ORIGEN2 that require some explanation. These are: (1) the method for storing the equations that describe the buildup and decay of nuclides, and, (2) the methods employed to solve these equations.

In general, the rate at which the amount of nuclide changes as a function of time is described by a nonhomogeneous first-order ordinary differential equation. Since N nuclides are being considered, there are N equations of the same general form, one for each nuclide. Solution (integration) of this set of simultaneous differential equations by ORIGEN2 yields the amounts of each nuclide present at the end of each time step (integration interval). Storage of the equation coefficients works in the following manner:

(1) Input data containing the half-lives, decay branching fractions, cross-sections, and fission products yields for each parent nuclide are read from data bases.

(2) The daughter of each nuclear transformation, e.g. beta decay, neutron capture, is determined, and the transformation rate and identity of the daughter are stored temporarily in an array.

(3) The temporary array is then searched to find all of the parents of each daughter nuclide.

(4) The transformation rate of each parent daughter nuclide and the identity of that parent are stored sequentially in one-dimensional floating-point and integer arrays, respectively, with the decay transformations being stored first.

(5) Counters are maintained to indicate the array locations at which the transformations producing each daughter nuclide begin and the number of the transformations that are decay transformations.

The floating-point array of transformation rates, called the transition matrix, is stored permanently since it is invariant for a given case. The transition matrix and its accompanying integer arrays use <20 000 decimal words of storage as compared with the 2.9 million that would be required to store the entire matrix.

After the transition matrix and its associated arrays have been established, it is possible to begin irradiation and decay calculations. The user specifies an initial composition of the material to be irradiated, the flux or power that it is to produce, and the length of time step over which the flux, power, or radioactive decay is applicable. The composition of the material at the end of the irradiation step is then calculated in three general steps:

(1) The transition matrix parameters that are time-step dependent are set.

(2) The neutron flux is calculated from the power (or vice versa) and the transition matrix is adjusted accordingly.

(3) The nuclide composition at the end of the time step is calculated using a complementary set of mathematical techniques.

The final step in the calculational procedure is to solve the system of simultaneous differential equations represented by the coefficients in the transition matrix. The method employed by ORIGEN2 is really a composite of three solution methods, the center-piece of which is the matrix exponential technique for solving differential equations (described below). However, computational problems are encountered when the exponential technique is applied to a matrix with widely separated eigenvalues, which is certainly the case for ORIGEN2 since the coefficients in the matrix range from half-lives of seconds to billions of years. This difficulty can be circumvented by employing asymptotic versions of the analytical solutions to the nuclide buildup and depletion equations.

DESCRIPTION OF ORIGEN2 INPUT DATA BASES

Three principal types of input data bases are required by the ORIGEN2 computer code: radioactive decay, photon production, and cross section. Each of these data bases is divided into three segments. Only one or two of the segments may be required in a given case if they include the nuclides of interest.

The decay data base is required for all ORIGEN2 calculations. It supplies the following information:

(1) the list of nuclides to be considered,

(2) the decay half-lives and the decay branching fractions for beta decay to ground and excited states, positron plus electron capture decay to ground and excited states, internal transitions, alpha decay, spontaneous fission decay, and delayed neutron decay,

(3) the recoverable heat per decay for each radioactive parent,

(4) the isotopic composition of naturally occurring elements,

(5) the radionuclide maximum permissible concentration values.

The photon data base supplies the number of photons per decay in an 18-energy-group structure. These values are used to output a table giving the number of photons and the photon energy emission rate in 18 energy groups as a function of irradiation or decay time. They are also used to generate a summary table listing the principal nuclide contributors to each of the 18 energy groups. The types of photons that have been included in the data bases are gamma rays, x rays, conversion photons, prompt and fission product gamma rays from spontaneous fission, and bremsstrahlung. Prompt gamma rays from fission and neutron capture are not included.

At present, three photon data bases are available, depending on the type of bremsstrahlung (which is medium dependent) that is included. The first and second data bases include bremsstrahlung from a UO_2 matrix and an H_2O matrix, respectively; the third includes no bremsstrahlung. A master data base containing discrete gamma-ray and x-ray transitions and bremsstrahlung in a 70-energy group structure is maintained at ORNL to facilitate the generation of photon data bases in alternative energy group structures.

The function of the cross-section data bases is to supply ORIGEN2 with cross section and fission product yields. The types of cross sections normally included are (n,g) to ground and excited states, (n,2n) to ground and excited states, (n,3n) and (n, fission) for the actinides, and (n,p) and (n,a) for the activation products and fission products. In addition, a separate mechanism has been incorporated into ORIGEN2 to accommodate any other flux-dependent reaction that is not included in this list.

There are a large number of possible cross-section data bases for the ORIGEN2 computer code since the one-group cross-sections are highly reactor- and fuel-type specific. The types of reactors for which cross-section libraries are now available are as follows:

(1) U and U-Pu cycle pressurized water reactors (PWRs) and boiling water reactors (BWRs),

(2) alternative fuel cycle PWRs,

(3) once-through Canada deuterium uranium reactors,

(4) U-Pu cycle LMFBRs,

(5) thorium cycle LMFBRs,

(6) Fast Flux Test Facility,

(7) Clinch River Breeder Reactor.

Calculation of the one-group cross sections is a complex process that is specific to the reactor type being considered and must be performed by sophisticated reactor physics codes external to ORIGEN2. In general, such calculations involve generation of multiple-energy-group cross-section data bases. These are then weighted with an approximate neutron spectrum, resulting in a few-group cross-section data base that accounts for self-shielding effects within the fuel rods. The few-group cross-sections for the most important nuclides are subsequently used to perform a one- or two-dimensional depletion calculation, resulting in (a) a prediction of the composition of the spent fuel and (b) a set of burnup-dependent cross sections that can be incorporated into ORIGEN2 to enable it to account for concentration and neutron spectrum changes. The composition predicted by the depletion code is used to generate a multigroup neutron energy spectrum, which becomes the weighting function to generate one-group cross-sections and spectrum-weighted fission product yields for the ORIGEN2 cross-section data bases. This spectrum is also used to generate the ORIGEN2 flux parameters which are employed to weight thermal cross sections, resonance integrals, and threshold cross sections, respectively, when they cannot be obtained in multigroup format.

The multigroup cross sections were obtained from ENDF/B-IV and/or ENDF/B-V, depending on the availability of data at the time the calculations were performed. Virtually all of the fission product yields are independent yields and were taken from ENDF/B-IV. The exceptions are the fission yields of the very light nuclides that result from ternary fission, which were based on a search of the literature.

SP-100 OPERATING REACTOR FLUXES

Neutron and gamma fluxes for the beginning-of-life (BOL) of an SP-100 reactor operating at 2.5 MW$_{th}$ were calculated by General Electric (GE) using the TWODANT code. For the purposes of this project, the fluxes computed by GE were utilized and appropriately scaled-up to represent a 25 MW$_{th}$ SP-100 reactor used in an NEP vehicle. Furthermore, only fluxes at the bottom of the core were of interest in this project, because the core-reflector interface comprised the man-made source term for the particle transport calculations performed using the MCNP code. Tables 3.1 and 3.2 depict the energy ranges for the neutron and gamma groups used in the TWODANT calculations for the 2.5 MW$_{th}$ SP-100 reactor, respectively.

Table 3.1 SP-100 Neutron Energy Group Ranges.

Group	Lower Energy (MeV)	Upper Energy (MeV)
1	2.23	20.00
2	1.35	2.23
3	0.82	1.35
4	0.50	0.82
5	0.30	0.50
6	0.11	0.30
7	4.09E-02	1.11E-01
8	5.53E-03	4.09E-02
9	1.67E-04	5.53E-03
10	4.14E-07	1.67E-04
11	1.39E-10	4.14E-07

Table 3.2 SP-100 Gamma Energy Group Ranges.

Group	Lower Energy (MeV)	Upper Energy (MeV)
1	2.50	30.00
2	0.75	2.50
3	0.30	0.75
4	0.01	0.30

Table 3.3 below depicts the radial distribution of the neutron fluxes at the core-reflector interface of the 25 MW$_{th}$ SP-100 reactor. All 11 energy groups are listed. Figure 3.2 also depicts the radial neutron fluxes at the same axial location (core-reflector interface).

Table 3.3 25 MW$_{th}$ SP-100 Operating Neutron Fluxes at the Core-Reflector Interface.

Radial Location	0 cm	4 cm	8 cm	12 cm	16 cm	20 cm	24 cm	28 cm
Energy Group								
1	2.93E+13	2.86E+13	2.65E+13	2.31E+13	1.88E+13	1.40E+13	8.99E+12	4.52E+12
2	3.41E+13	3.33E+13	3.08E+13	2.69E+13	2.19E+13	1.62E+13	1.04E+13	5.23E+12
3	4.67E+13	4.55E+13	4.22E+13	3.70E+13	3.02E+13	2.25E+13	1.46+13	7.52E+12
4	7.67E+13	7.48E+13	6.93E+13	6.05E+13	4.93E+13	3.65E+13	2.35E+13	1.18E+13
5	6.98E+13	6.80E+13	6.30E+13	5.50E+13	4.46E+13	3.29E+13	2.11E+13	1.04E+13
6	1.60E+14	1.56E+14	1.45E+14	1.26E+14	1.02E+14	7.45E+13	4.70E+13	2.26E+13
7	1.20E+14	1.17E+14	1.08E+14	9.41E+13	7.60E+13	5.56E+13	3.50E+13	1.67E+13
8	1.35E+14	1.32E+14	1.21E+14	1.05E+14	8.50E+13	6.19E+13	3.87E+13	1.82E+13
9	6.68E+13	6.50E+13	6.00E+13	5.20E+13	4.18E+13	3.03E+13	1.88E+13	8.71E+12
10	2.80E+13	2.73E+13	2.51E+13	2.18E+13	1.75E+13	1.26E+13	7.80E+12	3.58E+12
11	5.14E+12	5.00E+12	4.60E+12	3.97E+12	3.16E+12	2.26E+12	1.37E+12	5.99E+11

SP-100 POST-SHUTDOWN FLUXES

Table 3.4 depicts the gamma post-shutdown fluxes at the core-reflector interface of the 25 MW$_{th}$ SP-100 reactor following operation at full power. All 18 energy groups are listed. Figures 3.3 and 3.4 also depict the gamma post-shutdown fluxes and dose at the same axial location (core-reflector interface).
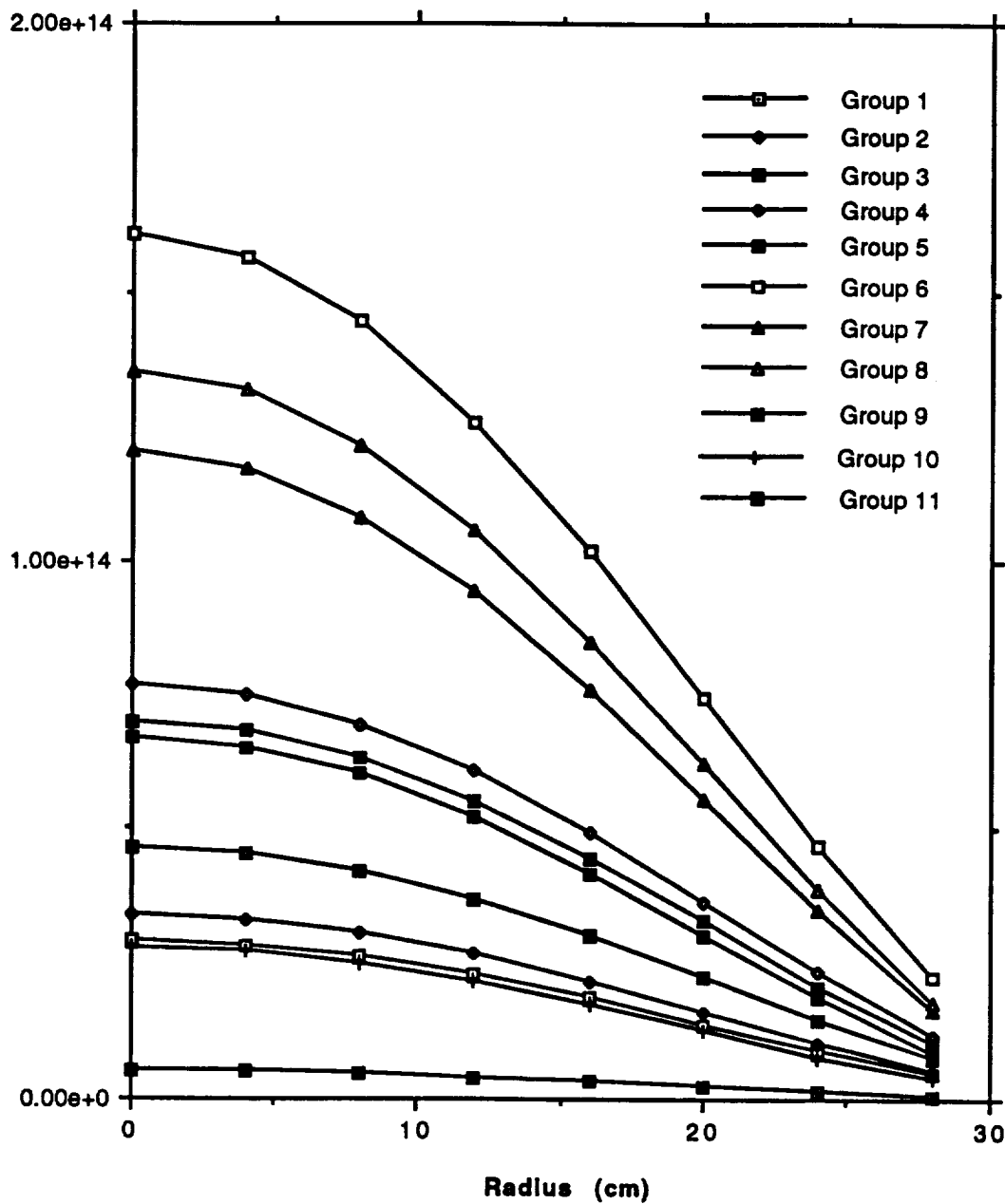
Figure 3.2 25 MW$_{th}$ SP-100 Operating Neutron Fluxes at the Core-Reflector Interface.

Table 3.4 25 MW$_{th}$ SP-100 Post-Shutdown Gammas Fluxes at the Core-Reflector Interface.

| Time After Shutdown	1 days	5 days	10 days	20 days	30 days
Energy Group					
1	1.72E+17	1.04E+17	8.42E+16	6.49E+16	5.41E+16
2	6.38E+16	3.71E+16	2.62E+16	1.77E+16	1.39E+16
3	8.08E+16	4.59E+16	3.20E+16	2.07E+16	1.57E+16
4	3.59E+16	1.98E+16	1.54E+16	1.18E+16	9.99E+15
5	4.04E+16	2.63E+16	1.81E+16	1.06E+16	7.70E+15
6	7.54E+16	4.59E+16	3.29E+16	2.43E+16	2.00E+16
7	8.21E+16	2.60E+16	1.39E+16	7.69E+15	5.90E+15
8	4.20E+16	2.85E+16	2.02E+16	1.11E+16	6.68E+15
9	1.55E+17	7.13E+16	4.80E+16	3.02E+16	2.23E+16
10	1.63E+17	1.15E+17	9.82E+16	8.32E+16	7.45E+16
11	1.58E+16	3.74E+15	1.61E+15	6.10E+14	4.38E+14
12	4.22E+16	3.48E+16	2.69E+16	1.57E+16	9.13E+15
13	1.37E+15	7.94E+14	5.59E+14	3.62E+14	2.76E+14
14	1.54E+15	1.32E+15	1.02E+15	5.96E+14	3.47E+14
15	1.33E+13	1.09E+13	8.45E+12	4.95E+12	2.91E+12
16	1.38E+11	9.12E+00	1.55E-05	1.55E-05	1.56E-05
17	1.00E-06	1.00E-06	1.00E-06	1.00E-06	1.00E-06
18	6.34E-08	6.35E-08	6.36E-08	6.37E-08	6.39E-08
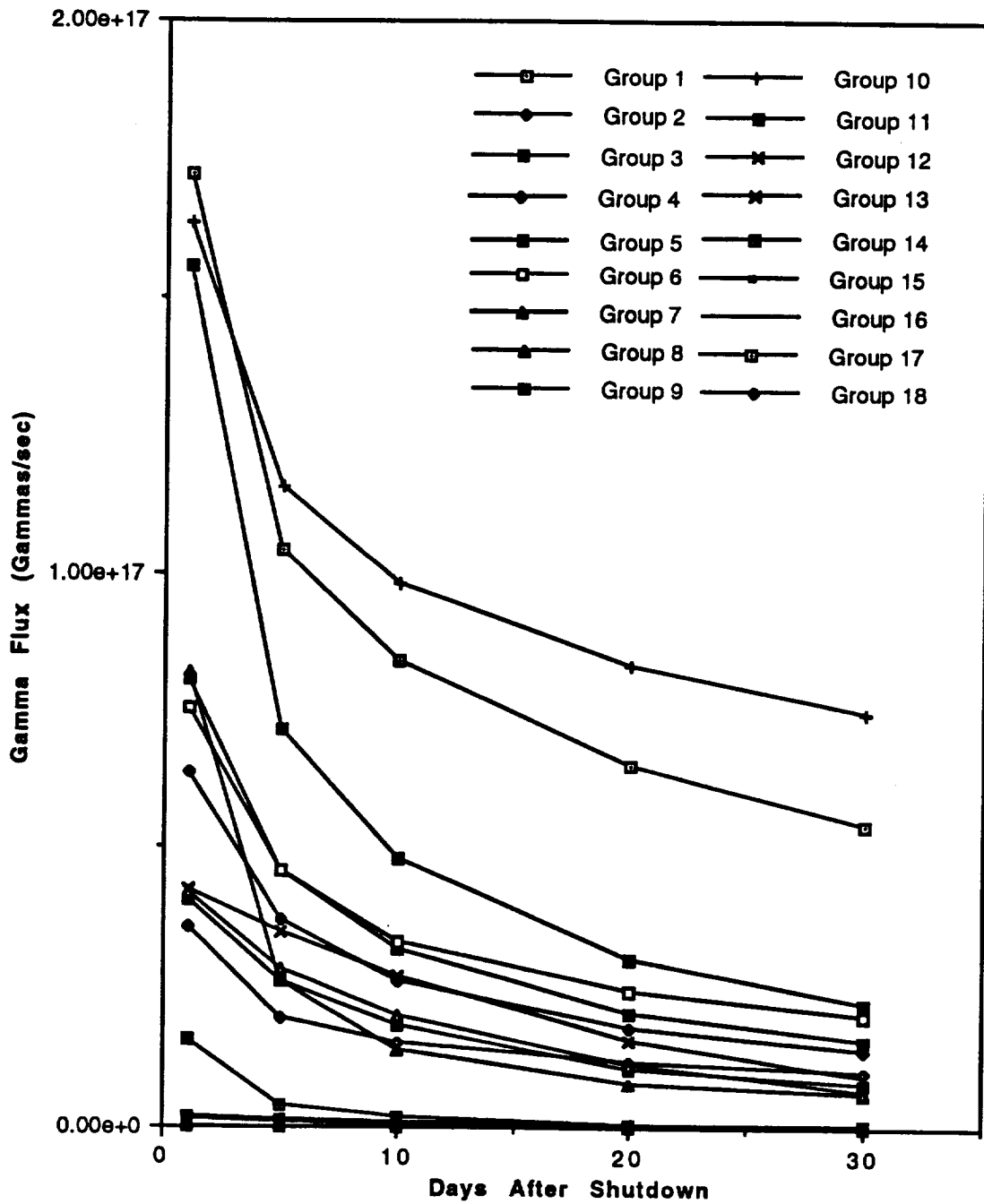
Figure 3.3 25 MWth SP-100 Post-Shutdown Gamma Fluxes at the Core-Reflector Interface.
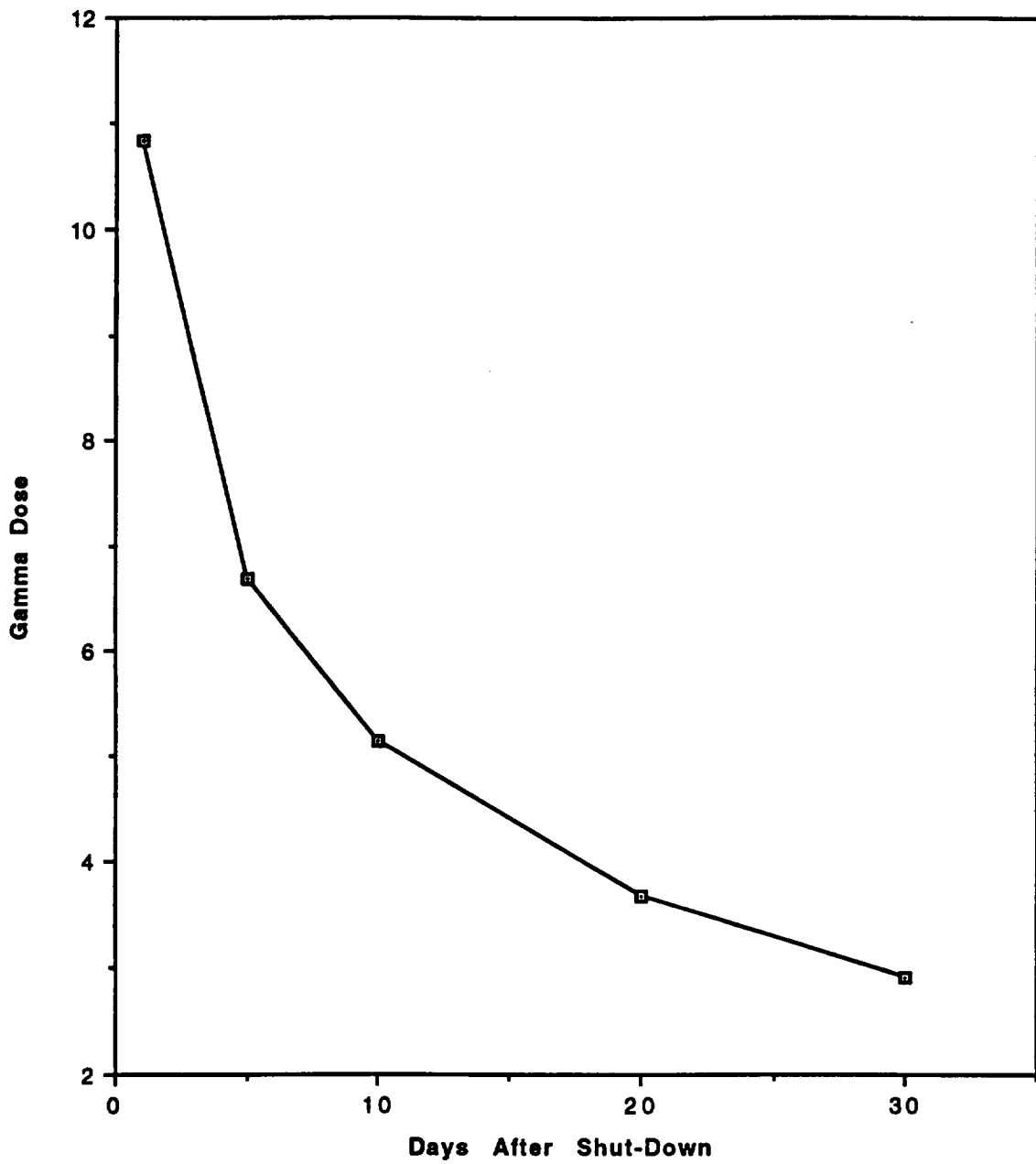
Figure 3.4 25 MW$_{th}$ SP-100 Post-Shutdown Dose at the Core-Reflector Interface.

CHAPTER IV

SPACE VEHICLE MODELING FOR RADIATION TRANSPORT CALCULATIONS

INTRODUCTION

In this chapter the nuclear electric propulsion (NEP) space vehicle is modeled using the neutron and photon transport code MCNP. Furthermore, the computational tool used in this modeling, namely MCNP, is briefly outlined. The source terms used in the space vehicle modeling include both the SP-100 reactor (man-made) and natural radiation.

MCNP: A GENERAL MONTE CARLO CODE FOR NEUTRON AND PHOTON TRANSPORT

The Monte Carlo method is a mathematical technique for solving problems that contain statistical processes. The method is very useful for complex problems that cannot be modeled by computer codes using deterministic methods or when experimental measurements may be impractical. The Monte Carlo method constructs a stochastic model representing the process of interest. The individual probabilistic events of a process are simulated sequentially, and the probability distributions governing these events are statistically sampled to describe the total phenomenon. The result is an estimate of a physical quantity characteristic of the process, specified with a measured degree of confidence.

The Monte Carlo method was named by Von Neumann (McCracken 1955). Von Neumann, Ulam, and Fermi applied the method towards neutron diffusion problems in the Manhattan Project at Los Alamos during World War II. Monte Carlo techniques have found numerous applications within the radiation sciences because of the random nature of radioactive decay and transport processes.

In radiation transport problems, the Monte Carlo technique consists of following each of many particles from a source throughout its life to its death in some terminal category such as absorption or escape. Probability distributions are randomly sampled from the transport data to determine the outcome at each step of the life of the particle.

Random numbers are used to sample the probability, type, and outcome of interactions in the model, thus simulating the paths of the particles in the media. After sampling numerous values of the physical quantity of interest (e.g., particle flux, fluence, etc.), the expected value is estimated as the average value of all histories. Associated with this estimate is a measure of its statistical significance. Greater confidence or precision is achieved in the average value as the number of histories sampled is increased. The accuracy of the estimate is dependent upon the appropriateness of the stochastic model to represent the true physical process. For radiation transport problems, the model includes geometry and material specifications. Cross-section data for the interaction types of interest (incoherent scattering, pair production, etc.) must be supplied for each material present. The model also consists of algorithms used to compute the result of interactions (changes in particle energy, direction, etc.) based on the physical principles that describe the interaction of radiation with matter and the cross-section data provided. Therefore, it is extremely important to model the situation well as the Monte Carlo result is only as valid as the data supplied.

The increased speed and capabilities of computers, coupled with their widespread availability and decreasing costs, has further simplified use of the Monte Carlo method in solving transport problems. Much emphasis has been placed upon developing generalized computer programs that can process a variety of transport problems. A large number of codes currently exists for this purpose, requiring only a limited amount of user supplied information regarding the specific problem to be examined. One of these codes is MCNP, a general Monte Carlo code for Neutron and Photon transport.

MCNP CODE

MCNP is a general purpose radiation transport code that is the result of 50 years of development efforts at the Los Alamos National Laboratory (LANL) (Briesmeister 1986; Briesmeister and Hendricks 1991). The code is the union of previously independent codes for transporting source neutrons (MCN) (Cashwell et al. 1972), photons (MCG) (Cashwell et al. 1973), and electrons (Integrated Tiger Series/"ITS") (Halbleib and Mehlborn 1986), separately. The first coupled neutron/photon version of MCNP was published in 1977. Primary and secondary electron transport capabilities were included in the most recent version released, MCNP4. Only neutron and photon sources of transport

relevant to the work described here. Therefore, the following discussion of the MCNP code will be restricted to neutron and photon transport.

MCNP is currently supported by the Radiation Transport Group (X-6) in the Applied Theoretical Physics Division (X-Division) at Los Alamos National Laboratory (LANL). The code has an extensive library of continuous-energy cross-section data. Photon cross-section tables span the energy range 1 keV - 100 MeV, and were extracted from the Evaluated Nuclear Data File (ENDF) (Kinsey 1979). MCNP features state-of-the-art computational methods modeling the physics of interaction events. With regard to photon transport, this includes coherent scattering, annihilation radiation emission following absorption by pair production, and potential fluorescent emission following photoelectric absorption. A generalized three-dimensional geometry capability is supplied supporting first-, second-, and some specialized fourth-degree surfaces. User-supplied geometries of a more complex nature are permitted. Numerous variance reduction techniques are also available. Random numbers are generated using the Lehmer scheme (Lehmer 1951). MCNP was written in pure FORTRAN 77, i.e., it contains no system dependent features, and thus is portable to numerous machines and operating systems. The quality of the code has been validated by countless user-years producing credible results for a variety of applications.

Even if Monte Carlo radiation transport is not easily suited for deep penetration problems, MCNP is currently the most reliable code on the market for neutron and photon transport at the macrodosimetric level and it appeared to be the best solution to the current problem. Second, the geometry set-up for one reactor could easily be modeled by MCNP standard geometrical surfaces. Third, MCNP is portable on the Vax and UNIX systems, the available systems on the Texas A&M University campus. These are the main reasons why this research was performed using the MCNP transport code.

USER-SUPPLIED INFORMATION REQUIRED BY MCNP

The MCNP input file contains information about the problem in areas such as the geometry, the materials, the source, and output tallies. The file consists of three sections: cell cards, surface cards, and data cards. The first cards, cell cards, describe the geometry of a problem. MCNP defines each region of the problem to be a "cell" bounded by geometrical surfaces and having unique characteristics such as material composition. Each

of the cells in a problem may be defined by the intersection and union of various types of MCNP standard or user-defined surfaces allowed by MCNP. MCNP supplies generalized mnemonics for describing the standard surfaces, requiring only numerical entries to specify the scale of the problem. The sign of the numerical entry defines the important concept of sense. The sense refers to the direction in which all points in a cell lie relative to a bounding surface. By convention the interior of a cylinder or sphere is taken to be the negative (-) direction; the exterior of a cylinder or sphere is taken to be the positive (+) direction. A cell defined by the shorthand notation "#n" sign, contains everything that is not in cell "n". The information presented above constitutes the "cell cards" of a MCNP input file. Material specifications must also be defined using these cards, including the material density and an arbitrary material reference number defined in the material card section. Atomic densities (atom barn^{-1} cm^{-1}) are denoted by a positive sign entry on the cell card; mass densities (g cm^{-3}) are denoted by a negative sign. The data cards include source and tally information, the composition of the materials used in the problem, the number of particles to be launched, variance reduction information, and options for the output file.

INPUT FILE

A complete listing of the input files for the four types of calculations performed (neutron transport through the shield, photon transport through the shield, neutron transport through the crew compartments, photon transport through the crew compartments) is given in Appendix B. As it can be seen in Fig. 4.1, the three reactors of the NEP vehicle design are in a same plane, and are symmetric by a rotation of 120°. Thus the calculations could be simplified and consequently the computer time could be decreased by modeling only one of the three reactors and its shield complex. The central structures of the vehicle, such as the crew compartment, the ion thrusters, the argon tanks, and the Earth Crew Capture Vehicle (ECCV), are modeled separately in full detail since particle fluxes vary with the location inside the crew compartment. As shown in Fig. 4.2, the crew compartment is modeled as a series of six cylindrical regions with MCNP cell designations 110, 111, 112, 113, 139, and 150 (see Appendix B). Crew compartment 110 is directly exposed to the particle fluxes from the single reactor modeled in the simulations and thus receives a higher dose than the other crew compartments. The compartment numbers on Fig. 4.2 are identical to these used in the MCNP input file and in the presentation of the results in chapter IV. The other structures are modeled to take

into account scattered particles. Due to the geometrical symmetry of the central vehicle structures, the total particle fluxes and resulting doses when all three reactors are in operation may be found by simple summation of the simulation results obtained for the single reactor considered here.

The photon and neutron sources are treated separately because MCNP allows only one kind of source particle per run. Nevertheless, during neutron source runs, photons created by inelastic scattering and radiative capture are followed until their entire kinetic energy is spent or until they exit the vehicle geometry and are tallied in the output file.

15 MWe
Piloted
Vehicle
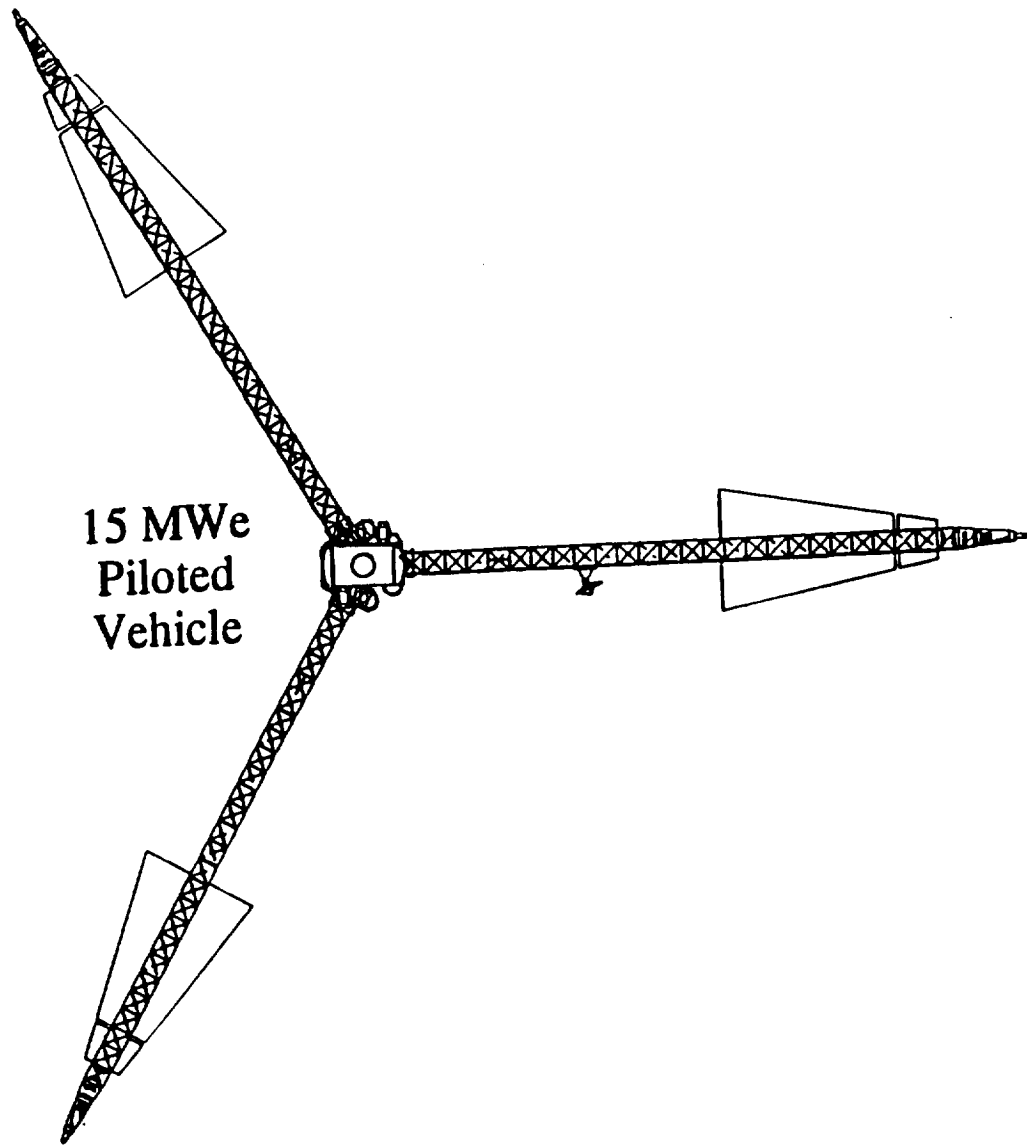
**Figure 4.1** Representation of a NEP vehicle.
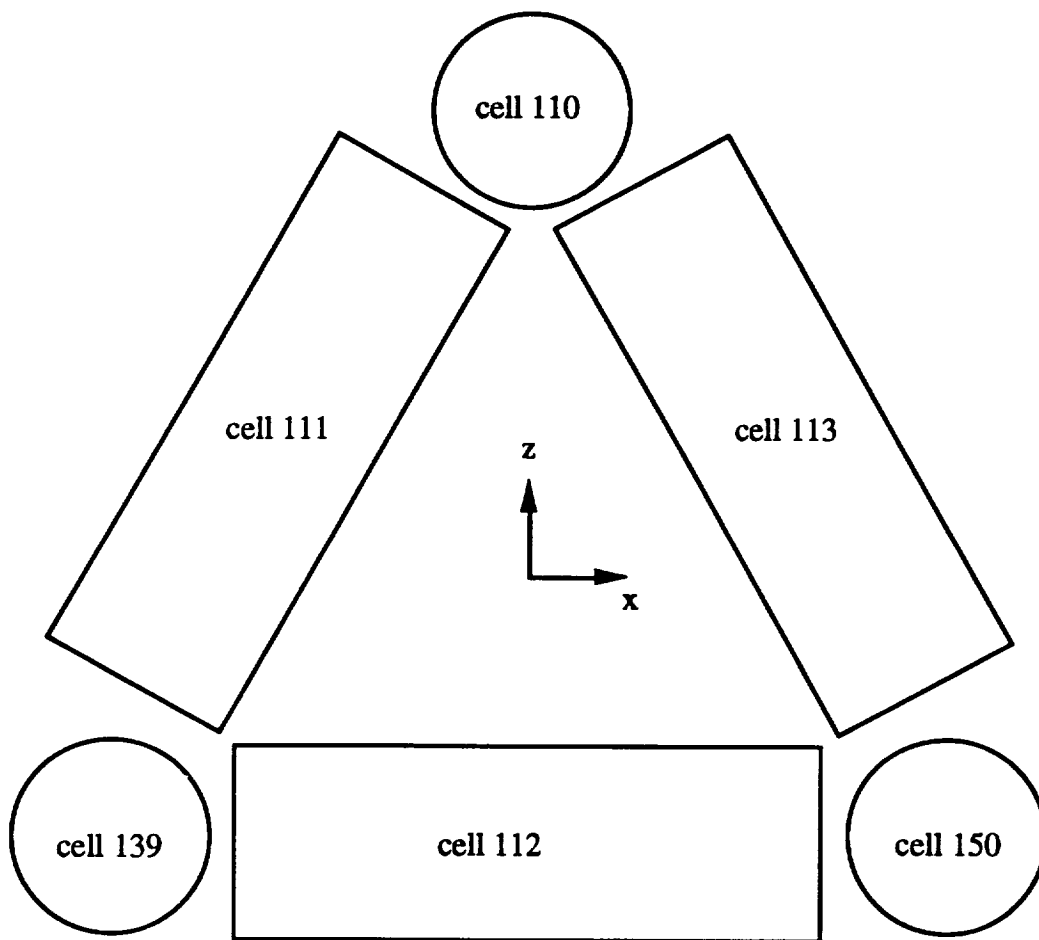
Figure 4.2 Crew compartment cell definition. The notations given in this figure are used in Chapter IV for the presentation of the results. The Y axis is coming out of the figure.

Moreover, the transport problem is handled in two geometry sets. The first set considers the transport of the particles from the bottom of the reactor through the entire shield assembly. This set is run for various combinations of the tungsten and lithium hydride layer thickness. The resulting fluxes at the bottom of the shield are then collapsed and treated as a point source for the second set of transport calculations. The second geometry set includes the crew compartment, the ECCV, the argon tanks, and the ion thrusters. The various elements of the geometry included in this model are now described in more detail in the following paragraphs.

The first geometry set allows the transport of source particles through a layer of liquid lithium coolant and then through a multilayered shield (Fig. 4.3). The source and the shield are surrounded by a sphere outside of which particle transport is terminated. In MCNP terminology, the exterior of this sphere is referred to as the outside world. Liquid lithium is used as the reactor coolant in the adopted SP-100 reactor design. The liquid lithium layer is located between the shield and the reactor bottom; it is modeled as a cylinder 28 cm in radius and 22.25 cm in height. The shield itself consists of various materials layered in a cylinder 108.00 cm in radius. The designed shield is a shadow shield, which means it shields a specific conical area of space including the crew compartment. For computer modeling simplification, the shield is modeled as a cylinder, whereas the design includes a conically shaped shield. The conical shape allows a reduction of the total shield mass without a decrease in the shielding performance. The weight factor is very important for space vehicles, but the use of a cylindrical shield instead of a conical one should not affect the dose calculations to any significant degree. The diameter of the cylinder was taken to be equal to the maximum diameter of the cone. The first layer considered in the model is the bottom-core reflector consisting of pure beryllium (Be). Contrary to the radial Be reflectors, whose primary function is to return a large fraction of neutrons to the core through elastic collisions, the primary purpose of the bottom layer of Be is to scatter neutrons away from the crew compartment. Because the distance between the reactor core and the Be layer is rather large, the reflecting property of Be is not used to control the reactor flux. Although, not usually considered in Earth-based reactor shield designs, this layer is included in the shadow shield design because of the neutrons scattered into free space result in a reduction of the doses to the crew. On Earth, radiation sources can not be simply scattered away from a specific area, radiation has to be shielded by absorption, because of the population living near the nuclear facility area. In
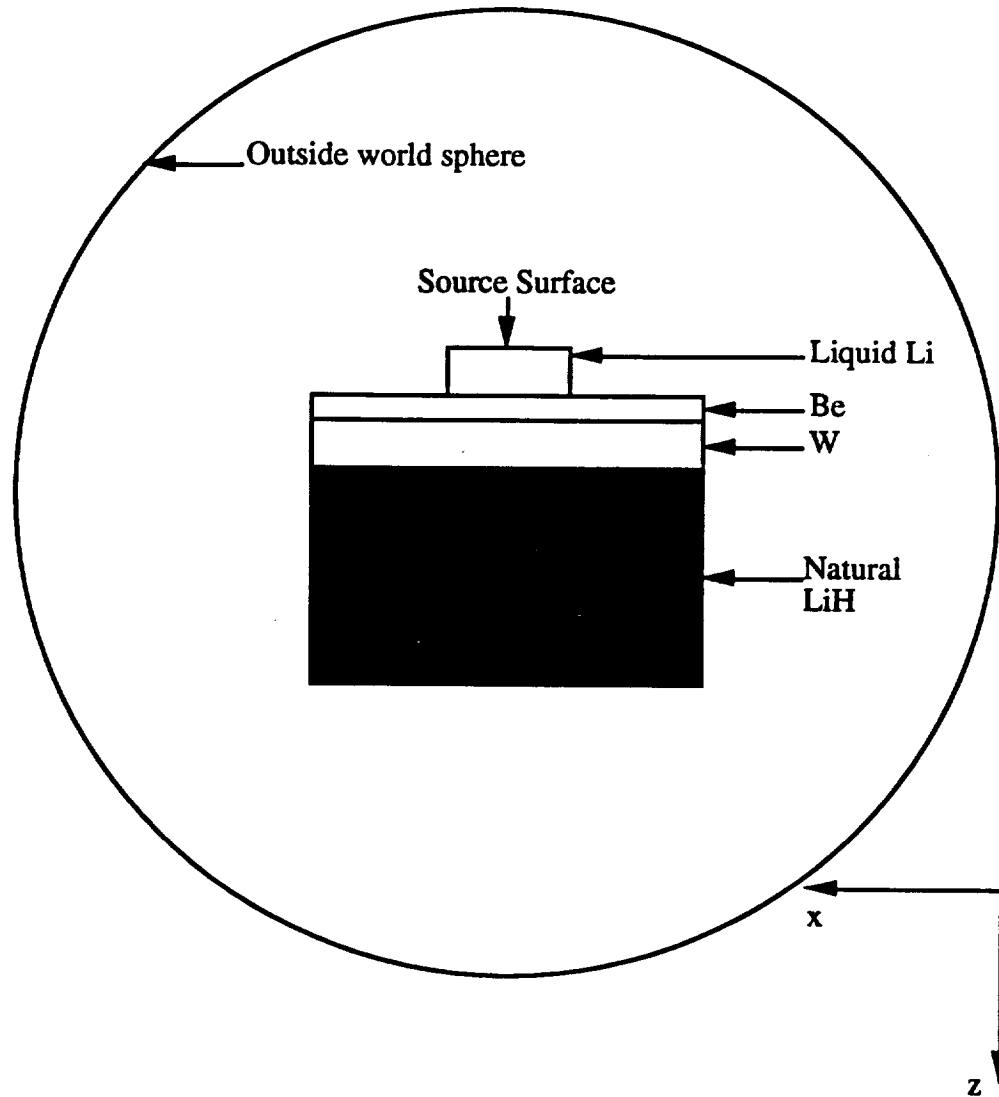
Figure 4.3 NEP bottom coolant and shadow shield as modeled in MCNP. The particle sources are distributed on the top surface of the small cylinder. The vertical lines represent cylinders. The outside circle is a sphere defining the "outside world". The first layer of the larger cylinder represents the bottom beryllium reflector, the second represents the tungsten gamma-ray shield, and the third represents the LiH neutron shield. The axes correspond to the input file for first set of geometries. The origin is at the center of the sphere. This coordinate system is not consistent with the coordinate system adopted for the vehicle but the MCNP source definition is simplified in this case.

space, the astronauts are the only population. The beryllium (Be) layer is 9.34 cm thick. The next layer is in tungsten (W) and its thickness is variable. The following layer of natural lithium hydride (LiH) has also a variable thickness. The tungsten layer serves as a gamma-ray shield. Materials with high atomic number (high Z) and a high density are the shielding materials of choice in applications of gamma-ray attenuation. For tungsten, its atomic number is 74 and its density is equal to 19.3 g cm^{-3}. The lithium hydride layer is a neutron shield. Optimal neutron shielding materials have a high hydrogen content or otherwise a low atomic number (low Z). Hydrogen constitutes 50% of the atomic density of the natural lithium hydride; the remainder constituents include 3.75% lithium-6 and 46.25% lithium-7. Lithium-6 has a high thermal neutron capture cross section.

The first geometry set origin is at the center of the disk located between the reactor and the liquid lithium coolant. The X and Z axes are shown in Fig. 4.3, the Y axis is directed toward the back of the figure. The second geometry set origin has the same X and Z coordinates as the origin in Fig. 4.4 but the Y coordinate of Fig. 4.4 origin is 750. The origin of the second geometry set is on the rotation axis of the NEP vehicle (axis Y in the model referential system) and in the same plane as the centers of the reactors and the argon spheres. The Y axis is directed from the ion thrusters toward the crew compartment.

The crew compartment is modeled as a complex of six cylinders (Fig. 4.4). Three long cylinders form a triangle and the three smaller cylinders form the vertexes of this triangle. The vertex cylinder axes are orthogonal to the long cylinder axes. The larger cylinders are 12 m long (outer dimension), with a 200 cm radius. Their axes are in the (X, Z) plan of the model used for the MCNP input file. The small cylinders are 400 cm high and 200 cm in radius. Their axes are parallel to the Y axis in the model All the cylindrical shells are in aluminum and they have the same thickness of 3.7 cm. This thickness was determined from the literature review on GCR shielding when the shielding material is aluminum and corresponds to an annual dose equivalent to bone marrow of approximately 0.35 Sv. In the model, the inside of the inner cylinders is void (zero density).

The ECCV is located in the center of the crew compartment triangle. Figure 4.5 gives a view in the (X, Y) plane cutting the ECCV in the middle. The ECCV is represented as an aluminum solid cone. The apex of the cone is at a height of 7.0 m (Y
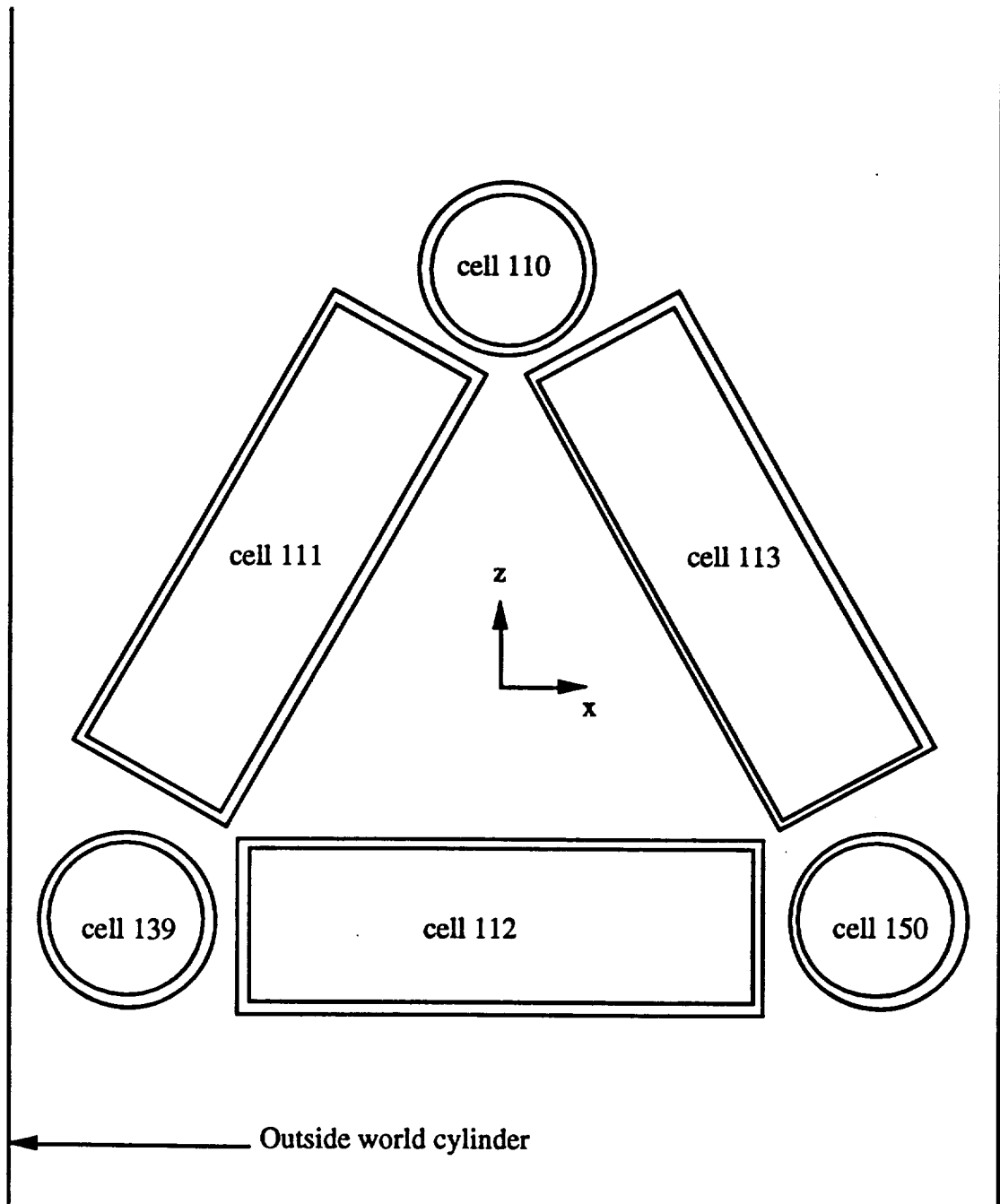
Figure 4.4 Crew compartment. Section in plane (X, Z) at Y= 750 cm.

axis) in the model coordinate system and its base at a height of 13.5 m. The cone axis corresponds to the Y axis and the cone angle is 30 degrees.

The argon tanks are located below the crew compartment and their centers are in the same (X, Z) plane as the reactors' centers (Figs. 4.5 and 4.6). The six argon tanks are modeled as six spheres. Each sphere has an aluminum shell and is filled with liquid argon (Fig. 4.7). Each spherical shell has a 200.32 cm outer radius and is 10.32 cm thick.

The ion thrusters are located in-between two (X, Z) planes below the origin. These units are represented as three solid titanium rectangles 100 cm in width, 550 cm in length, and 50 cm thick (Fig. 4.8). This model greatly simplifies the description of the ion thrusters. In reality, the ion thrusters are a very complex assembly of electronics components enclosed in a titanium box. Nevertheless, this simplification should not influence the results because the ion thrusters have been incorporated in the model so that the particles scattering from them toward the crew compartment would not be neglected. In that case the outside material and the shape of the ion thrusters constitute the essential structural data.

All the structures of the second geometry set are surrounded by a large cylinder defining the "outside world". This cylinder also contains the reactor point source located 120 m away from the crew compartment (Fig. 4.9).

The materials which have been described in this chapter are summarized in Tables 4.1 and 4.2. Table 4.1 describes the materials included in the neutron runs. Because neutrons undergo atomic interactions, the isotopic composition of the materials needs to be specified for neutron runs. Table 4.2 describes the materials included in the photon runs. The tables give for each material listed: the spacecraft structure which includes the material, the material density, and its elemental composition as described in the code. The neutron and photon MCNP runs do not require the same material information.

The neutron source in this problem is a surface source located at the bottom of the reactor adjacent to the lower layer of liquid lithium. The neutron fluxes are given for 11 energy groups and their values are shown in Table 4.3. The neutron energies range from 1.39×10^{-4} eV to 2.23 MeV. The total neutron flux is 7.721×10^{14} neutrons cm^{-2} s^{-1}.
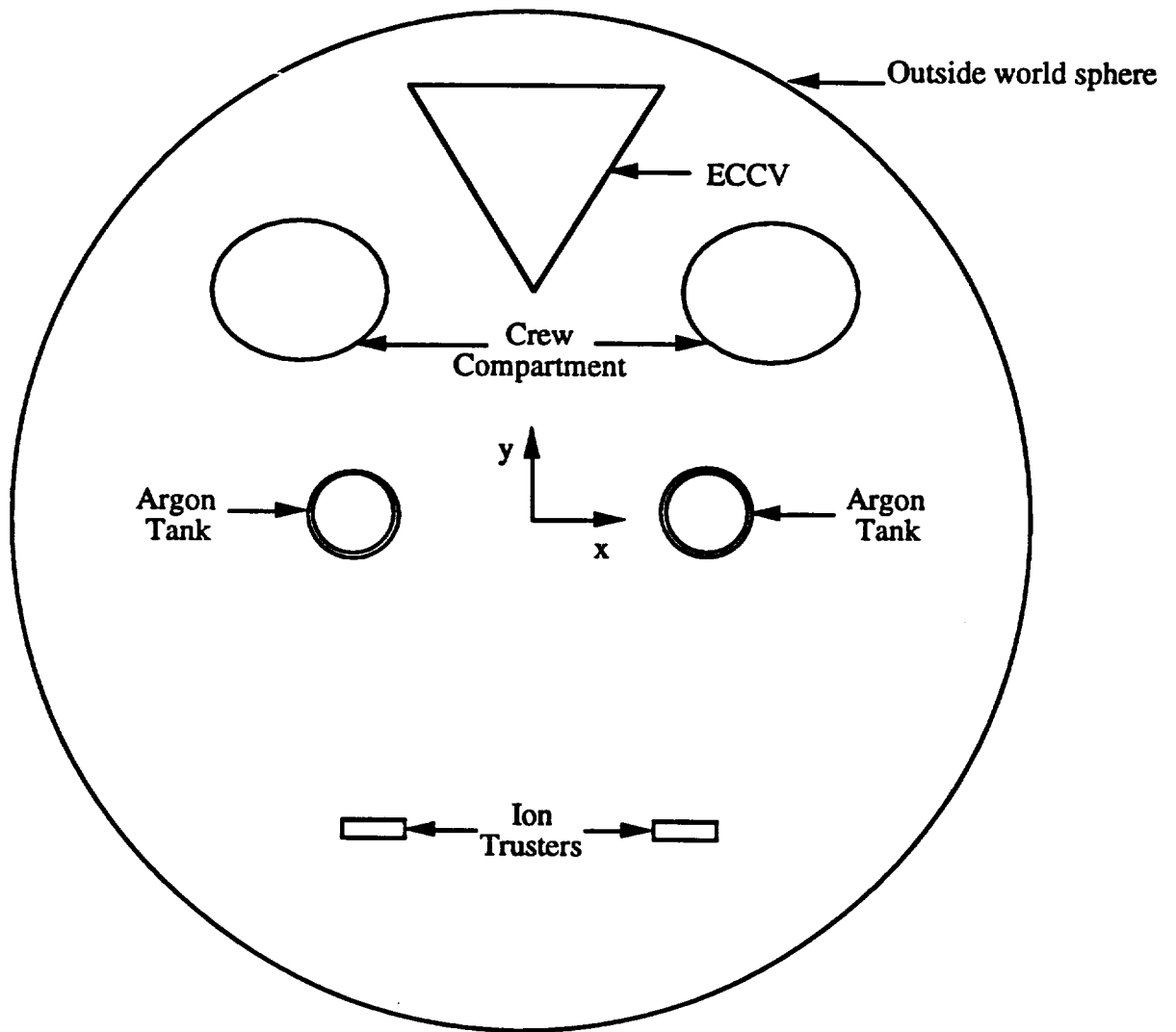
Figure 4.5 ECCV, crew compartment, argon tanks, ion thrusters (from top to bottom). All the structures are inside the outside world cylinder. Section in plane (X, Y) passing through the origin.
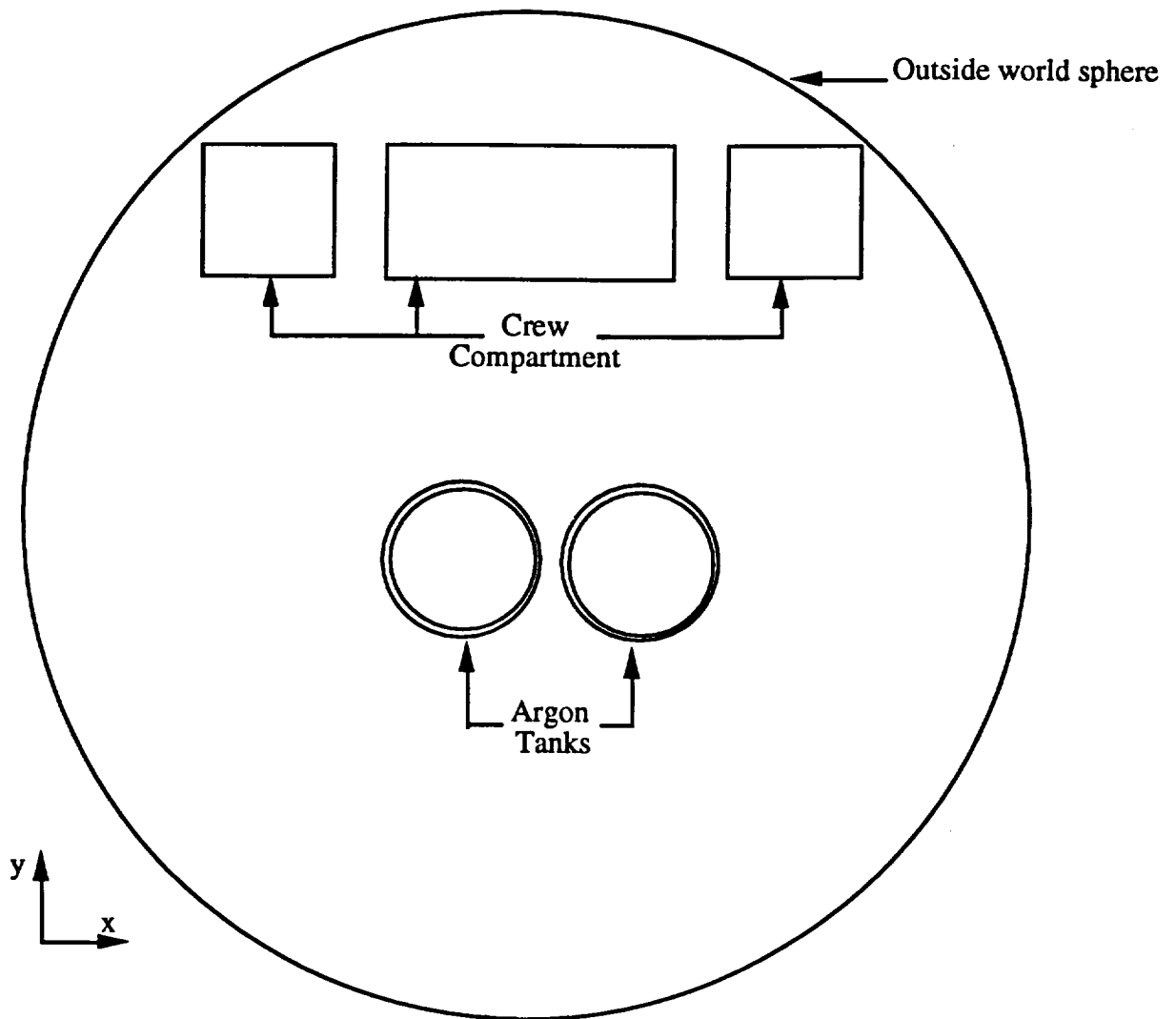
Figure 4.6 Crew compartment and argon tanks inside the outside world cylinder. Section in plane (X, Y) at Z = - 600 cm.
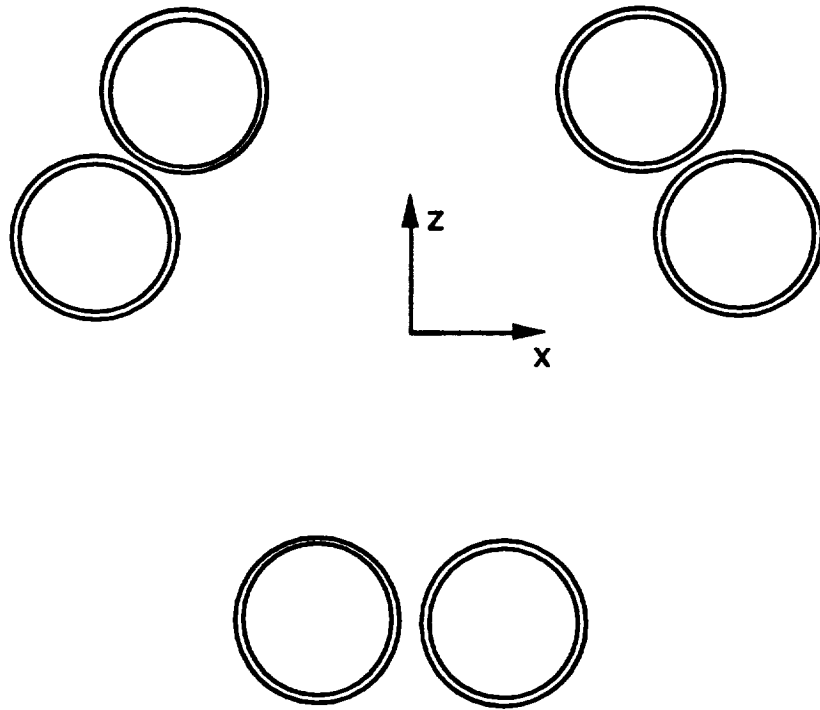
Figure 4.7 Argon tanks. Section in plane (X, Z) at Y = 0.
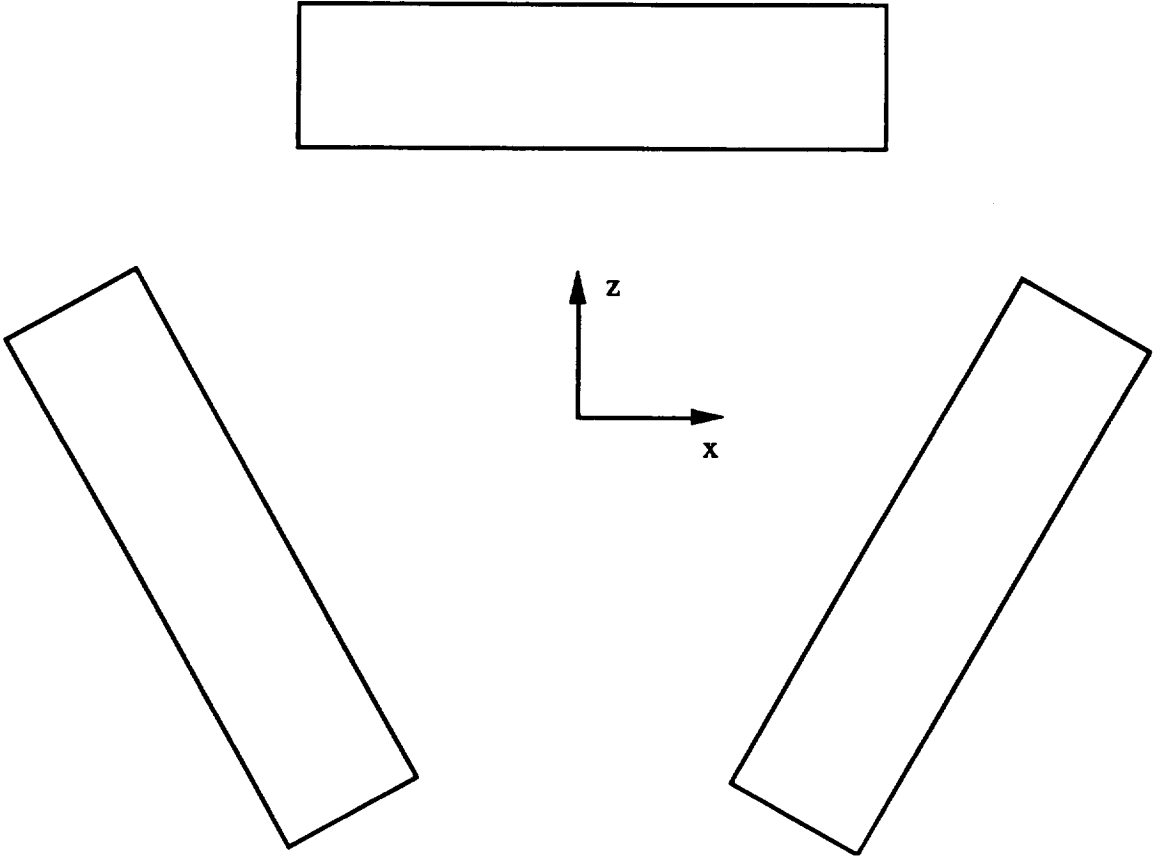
Figure 4.8 Ion thrusters. Section in plane (X, Z) at Y = -775 cm.
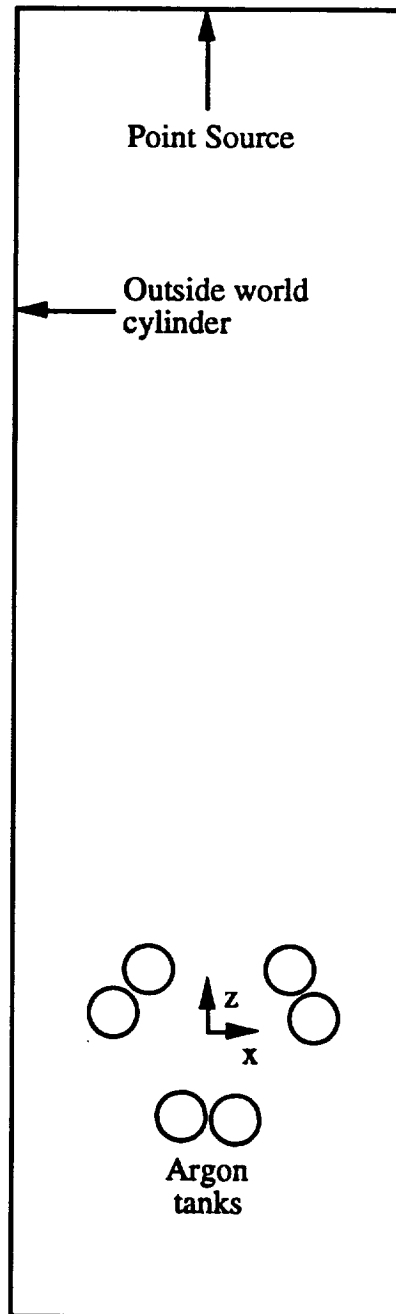
Figure 4.9 Outside world cylinder and argon tanks. Section in plane (X, Z) at Y = 0. The source particles start in the center of disk represented by the segment on top of the figure.

Table 4.1 Description of the materials included in the neutron runs. The table gives for each material listed: the spacecraft structure composed of the material, the material density, and its elemental composition as described in the code.

Spacecraft structure	Material	Density (g cm^{-3})	Isotopic Composition
Neutron Shield	Natural Lithium Hydride	0.775	Li-6 : 3.75%; Li-7 :46.25% H-1 : 50%
Photon Shield	Tungsten	19.3	Natural W
Neutron Shield Reflector	Beryllium	1.85	B x 10-9
Coolant	Liquid Lithium	0.479	Li-6 :7.5%; Li-7 : 92.5%
Crew Compartment, Argon Tank, ECCV	Aluminum	2.7	Al-27
Ion thruster	Titanium	4.5	Natural Ti
Inside Tank	Liquid Argon	1.4	Natural Ar

Table 4.2 Description of the materials included in the photon runs. The table gives for each material listed: the spacecraft structure composed of the material, the material density, and its elemental composition as described in the code.

Spacecraft structure	Material	Density (g cm^{-3})	Isotopic Composition
Neutron Shield	Natural Lithium Hydride	0.775	Natural LiH
Photon Shield	Tungsten	19.3	Natural W
Neutron Shield Reflector	Beryllium	1.85	Natural Be
Coolant	Liquid Lithium	0.479	Natural Li
Crew Compartment, Argon Tank, ECCV	Aluminum	2.7	Natural Al
Ion thruster	Titanium	4.5	Natural Ti
Inside Tank	Liquid Argon	1.4	Natural Ar

The initial source varies radially following a Bessel function distribution, but with the distance between the crew compartment and the reactor being approximately 120 m, the transport was simplified by assuming that the neutron source is uniformly distributed over the bottom surface of the reactor. This assumption greatly simplified the description of the source term in MCNP and thus general source descriptions in the code could be utilized. The MCNP general source can use source distribution functions, which are specified on various cards.

The photon source for the operating reactor is a surface source located at the bottom of the reactor just prior to the liquid lithium layer. Photon fluxes are uniformly distributed on the disk area and are given in four energy groups as shown in Table 4.4. The photon energy varies from 10 keV to 30 MeV.

The shield run results are given as surface fluxes for determined energy groups at the bottom of the shield complex. In MCNP, these results correspond to an F2-type tally. The particle flux is given for various energy groups. The energy groups were selected to match the energy groups of the dose conversion factors given in ICRP Publication 51. The energy groups for photons and neutrons are given in Table 4.5 with the corresponding dose conversion factors.

The crew compartment run results are cell fluxes within each crew compartment. As it has been explained in the first part of this chapter, one or more surfaces define a cell. These results correspond to an F4 type MCNP tally. The flux unit is given in particles per cm^2. With the source unit being particles per second, the results are thus expressed in particles s^{-1} cm^{-2}.

The error corresponding to the flux results for each energy group is printed in the output file. The interpretation of MCNP error R is listed in Table 4.6. R is the relative error, defined as the ratio of the estimated standard deviation of the mean to the mean value. It represents the estimated statistical error at the 1s level. An example of the tally results and errors as presented in MCNP output files is presented in Appendix C.

Table 4.3 Distribution of the source neutron energies and fluxes. The source neutrons are exiting the bottom surface of a 25 MW$_{th}$ SP-100 class reactor operating at full power at beginning-of-life.

Energy (MeV)	Neutron Flux (cm^{-2} s^{-1})
0.00	0.000
1.39×10^{-10}	5.136×10^{12}
4.14×10^{-7}	2.798×10^{13}
1.67×10^{-4}	6.677×10^{13}
5.53×10^{-3}	1.350×10^{14}
4.09×10^{-2}	1.202×10^{14}
1.11×10^{-1}	1.605×10^{14}
3.02×10^{-1}	6.979×10^{13}
4.98×10^{-1}	7.668×10^{13}
8.21×10^{-1}	4.665×10^{13}
1.35	3.413×10^{13}
2.23	2.931×10^{13}

Table 4.4 Distribution of the source photon energies and fluxes. The source photons are exiting the bottom surface of a 25 MW$_{th}$ SP-100 class reactor operating at full power at beginning-of-life.

Energy (MeV)	Photon Flux (cm^{-2} s^{-1})
0.00	0.000
0.01	0.000
0.30	1.223 X 10^{13}
0.75	2.165 X 10^{13}
2.50	2.172 X 10^{13}
30.00	8.537 X 10^{12}

Table 4.5 Tally energies and corresponding dose conversion factors (DCF) for neutrons and photons.

Neutron Energy (MeV)	Neutron DCF (Sv cm^2)	Photon Energy (MeV)	Photon DCF (Sv cm^2)
		0.010	0.00
0.005	3.12×10^{-12}	0.015	0.00
		0.025	1.05×10^{-27}
		0.050	4.74×10^{-26}
		0.060	1.67×10^{-25}
0.252	1.67×10^{-11}	0.070	3.07×10^{-25}
		0.080	4.70×10^{-25}
		0.100	1.19×10^{-24}
		0.150	3.82×10^{-24}
1.000	6.87×10^{-11}	0.200	3.94×10^{-24}
		0.300	8.54×10^{-24}
		0.500	1.32×10^{-23}
		1.000	4.58×10^{-23}
4.500	2.10×10^{-10}	3.000	1.76×10^{-22}
		6.000	4.21×10^{-23}
		10.000	4.53×10^{-23}

Table 4.6 Interpretation of the relative error R accompanying the tally data in the output file of any MCNP run. R represents the estimated statistical error at the 1s level.

| Range of Error	Quality of the tally
0.5 to 1	"Garbage"
0.2 to 0.5	Factor of a few
0.1 to 0.2	Questionable
< 0.1	Generally reliable

CHAPTER V

ESTIMATES OF NEUTRON AND PHOTON DOSE RATES

INTRODUCTION

This chapter presents calculated results as dose rates inside the crew compartment from the tallies of the MCNP output files. MCNP final results are fluxes within the six crew compartments of the NEP vehicle over a range of particle energies. These fluxes are then multiplied by the ICRP Publication 51 dose conversion factors and summed over all energy groups to give estimates of the total dose rate. Total dose rates are expressed in terms of annual doses to enable comparisons with the 0.05 Sv y^{-1} limit for man-made sources. Fig. 5.1 gives a flow chart of the various steps followed to convert MCNP tallies into meaningful dosimetric results.

MCNP tallies are normalized per starting particle. The simplest Monte Carlo model for particle transport problems uses the natural probabilities with which various events occur (for example, collision, fission, capture, etc.). Particles are followed from event to event by the computer, and the next event is always sampled (using the random number generator) from a number of possible events according to events probabilities. This process is called the analog Monte Carlo model because it is directly analogous to the naturally occurring particle transport.

The analog Monte Carlo model works well when a significant fraction of the particles contributes to the estimate of interest in a manner comparable to detecting a significant fraction of the particles in the physical situation. There are many cases for which the fraction of particles detected is very small (less than 10^{-6}). For these problems analog Monte Carlo fails because few, if any, of the particles are tallied, and the statistical uncertainty in the answer is unacceptable.

Although the analog Monte Carlo model is probably the simplest conceptual probability model, there are other probability models for particle transport that will estimate the same average value as the analog Monte Carlo models. They are useful because although the average value remains unchanged, the variance (uncertainty) of the
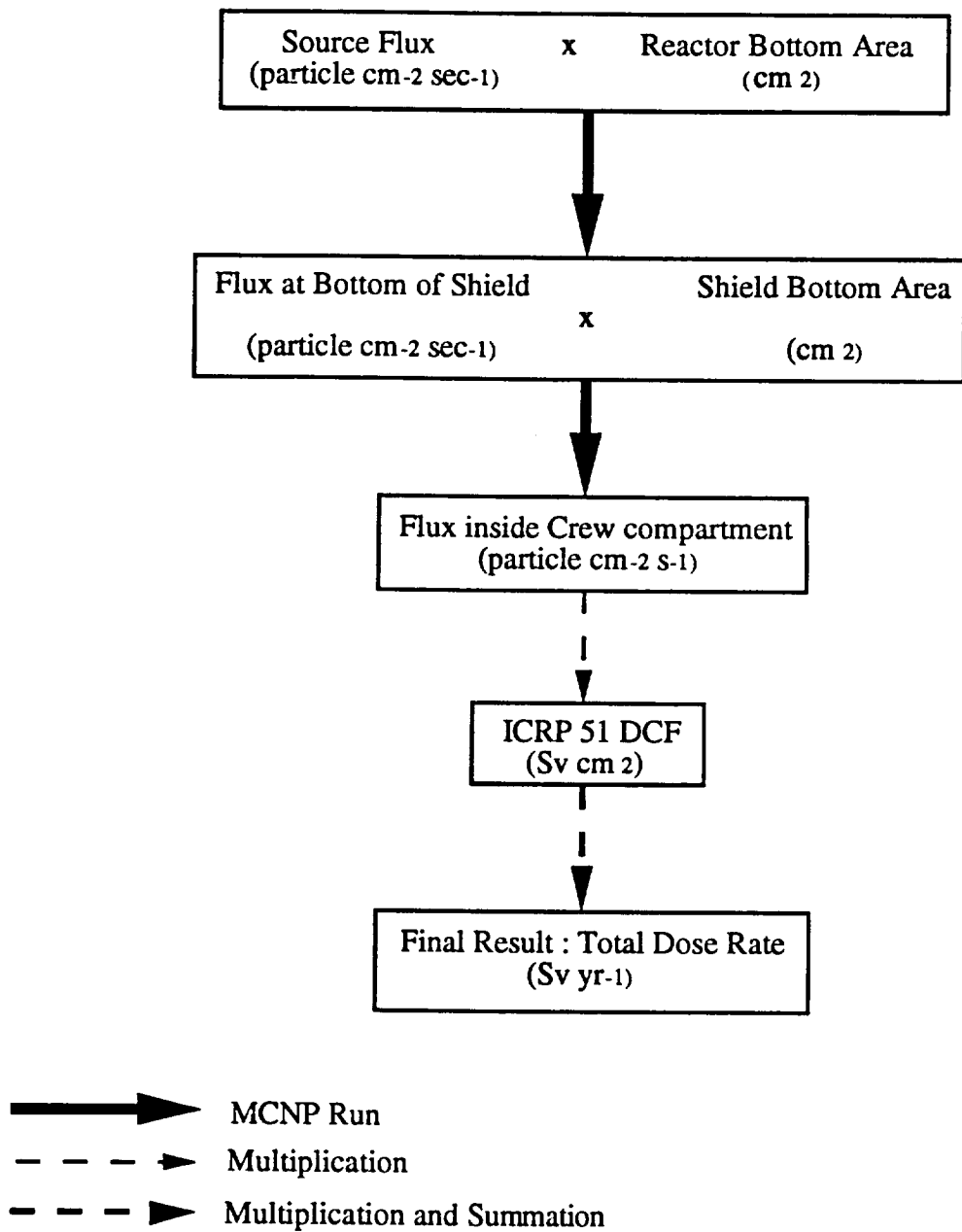
Figure 5.1 Description of the steps in the data treatment to obtain dose rates inside the various crew compartments of the NEP vehicle.

estimate can often be made much smaller than the variance for the analog estimate. Practically, this means that problems which would be impossible to solve in days of computer time can be solved in minutes of computer time.

A non-analog Monte Carlo model attempts to follow "interesting" particles more often than "uninteresting" ones. An "interesting" particle is one which contributes more substantially to the quantity (or quantities) to be estimated. There are several non-analog techniques, and they are all meant to increase the odds that a given particle contributes to the final result. To ensure that the average score is the same in the non-analog run as in the analog run, the score is modified to remove the effect of biasing the natural odds. Thus, if a particle is artificially made X times as likely to execute a given random walk, then the particle's score is weighted by 1/X. The average score is thus preserved because the average score is the sum, over all random walks, of the probability of a given walk multiplied by its resulting score.

A non-analog Monte Carlo technique will have the same expected tallies as an analog technique if the expected weight executing any given random walk is preserved. For example, a particle can be split into two identical pieces and the tallies of each piece are weighted by half of what the tallies would have been without the split. Such non-analog, or variance reduction, techniques can often decrease the relative error by sampling naturally rare events with an unnaturally high frequency and weighting the tallies appropriately.

In deep penetration problems such as particle transport through a thick shield, the particle fluxes are expected to drastically decrease as the shield thickness increases. The problem analyzed in this research is a typical example where variance reduction methods are required. For the shield runs, the variance reduction method was indicated in the importance cards of each cell. The importance of a cell is used for geometry splitting and Russian roulette to help the particles move to the more important regions of the geometry, or, if the importance is zero (such as in the "outside world"), to terminate the particle's history.

For the crew compartment runs, the source was directed toward the crew compartment by emitting the particles into a cone surrounding the compartment. The results are then weighted by the ratio of the cone solid angle and the half space (2p

steradians). By biasing the source, all particles are emitted toward the interesting region, and the number of particles which contribute to a tally is maximized.

The results can be classified depending on the source particles and the particles tallied. Three cases are differentiated in this thesis: (a) the neutron dose, (b) the photon dose from reactor photon sources, and (c) the photon dose from photons created by the neutron interactions with the shield materials. This chapter presents the variations of the dose rate inside the crew compartment as a function of the LiH layer thickness and for W layer thicknesses: 10, 20, and 30 cm. Under the assumption that all three reactors of the NEP vehicle are operating simultaneously, the annual dose limit per reactor would be (0.05/3 Sv) or 0.0166 Sv per year per reactor. This value is indicated as a horizontal line on each figure. Each graph gives five additional curves showing variations in dose rate with location inside the six crew compartments. For this vehicle design it is obvious that the higher dose rates occur inside the smaller cylinder positioned closest to the reactor in question.

NEUTRON RESULTS

Figures 5.2 through 5.4 show the calculated values of the variations of the neutron dose rates inside the crew compartment for the three W layers previously mentioned, each as a function of the LiH thickness. From Fig. 5.2, the minimum LiH thickness required to lower the neutron dose below 0.0166 Sv y^{-1} is 50 cm, if the W layer is 10 cm thick. The 50 cm of LiH will only lower that component of the dose rate which is due to the neutron source term. It should be kept in mind that there is always a photon source term and that the final design will have to consider the total dose rate from both contributions. The lower-weight solid line (cell union) indicates the crew dose rate per operating reactor averaged over all six crew compartments. Error bars are not plotted on any of the graphs as they are too small to be visible relative to the graph scales. The calculational percent errors on the dose rates were on the order of maximum 5% for all cases simulated.

Fig. 5.3 shows the neutron dose rate variations inside the crew compartments for a 20-cm thick W layer as a function of the LiH layer thickness. This plot defines an approximately 40 cm minimal thickness necessary to lower the neutron dose below the 0.0166 Sv y^{-1} limit when the tungsten layer is 20 cm thick. This minimal LiH thickness
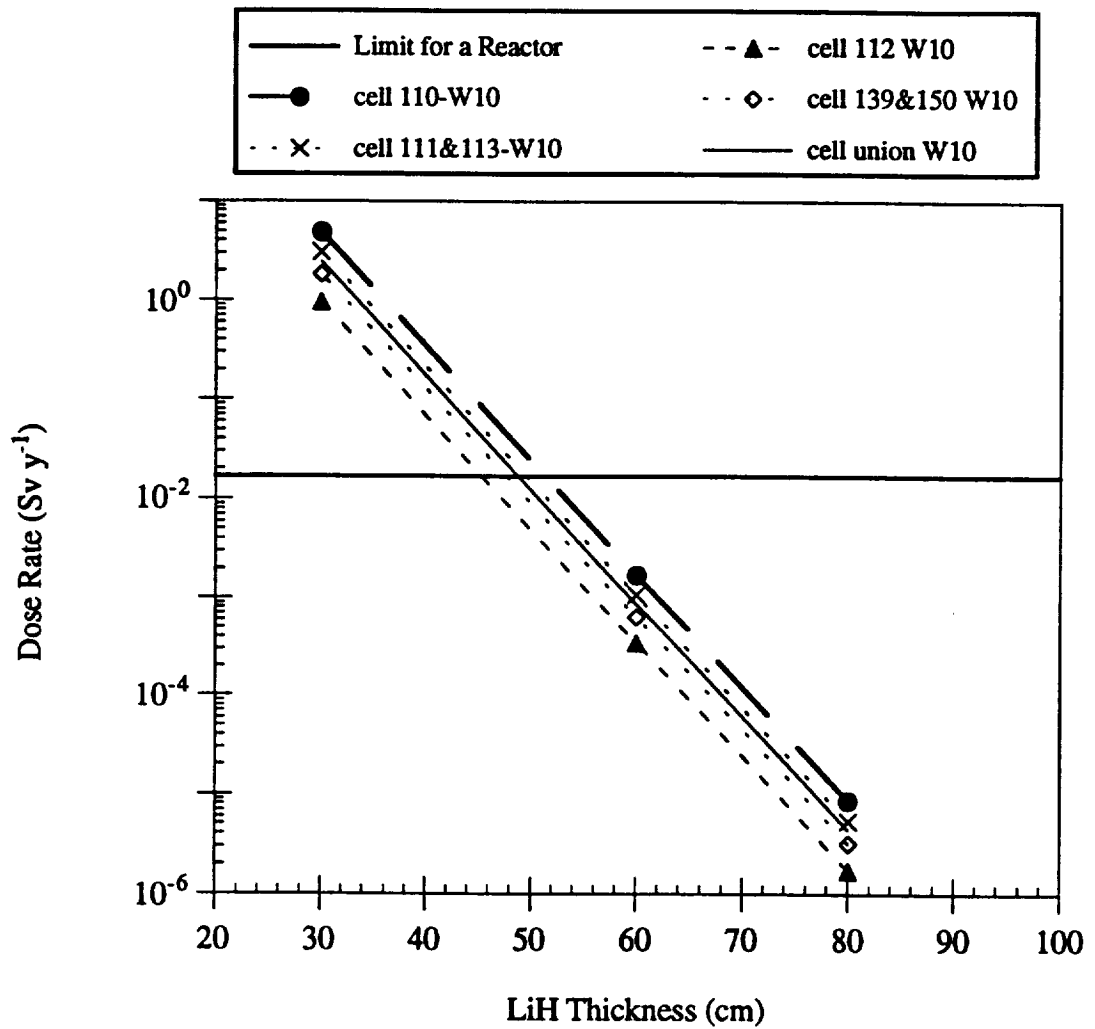
Figure 5.2 Neutron dose rates inside the six crew compartments due to the neutron source of one SP-100 reactor with a 10-cm thick tungsten layer and a variable lithium hydride thickness.
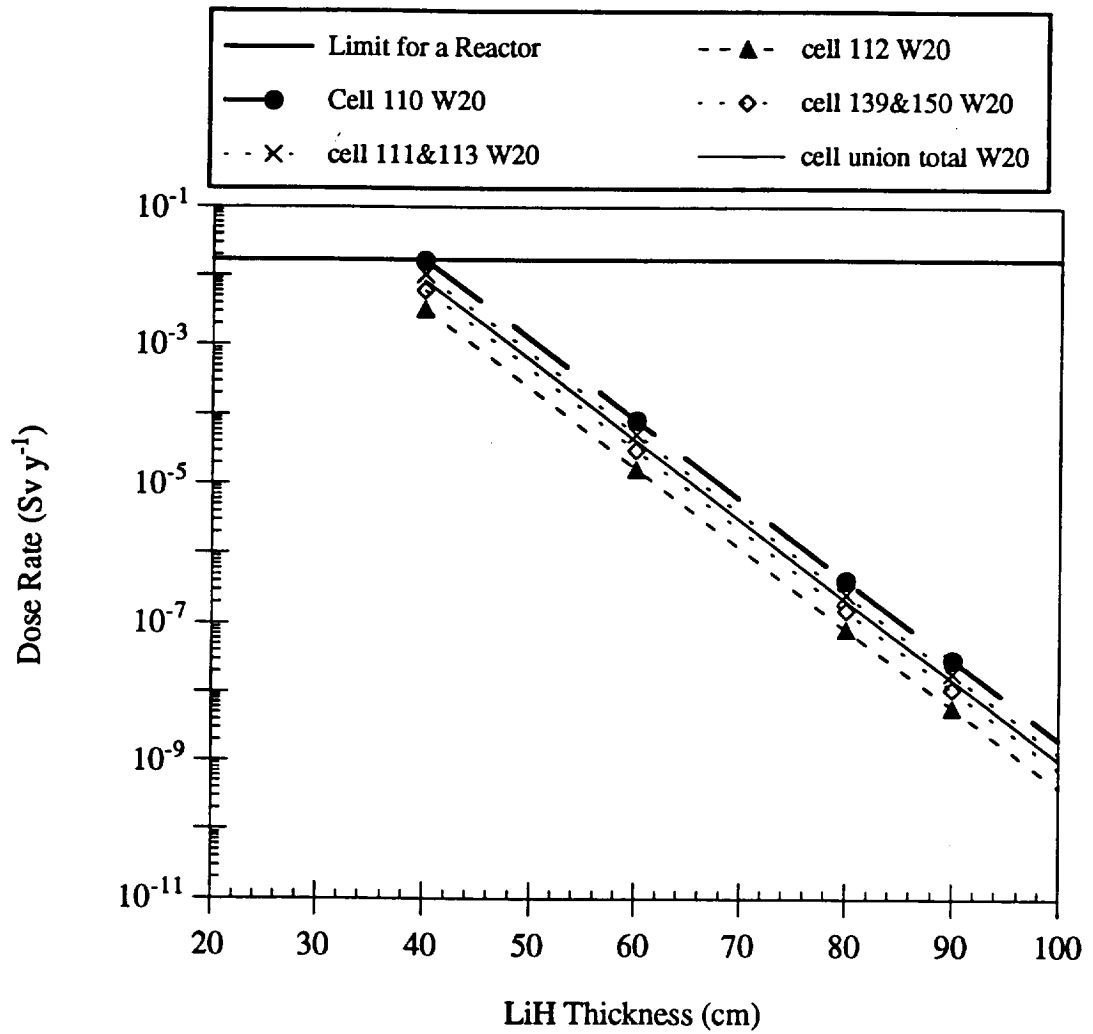
Figure 5.3 Neutron dose rates inside the six crew compartments due to the neutron source of one SP-100 reactor with a 20-cm thick tungsten layer and a variable lithium hydride thickness.
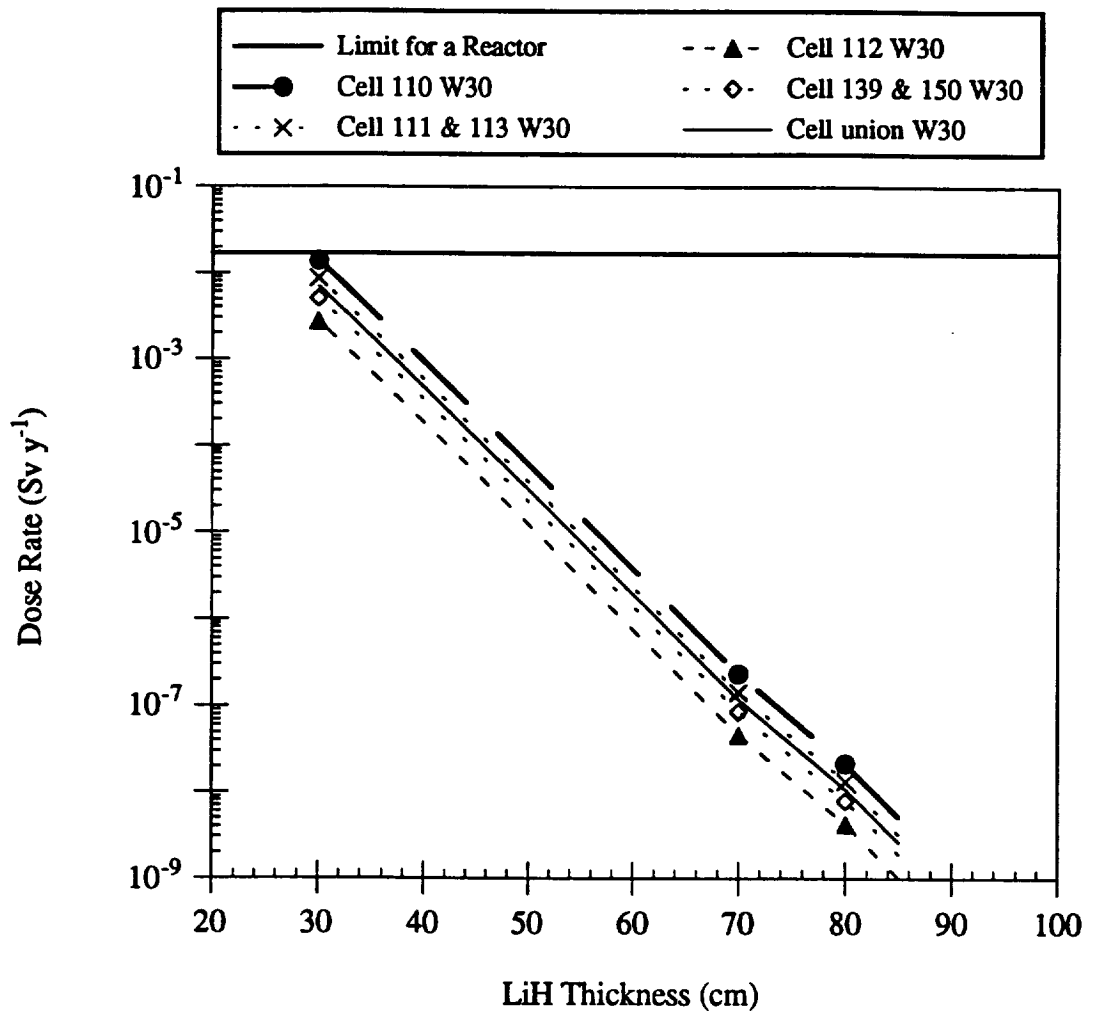
Figure 5.4 Neutron dose rates inside the six crew compartments due to the neutron source of one SP-100 reactor with a 30-cm thick tungsten layer and a variable lithium hydride thickness.

is lower than the 50 cm LiH necessary in the case of a 10-cm W shield. It is interesting to note that, even if the tungsten is included in the design as a photon shield, the neutrons interact with the tungsten. The neutrons undergo elastic scattering within the tungsten, over their energy range. Moreover, thermalized neutrons undergo (n, g) reactions in tungsten, while fast neutrons undergo inelastic scattering.

Fig. 5.4 shows the neutron dose rate variations inside the crew compartment for a 30-cm thick W layer as a function of the LiH layer thickness. This plot defines a 30 cm minimal thickness to lower the neutron dose below the annual limit when the tungsten layer is 30 cm. Once again, this minimal LiH thickness is lower than the 50 cm of LiH necessary in the case of a 10-cm W shield. The neutron dose rate decreases exponentially with increasing LiH thickness. In addition, it decreases with increasing W thickness. The shield design can not be determined from the neutron dose rates exclusively; the photon dose rates have to be taken into account in the overall dose estimates.

PHOTON RESULTS

Figures 5.5 through 5.7 show the calculated values of variations of photon source term dose rates inside the various crew compartments for the three W layers previously mentioned, as a function of the LiH thickness. In Fig. 5.5, the minimum LiH thickness for a 10-cm W layer is greater than 50 cm. The results for the maximum LiH layer computed are above the limit, but to estimate the minimal thickness of LiH, the curves are extrapolated by a curve fit procedure. In Appendix D, the curve fit data are plotted. The minimal LiH thickness is found by extrapolation to be 150 cm. The photon dose rates decrease very slowly with increasing LiH thickness, compared to the corresponding neutron attenuation through the shield.

Fig. 5.6 shows the reactor photon dose rate variations inside the crew compartments for a 20-cm thick W layer as a function of the LiH layer thickness. For any LiH thickness the photon dose is below the 0.0166 Sv y^{-1} limit. The dose rates are lower by a factor of 1000 compared to the values for a 10-cm thick W layer. The variations in the photon dose rates are much more sensitive to the W layer thickness than to the LiH layer thickness.
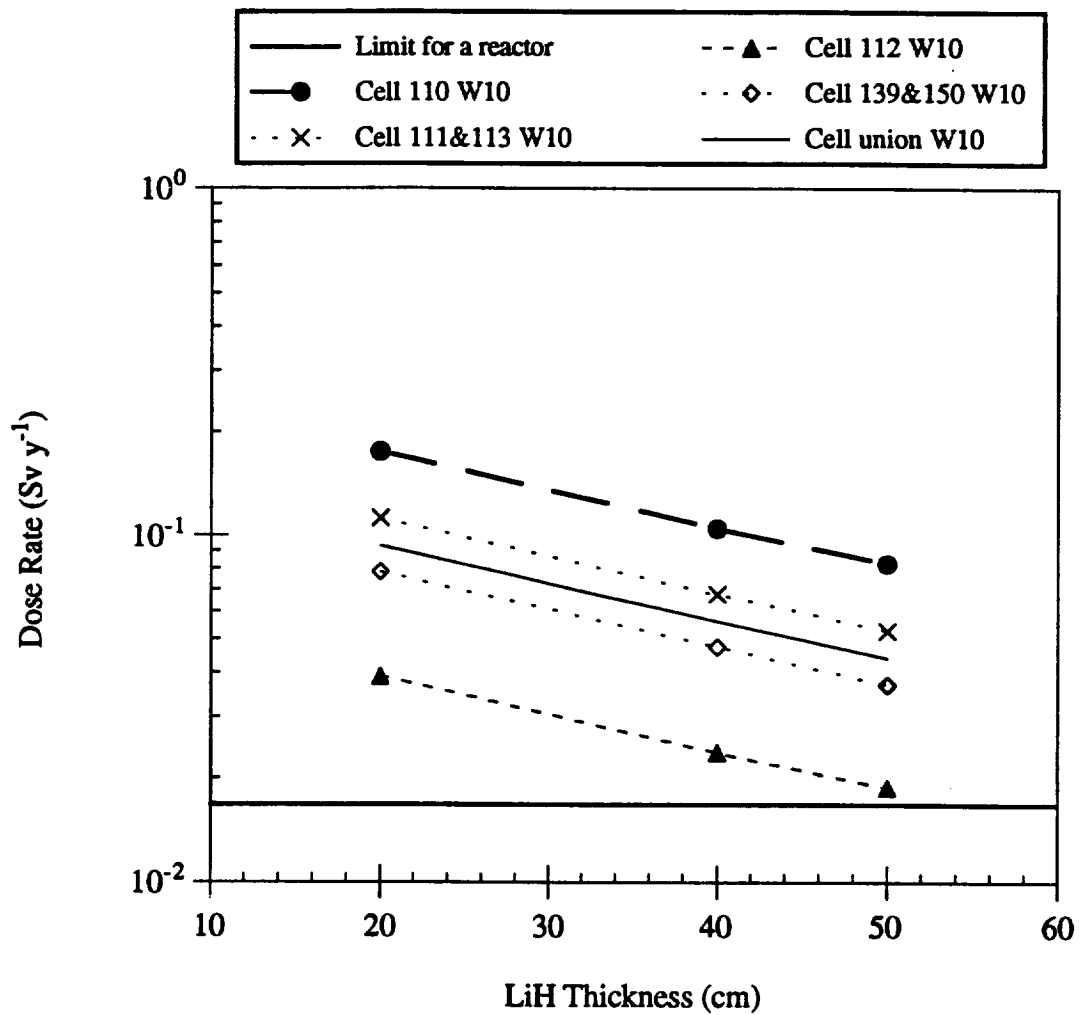
Figure 5.5 Photon dose rates inside the six crew compartments due to the photon source of one SP-100 reactor with a 10-cm thick tungsten layer and a variable lithium hydride thickness.
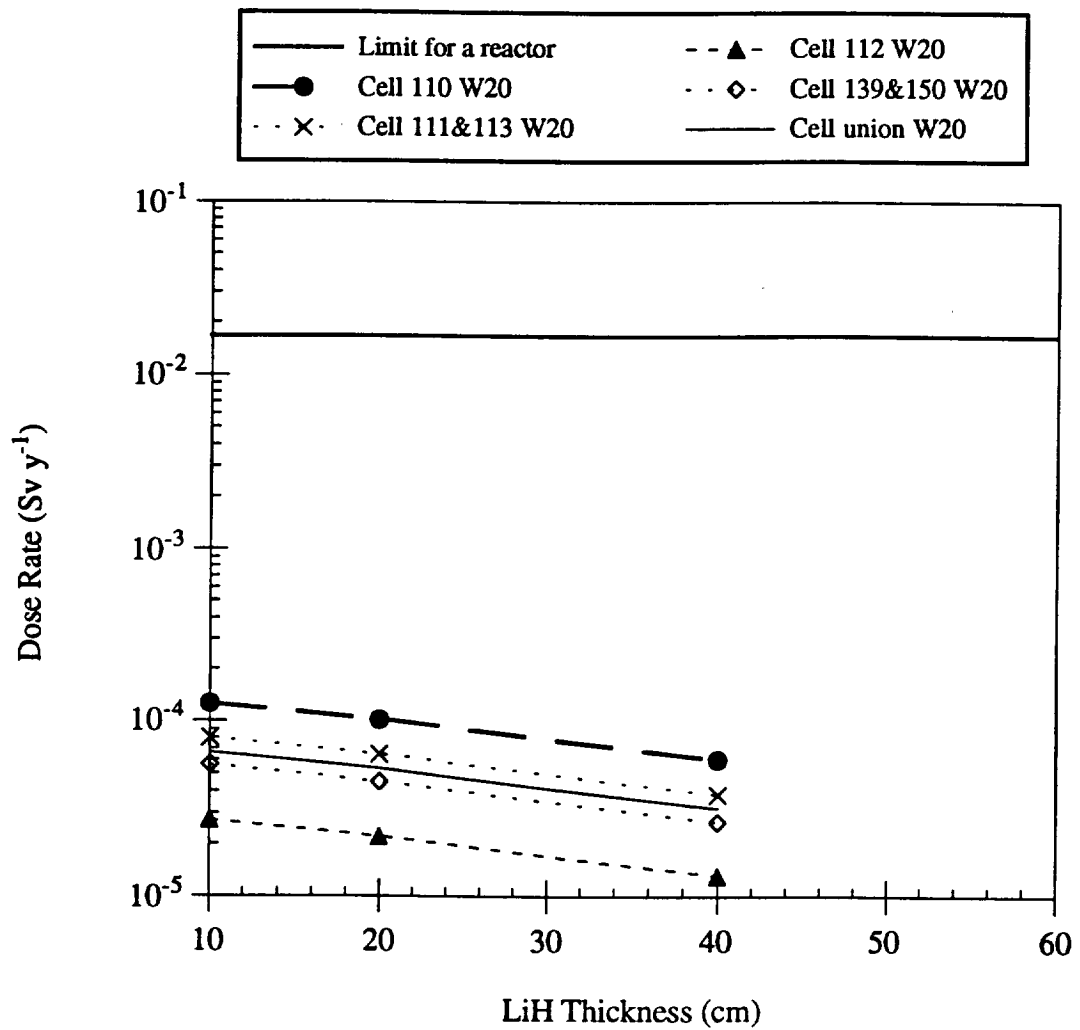
Figure 5.6 Photon dose rates inside the six crew compartments due to the photon source of one SP-100 reactor with a 20-cm thick tungsten layer and a variable lithium hydride thickness.
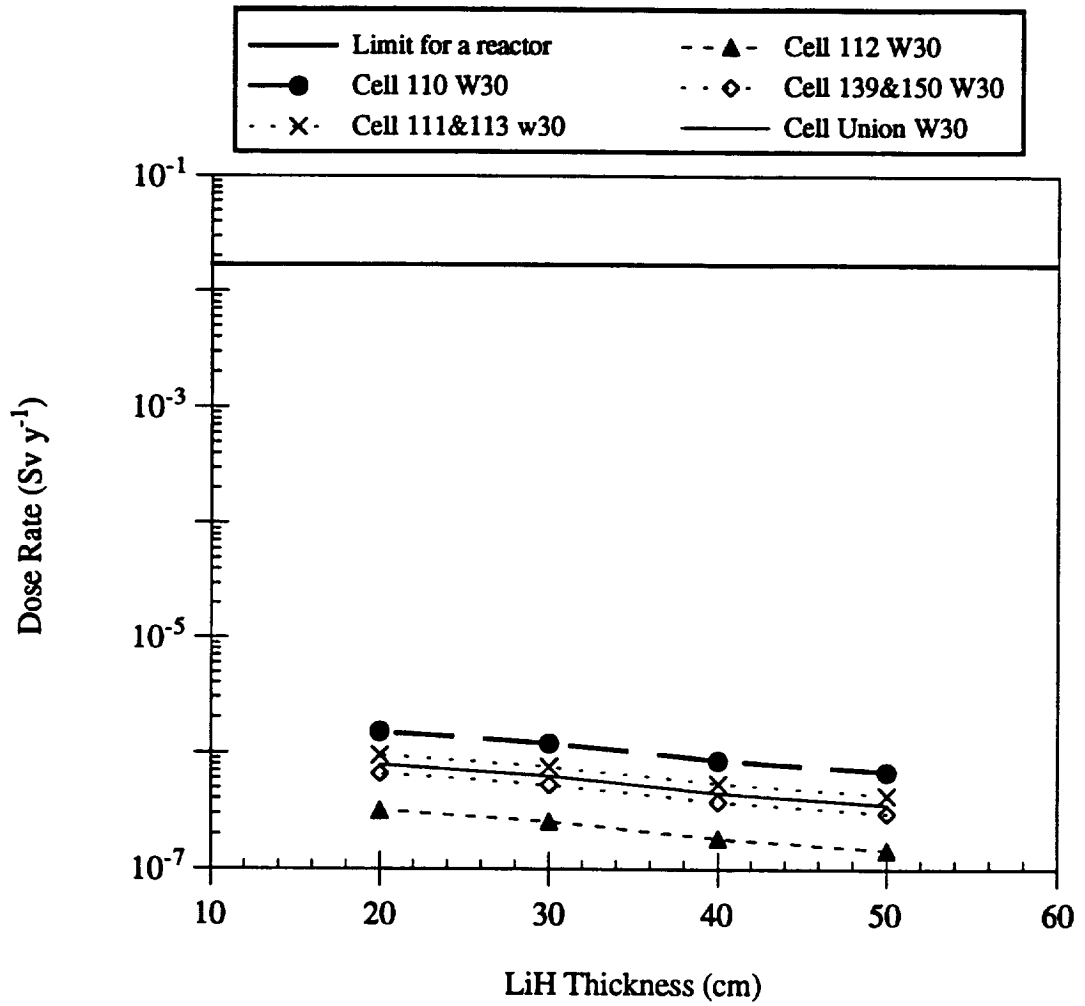
Figure 5.7 Photon dose rates inside the six crew compartments due to the photon source of one SP-100 reactor with a 30-cm thick tungsten layer and a variable lithium hydride thickness.

Fig. 5.7 shows the reactor photon dose rate variations inside the crew compartment for a 30-cm thick W layer as a function of the LiH layer thickness. There is no necessary minimal LiH thickness since the photon dose is always below the 0.0166 Sv y^{-1} limit when the tungsten layer is 30-cm thick.

These figures show the dose rates inside the crew compartment due to the photons exiting the reactor. However, neutron interactions within the shield materials generate additional photons through inelastic collisions and radiative capture reactions and thus need to be considered in a total shielding assessment.

Figures 5.8 through 5.10 show the calculated values of the variations of the neutron-generated photon dose rates inside the crew compartments for the three W layers previously mentioned, as a function of the LiH thickness. The computer run results are above the limit for the three figures and thus, to estimate the minimal thickness of LiH, a curve fitting procedure is employed. The curve fit graphs are presented in Appendix D. In Fig. 5.8, the minimum LiH thickness for a 10-cm W layer exceeds 120 cm. The dose rates inside the crew compartment for a 120-cm thick LiH layer are in the order of 12 to 100 Sv y^{-1} depending on the crew compartment location, which is about 10,000 times the yearly limit. For a number of reasons, these results are considered questionable and are believed to greatly overestimate this component of crew dose.

The overestimate of photon generation by neutron interactions is mostly due to the neutron cross sections which were available at the time this transport calculations were performed. These cross sections are not the most recent as they were published in the early 1980's. The photon production data contained in older MCNP libraries are referred to as "30 x 20 photon production" data in the MCNP manual. There is no information concerning individual photon production reactions in the 30 x 20 data. The only secondary photon data are a 30 x 20 matrix of photon energies; this means that for each of 30 incident neutron energy groups there are 20 equally probable exiting photon energies. In more recent MCNP libraries, compiled by Fisher in 1989 (Fisher 1989), the secondary photon energy distributions are a function of incident neutron energy. These revised cross sectional libraries were not implemented into MCNP until recently and thus were not available for use in the current modeling effort. In addition, the cross sections used in this work contain no information regarding secondary photon angular distributions; therefore, all photons are taken to be produced isotropically in the laboratory system.
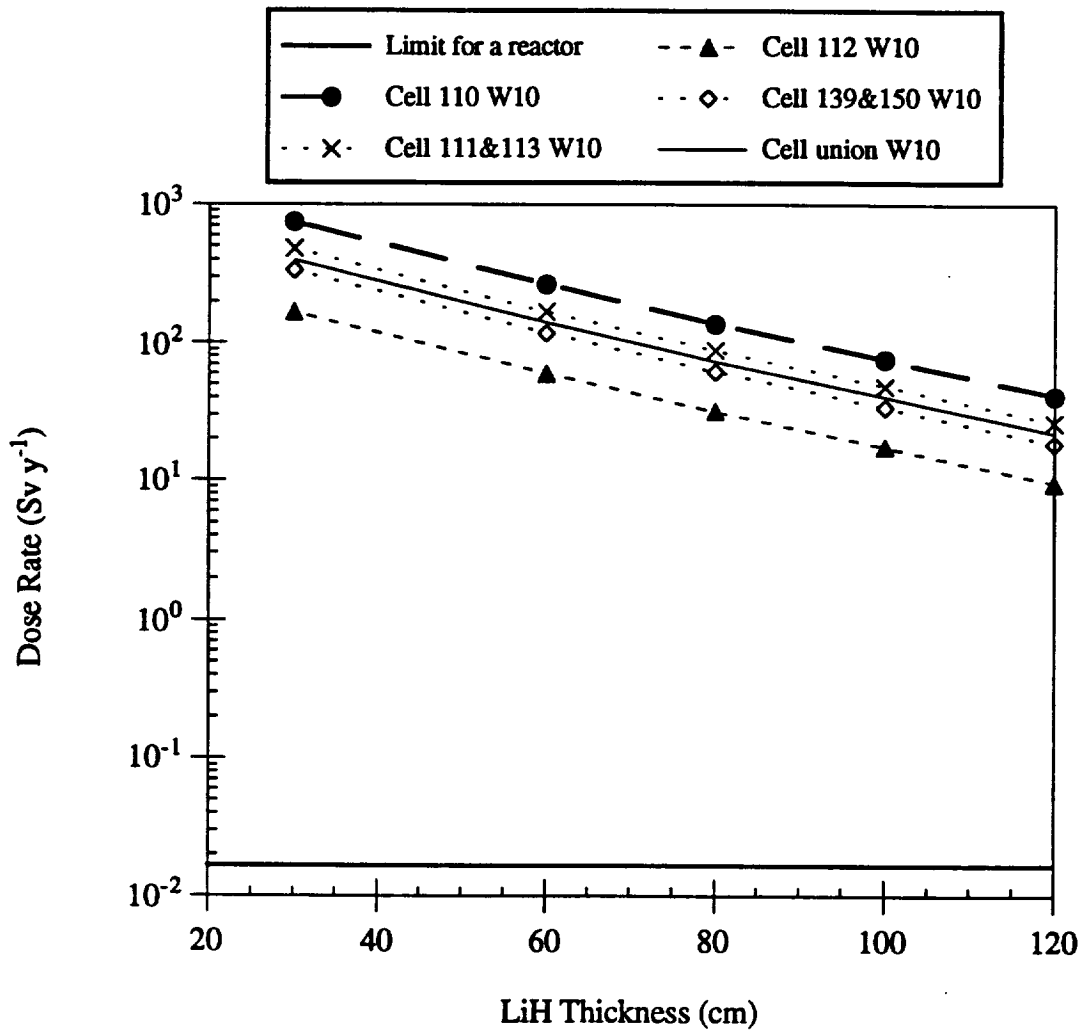
Figure 5.8 Photon dose rates inside the six crew compartments due to one SP-100 reactor neutron interactions through the shield with a 10-cm thick tungsten layer and a variable lithium hydride thickness.
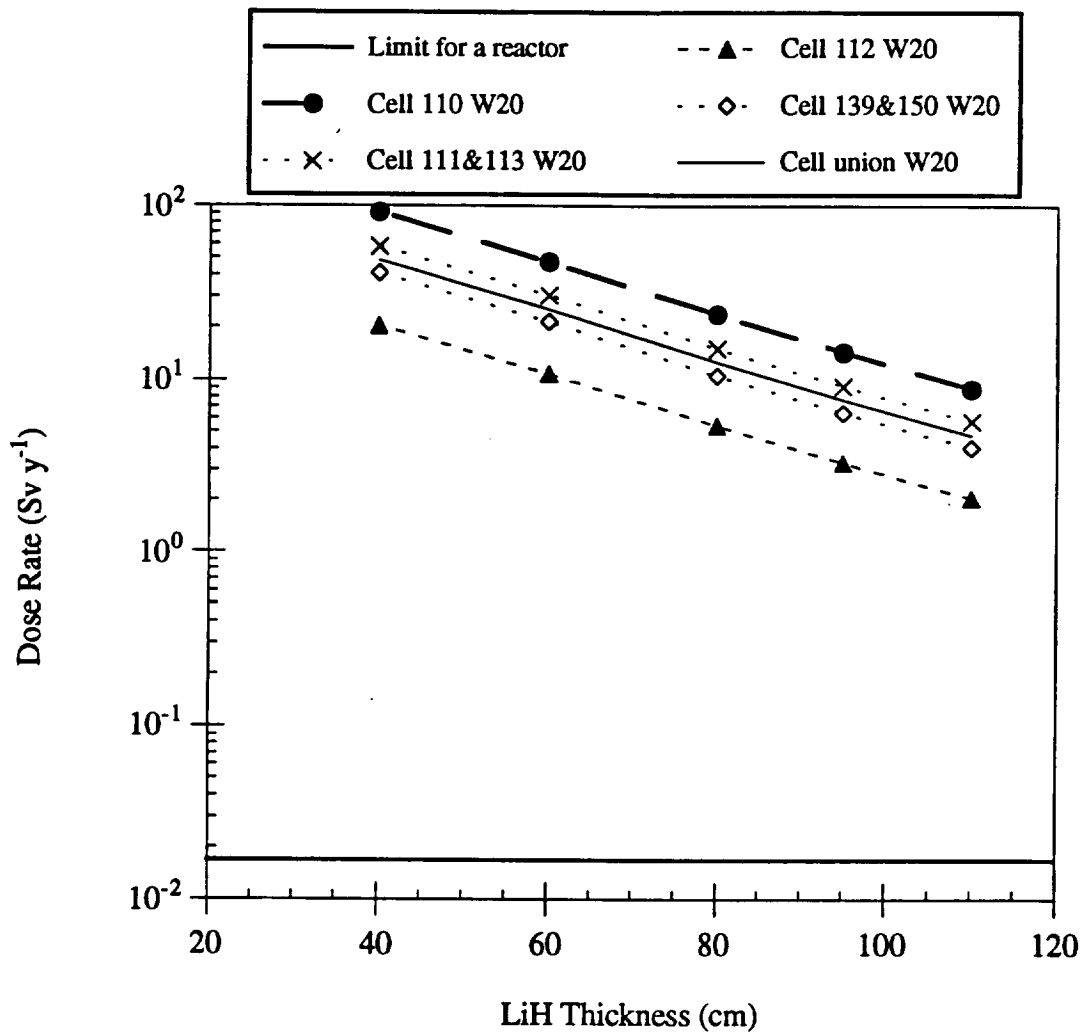
Figure 5.9 Photon dose rates inside the six crew compartments due to one SP-100 reactor neutron interactions through the shield with a 20-cm thick tungsten layer and a variable lithium hydride thickness.
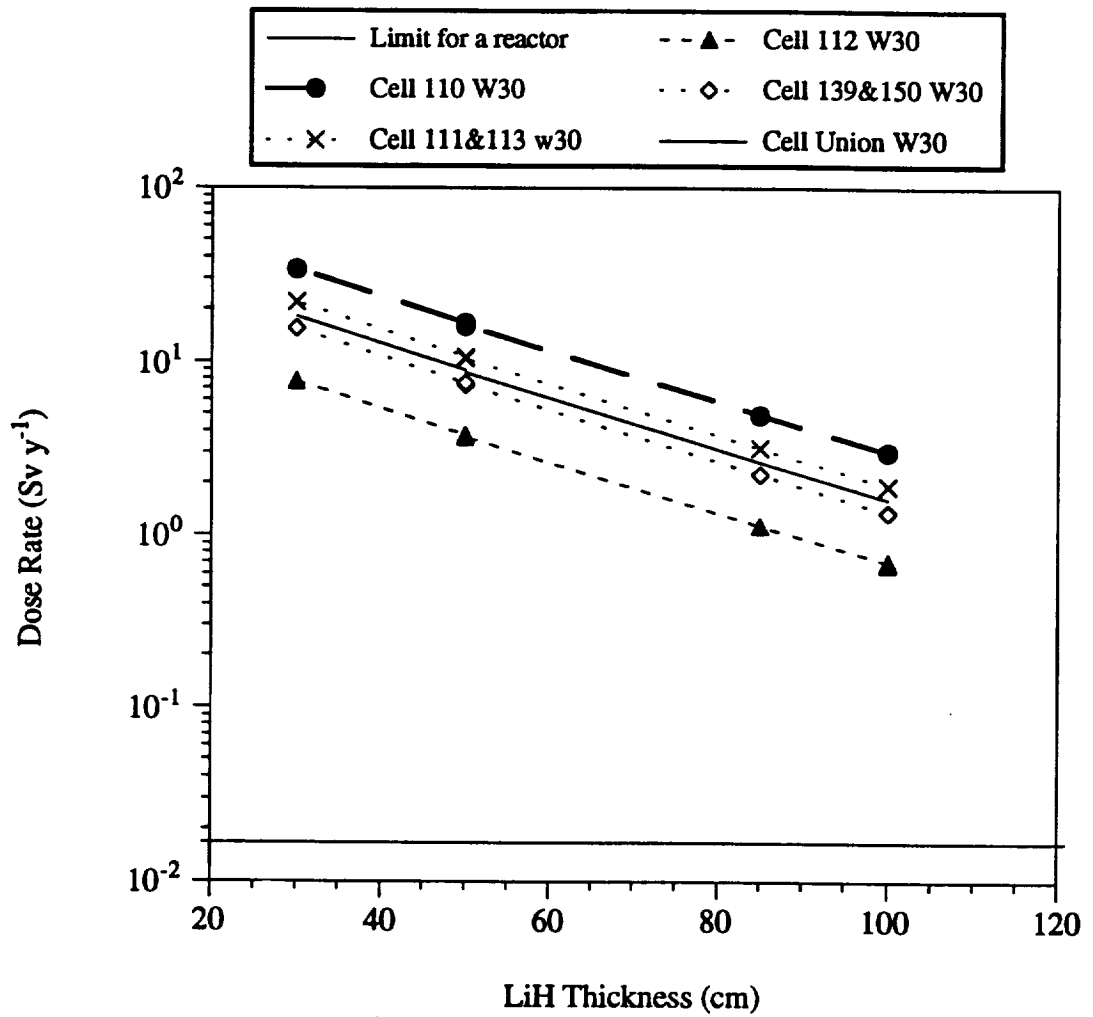
Figure 5.10 Photon dose rates inside the six crew compartments due to one SP-100 reactor neutron interactions through the shield with a 30-cm thick tungsten layer and a variable lithium hydride thickness.

There are several problems associated with 30 x 20 photon production data. The 30 x 20 matrix is an inadequate representation of the actual spectrum of photons produced. In particular, discrete photon lines are not well represented, and the high-energy tail of a photon continuum energy distribution is not well sampled. Also, the multigroup representation is not consistent with the continuous energy nature of MCNP. Finally, not all photons should be produced isotropically.

Fig. 5.9 shows the neutron-generated photon dose rate variations, inside the crew compartment, for a 20-cm thick W layer, as a function of the LiH layer thickness, where these photons are generated by the neutron interactions inside the shield. The dose rates inside the crew compartments for a 110-cm thick LiH layer are in the order of 3 to 20 Sv y^{-1} depending on the compartment, which is still about 1000 times the yearly limit. The dose rates are lower by a factor of 10 compared to the values for a 10-cm thick W layer. The variations in the photon dose rates are more sensitive to the W layer thickness than to the LiH layer thickness.

Fig. 5.10 shows the neutron-generated photon dose rate variations, inside the crew compartment, for a 30-cm thick W layer, as a function of the LiH layer thickness; the photons are generated by the neutron interactions inside the shield. The dose rates inside the crew compartment for a 100 cm thick LiH layer are in the order of 0.7 to 4 Sv per year depending on the location inside the compartment, which is still about 100 times the yearly limit.

The photons are created in many different ways: (n, g) radiative capture reactions, de-excitation of the atom following an inelastic scattering, etc. An analysis of the various possibilities of gamma production from the neutron reactions is performed by looking at the neutron cross sections (Fisher 1989) of the various materials layered in the shield. Neutrons exiting the reactor bottom first traverse a liquid lithium layer (22-cm in thickness) where, with their energy range they can either have an (n, t) or an elastic scattering with ^{6}Li, or they can have an elastic or an inelastic scattering with ^{7}Li. The cross section for ^{7}Li gamma production increases to 0.20 barns in this energy region. Lithium-6 gamma production cross section is on the order of 10^{-5} barns. Neutrons next traverse a layer of beryllium 10 cm in thickness. Elastic scattering accounts for essentially 100% of the total interactions in this layer and thus there is no production of gamma-rays. Neutrons which pass through these layers have been slowed down. Most of the gamma-

5-16

ray production by neutron reactions inside the shield thus occurs in the tungsten layer. The gamma production cross section of tungsten is approximately 10^4 barns, and displays a broad a resonance peak for neutron energies between 10^{-6} and 10^{-2} MeV. The neutrons modeled in this work have energies into this resonance region and approximately 78% of the reactions are (n, g) reactions while approximately 22% are elastic scattering events. There is some gamma-ray production in the lithium hydride layer, but it is minor compared to that in the tungsten. Lithium hydride is not a good photon shield, so their fluxes are not substantially attenuated when they exit the shield. Nevertheless, because of MCNP cross sections deficiencies, these photon dose rates are overestimated and should not be considered in the design of the shield. Additional calculations should be performed with the more recent neutron cross sections to obtain more accurate estimates of the photons created by neutron interactions within the shield. Figures 5.8 to 5.10 show that there are photon creations inside the shield and that these photons should be considered in the dose estimates of a mission. For the reasons given above, these figures have only a qualitative rather than quantitative value.

TOTAL DOSE RATE RESULTS

Figures 5.11 to 5.13 show variations in total dose rate from the reactor sources of photons and neutrons of one SP-100 reactor, within each of the crew compartments, for the three W layers previously mentioned, and as a function of the LiH thickness. From Fig. 5.11, the minimum LiH thickness required to lower the total dose below 0.0166 Sv y^{-1}, varies from 60 cm to 150 cm if the W layer is 10 cm in thickness. The variations depend on the location of the crew compartment. These data have been extrapolated from the curve fits on the photon and neutron dose rates. The curve fits are calculated from the plots of the logarithm of the dose rates. The logarithm of the dose rates are fitted with quadratic equations, then the dose rates are calculated by taking the exponential of the curve fit values. With 10 cm of tungsten, the photon dose rate inside each crew compartment is more important than the neutron dose if the LiH layer is more than 45 cm thick.

Fig. 5.12 shows the total dose rate variations inside the crew compartments for a 20-cm thick W layer as a function of the LiH layer thickness. This plot defines a 40 cm minimal thickness to lower the neutron dose below the 0.0166 Sv y^{-1} limit when the
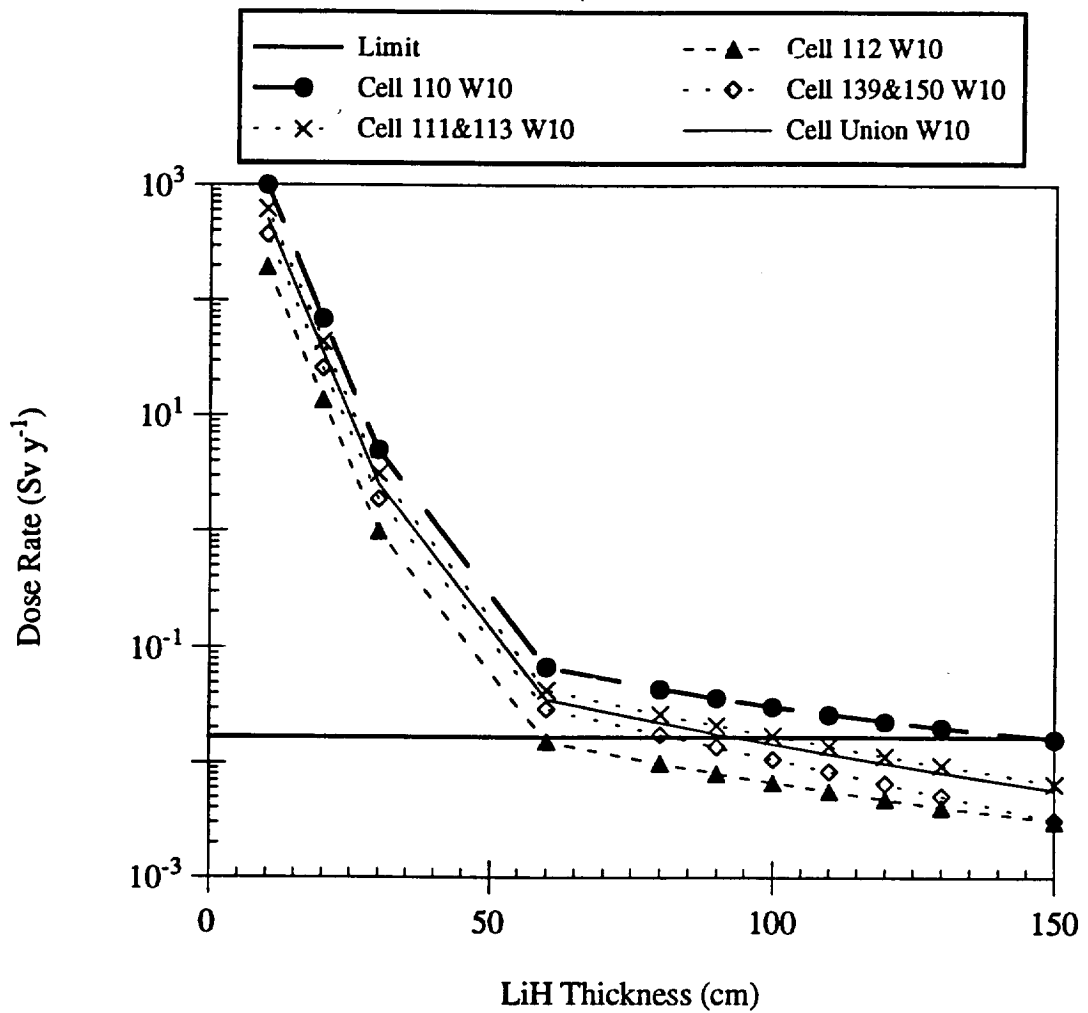
Figure 5.11 Total dose rates inside the crew compartment from the neutrons and photons created from one SP-100 reactor with a 10-cm thick tungsten layer and a variable lithium hydride thickness.
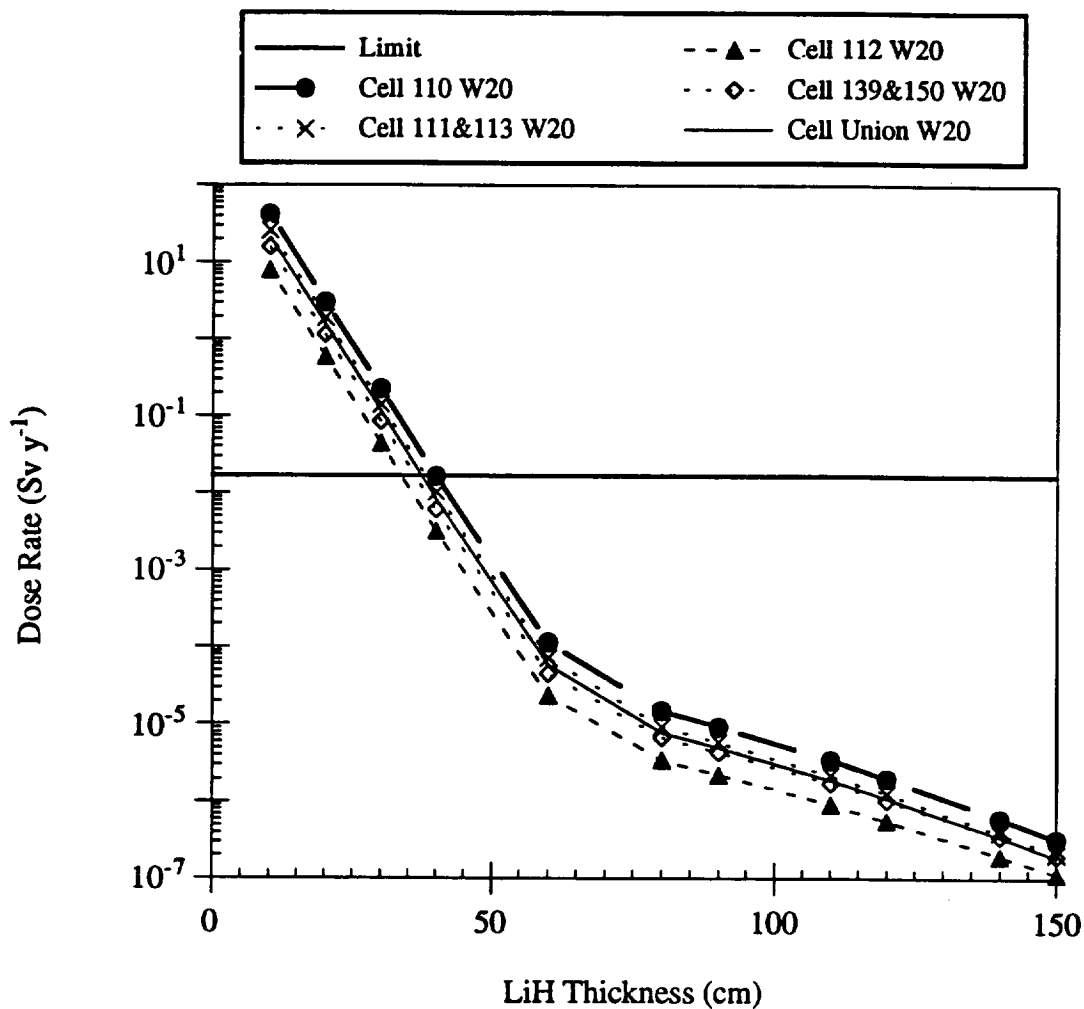
Figure 5.12 Total dose rates inside the crew compartment from the neutrons and photons created in one SP-100 reactor with a 20-cm thick tungsten layer and a variable lithium hydride thickness.
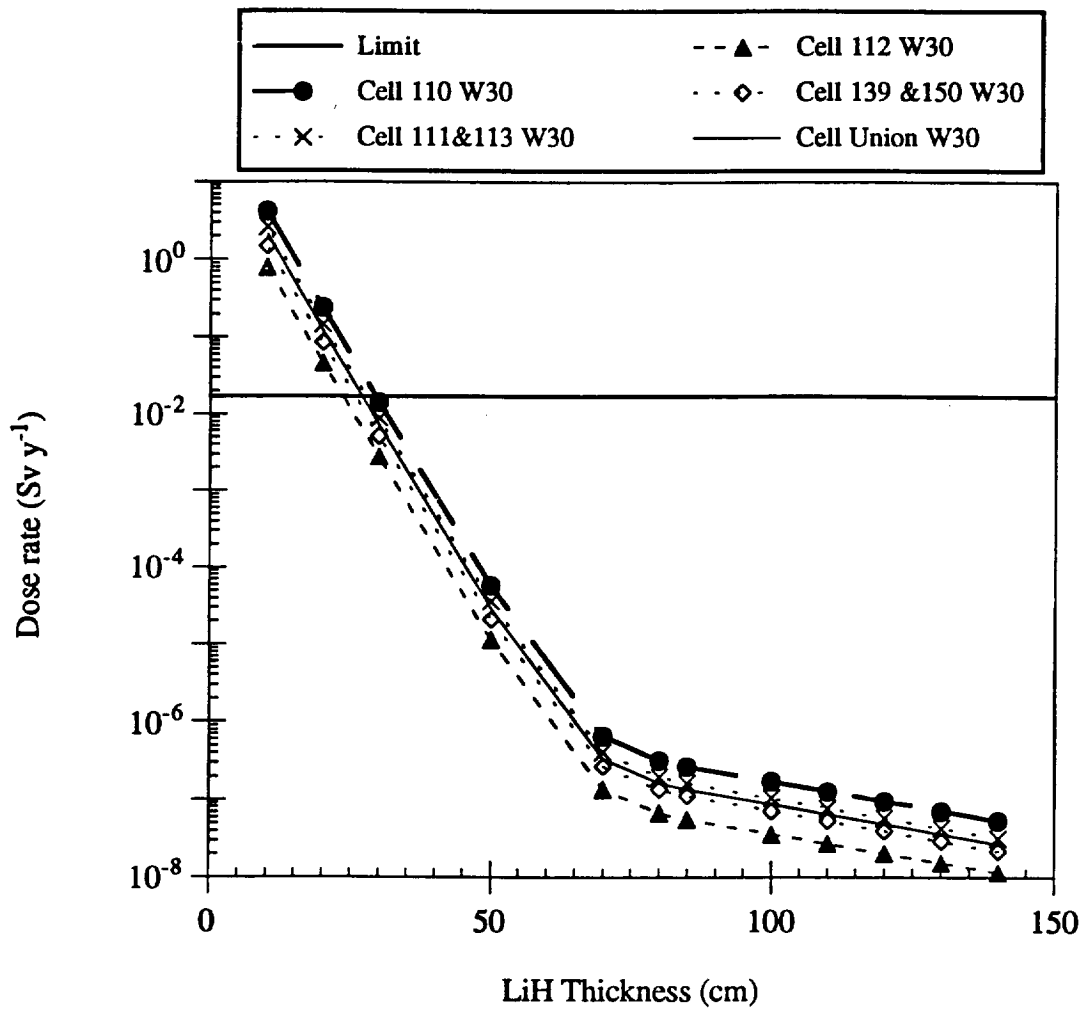
Figure 5.13 Total dose rates inside the crew compartment from the neutrons and photons created from one SP-100 reactor with a 30-cm thick tungsten layer and a variable lithium hydride thickness.

tungsten layer is 20-cm thick. This minimal LiH thickness is lower than the 60 cm of LiH necessary in the case of a 10-cm W shield. With a tungsten thickness of 20 cm, the photon dose rate inside the crew compartment is more important than the neutron dose if the LiH layer is more than 65 cm in thickness.

Fig. 5.13 shows the total dose rate variations inside the crew compartment for a 30-cm thick W layer as a function of the LiH layer thickness. This plot defines a 30-cm minimal thickness to lower the neutron dose below the 0.0166 Sv y^{-1} limit when the W layer is 30-cm in thickness. Once again, this minimal LiH thickness is lower than the 50 cm of LiH necessary in the case of a 10-cm W shield. With this W thickness, the neutron dose appears to be more of a concern than the photon dose from the reactor. There is no perfect shield design, but it seems that a minimum of 20 cm for the W layer can be recommended. With increasing W thickness, the minimal LiH thickness necessary to lower the dose rate below the annual limit decreases. Most of the photons generated by neutron interactions inside the shield are created in the W thickness. It should be noted that photon dose rates resulting from neutron interactions in the shield materials were not included in the total dose rate graphs. This neutron generated gamma dose rate could be comparable to the neutron dose itself. Therefore, additional transport calculations should be performed to account for this component of the total dose rate.

Figures 5.14 to 5.16 show the total dose rate variations inside the most exposed cell of the crew compartment, for 10-cm, 20-cm, and 30-cm thick tungsten layers, respectively, and as a function of the LiH layer thickness. These plots contain the neutron dose rates, the photon dose rates, and the total dose rates due to one reactor. The graphs explain the shape of the total dose rate curve by showing whether the neutron or photon dose rates are dominant.

Fig. 5.17 gives the three-reactor total dose rates inside the most exposed cell of the crew compartment, for 10-cm, 20-cm, and 30-cm thick tungsten layers. The three-reactor data are calculated by simply multiplying the dose rate within the most exposed crew compartment by a factor of three. This graph gives the estimates of total crew dose rates due to the neutrons and photons generated by three 5 MWe SP-100-class reactors during beginning-of-life, full-power operation.

Figure 5.14 Total dose rates inside the most exposed cell of the six crew compartments due to the neutrons, photons, and neutrons and photons generated by one SP-100 reactor with a 10-cm thick tungsten layer and a variable lithium hydride thickness.

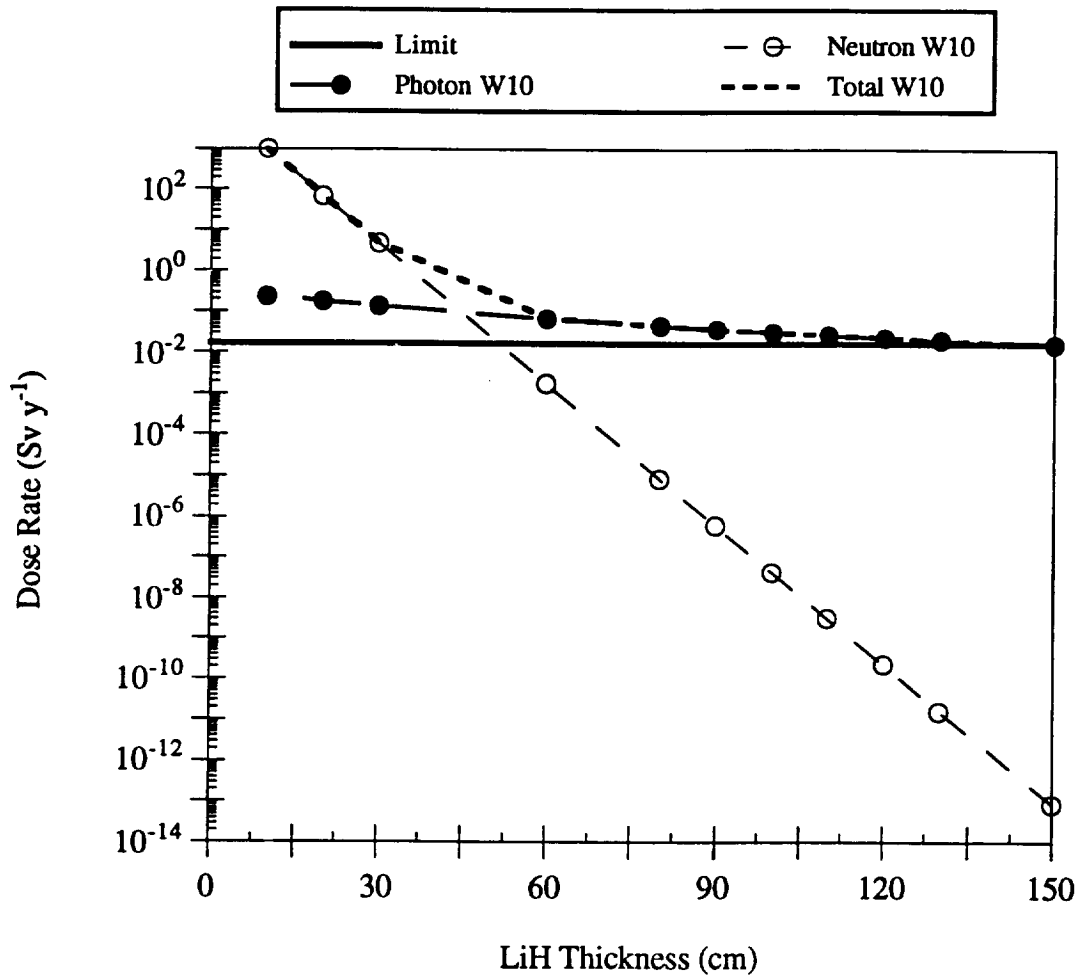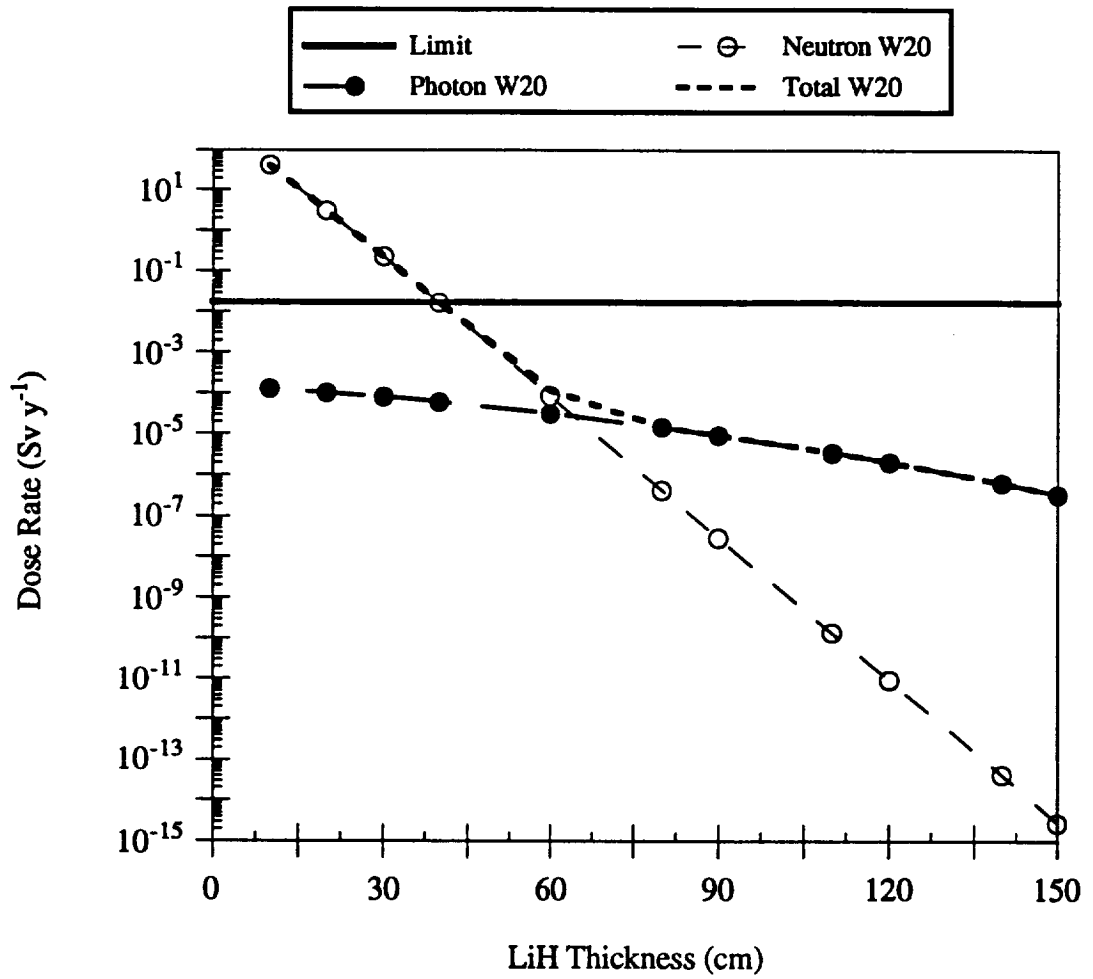**Figure 5.15** Total dose rates inside the most exposed cell of the six crew compartments due to the neutrons, photons, and neutrons and photons generated by one SP-100 reactor with a 20-cm thick tungsten layer and a variable lithium hydride thickness.
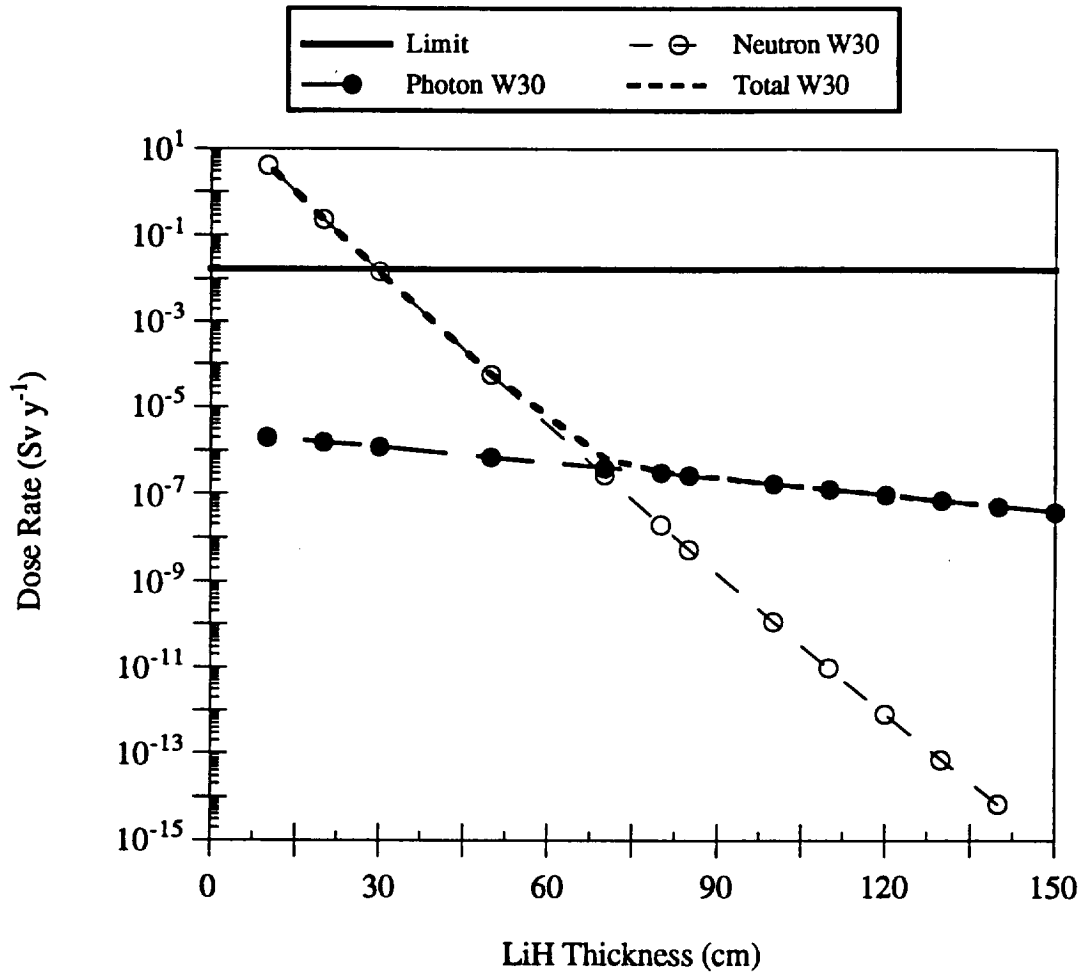
Figure 5.16 Total dose rates inside the most exposed cell of the six crew compartments due to the neutrons, and photons generated by one SP-100 reactor with a 30-cm thick tungsten layer and a variable lithium hydride thickness.
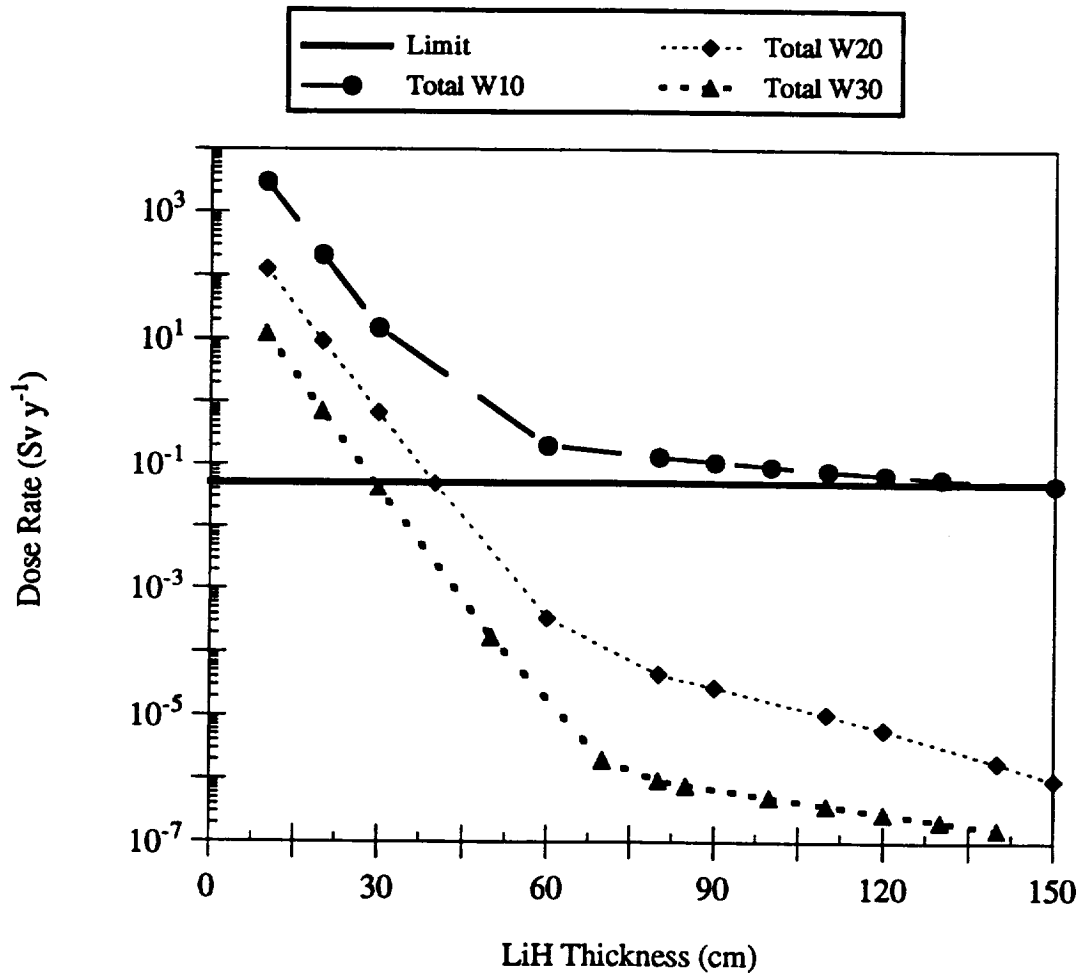
Figure 5.17 Total dose rates inside the most exposed cell of the crew compartment from the neutrons and photons created in three SP-100 reactors with 10, 20, and 30 cm thick tungsten layers and a variable lithium hydride thickness. The dose rate for three reactors was estimated by multiplying the highest dose rate for one reactor by a factor three.

CHAPTER VI

MacSpace™ USER'S GUIDE

INTRODUCTION

This chapter describes the skeletal version of the MacSpace™ software that embodies the computational results developed in this study. The chapter begins with a brief description of the computer system requirements for proper operation of MacSpace™. In the remainder of the chapter a summary menu reference is provided along with a brief description of a sample run.

COMPUTER SYSTEM REQUIREMENTS

MacSpace™ has been developed to operate with Macintosh computers. MacSpace™ requires System 7.0 or later, and MS Excel 5.0 or later installed. As a result of the need to install MS Excel 5.0 or later, at least 4 MB of RAM and approximately 10 to 20 MB of free hard disk space is required. A math co-processor (FPU) is required for proper execution and for speeding-up the numerical computations.

MacSpace™ MENU REFERENCE

MacSpace™ is developed to execute with Excel. Therefore, the main menu bar includes all of the standard MS Excel menus, as well as a MacSpace™ menu. The main menu bar menus allow the user to enter and manipulate all data necessary to work with MacSpace™.

The main menu bar includes the following menus:
- **File**
- **Edit**
- **View**
- **Insert**
- **Format**
- **Tools**

- **Data**
- **Window**
- **MacSpace™**

Now, these menus and the menu items they contain are briefly described. Detailed information is presented only for the MacSpace™ menu, whereas the other standard Excel menus are only mentioned. Additional information regarding these standard Excel menus can be found in the Excel User's Guide.

The File Menu

The **File** menu is for manipulating Excel files, i.e. workbooks that contain worksheets or other types of files. This menu contains, among others, menu items used for opening a new or an existing file, for closing a file, for saving a file, for reverting a file to a saved version, for printing a file, and for quitting Excel.

The command key equivalents of the menu items are shown adjacent to the menu item. The command key equivalents allow that menu item to be selected from the keyboard.

The following menu items are available in the **File** menu:
- **New**
- **Open...**
- **Close**
- **Save**
- **Save As...**
- **Save Workspace...**
- **Find File...**
- **Summary Info...**
- **Page Setup...**
- **Print Preview**
- **Print...**
- **Print Report...**
- *Recently Opened Documents*
- **Quit**

The Edit Menu

The **Edit** menu is for manipulating the Excel file contents. The main Excel file unit is a workbook, and it contains a number of worksheets. Each worksheet in the workbook contains cells in the form of rows and columns. This menu contains, among others, menu items used for cutting and pasting data and for publishing and subscribing to other files.

The command key equivalents of the menu items are shown adjacent to the menu item. The command key equivalents allow that menu item to be selected from the keyboard.

The following menu and sub-menu items are available in the **Edit** menu:
- **Undo**
- **Repeat**
- **Cut**
- **Copy**
- **Paste**
- **Paste Special...**
- **Fill**
  - **Down**
  - **Right**
  - **Up**
  - **Left**
  - **Across Worksheets...**
  - **Series...**
  - **Justify**
- **Clear**
  - **All**
  - **Formats**
  - **Contents**
  - **Notes**
- **Delete...**
- **Delete Sheet**
- **Move or Copy Sheet...**

- **Find...**
- **Replace...**
- **Go To...**
- **Publishing**
    - **Create Publisher...**
    - **Subscribe To...**
- **Links...**
- **Objects**

The View Menu

The **View** menu is for manipulating the various toolbars available and for determining the way the workbook windows are viewed. This menu contains, among others, menu items used for full-screen viewing and for zooming the Excel workbook windows.

The command key equivalents of the menu items are shown adjacent to the menu item. The command key equivalents allow that menu item to be selected from the keyboard.

The following menu items are available in the **View** menu:
- **Formula Bar**
- **Status Bar**
- **Toolbars...**
- **Full Screen**
- **Zoom...**
- **View Manager...**

The Insert Menu

The **Insert** menu is for adding the various objects available in Excel, such as cells, rows, columns, worksheets, charts, etc.. This menu contains, among others, menu items used for adding and defining new macros.

The command key equivalents of the menu items are shown adjacent to the menu item. The command key equivalents allow that menu item to be selected from the keyboard.

The following menu and sub-menu items are available in the **Insert** menu:
- **Cells...**
- **Rows**
- **Columns**
- **Worksheet**
- **Chart**
    - **On This Sheet**
    - **As New Sheet**
- **Macro**
    - **Module**
    - **Dialog**
    - **MS Excel 4.0 Macro**
- **Page Break**
- **Function...**
- **Name**
    - **Define...**
    - **Paste...**
    - **Create...**
    - **Apply...**
- **Note...**
- **Object...**

The Format Menu

The **Format** menu is for formatting the various objects available in Excel. This menu contains, among others, menu items used for changing the look and feel of the cells, worksheets, etc..

The command key equivalents of the menu items are shown adjacent to the menu item. The command key equivalents allow that menu item to be selected from the keyboard.

The following menu and sub-menu items are available in the **Format** menu:

- **Cells...**
- **Row**
  - **Height...**
  - **AutoFit**
  - **Hide**
  - **Unhide**
- **Column**
  - **Width...**
  - **AutoFit Selection**
  - **Hide**
  - **Unhide**
  - **Standard Width...**
- **Sheet**
  - **Rename...**
  - **Hide...**
  - **Unhide...**
- **AutoFormat...**
- **Style...**
- **Placement**
  - **Bring to Front**
  - **Send to Back**
  - **Group**

The Tools Menu

The **Tools** menu provides the various functions for expediting work with Excel. This menu contains, among others, menu items used for spell checking, recording macros, creating add-ins, etc..

The command key equivalents of the menu items are shown adjacent to the menu item. The command key equivalents allow that menu item to be selected from the keyboard.

The following menu and sub-menu items are available in the **Tools** menu:

- **Spelling**
- **Auditing**
    - **Trace Precedents**
    - **Trace Dependents**
    - **Trace Errors**
    - **Remove All Arrows**
    - **Show Auditing Toolbar**
- **Goal Seek...**
- **Scenarios...**
- **Solver...**
- **Protection**
    - **Protect Sheet**
    - **Protect Workbook**
- **Add-Ins...**
- **Macro...**
- **Record Macro**
    - **Record New Macro...**
    - **Use Relative References**
    - **Mark Position for Recording**
    - **Record At Mark**
- **Assign Macro...**
- **Options...**

The Data Menu

The **Data** menu is for manipulating and handling the data available on the worksheets. This menu contains, among others, menu items used for grouping and ungrouping data, consolidating data, etc..

The command key equivalents of the menu items are shown adjacent to the menu item. The command key equivalents allow that menu item to be selected from the keyboard.

The following menu and sub-menu items are available in the **Data** menu:

- Sort...
- Filter
    - Auto Filter
    - Show All
    - Advanced Filter...
- Form...
- Subtotals...
- Table...
- Text to Columns...
- Consolidate...
- Group and Outline
    - Hide Detail
    - Show Detail
    - Group...
    - Ungroup...
    - Auto Outline
    - Clear Outline
    - Settings...
- PivotTable...
- PivotTable Field...
- Refresh Data
- Get External Data...

The Window Menu

The Window menu is for determining which window within the Excel application will be visible. This menu contains, among others, menu items used for hiding and unhiding windows, splitting windows, and switching among open windows.

The command key equivalents of the menu items are shown adjacent to the menu item. The command key equivalents allow that menu item to be selected from the keyboard.

The following menu items are available in the Window menu:
- New Window

- **Arrange...**
- **Hide**
- **Unhide...**
- **Split**
- **Freeze Panes**
- **Show Clipboard**
- *Open Windows*

The MacSpace™ Menu

The MacSpace™ menu contains menu items specific to the application developed. This menu contains, among others, menu items used for selecting a mission, setting the various items for space vehicle configuration, and calculating the crew doses and crew radiation risk.

The following menu and sub-menu items are available in the MacSpace™ menu:
- **About MacSpace™...**

This menu item reveals the start-up dialog documenting the support provided for the development of **MacSpace™**. By clicking on the **Credits** button, additional information can be obtained regarding the developers of the software.
- **Help...**

This menu item contains the on-line help to be made available in a future version of **MacSpace™**. Currently, this menu item is visible, though no on-line help can be obtained.
- **Mission**

This menu item contains the missions considered in **MacSpace™**. Even though four mission options are currently provided, only the Mars mission option is operational. The following sub-menu items are included in the **Mission** menu:
- **Mars**

This sub-menu item contains the options available to choose from in performing a Mars mission. Execution of this sub-menu item results in the display of a dialog box which allows the user to choose one of the following options: (1) Nuclear Electric Propulsion (NEP), (2) Nuclear Thermal Rocket (NTR), or, (3) Non-Nuclear. Currently, only the NEP option to the Mars mission is operational.
- **Lunar**

This sub-menu item contains the options available to choose from in performing a Lunar mission. Execution of this sub-menu item currently results in a warning message, as there are no options for a lunar mission yet.

- **Asteroid**

This sub-menu item contains the options available to choose from in performing an Asteroid mission. Execution of this sub-menu item currently results in a warning message, as there are no options for an Asteroid mission yet.

- **Alternate**

This sub-menu item contains the options available to choose from in performing any Alternate mission. Execution of this sub-menu item currently results in a warning message, as there are no options for any Alternate missions yet.

- **Config Vehicle**

This menu item contains the vehicle components that can be altered for specific missions considered in **MacSpace™**. Even though four component options are currently provided, only the "Reactors" component can be altered. The following sub-menu items are included in the **Config Vehicle** menu:

- **Reactors...**

This sub-menu allows the user to select the various reactor options which impact the crew dose and risk calculations. Currently, the options available for change are the thickness of the tungsten shield and the thickness of the lithium-hydride shield in the reactor.

- **Tanks...**

This sub-menu allows the user to select the various propellant tank options which impact the crew dose and risk calculations. These options are only meaningful for an NTR-type mission. As NTR mission scenarios are not currently operational, the various propellant tank options cannot be set yet.

- **Habitat...**

This sub-menu allows the user to select the various crew habitat options which impact the crew dose and risk calculations. In future versions of the software, the option available for change will be the thickness of the aluminum shield in the crew habitat which protects against natural radiation.

- **Other...**

This sub-menu allows the user to select the various options present in other space vehicle components which impact the crew dose and risk calculations. Currently, no other space vehicle component can be changed.

- **Options...**

This menu item contains the various options that can be set for specific missions considered in **MacSpace™**. Currently, only natural radiation options are available. The following natural radiation options are available for selection:

(1) Solar Maximum, or,

(2) Solar Minimum, for Galactic Cosmic Radiation (GCR) fluxes,

and,

(1) February 1956,

(2) November 1960,

(3) August 1972,

(4) August 1989,

(5) September 1989, and,

(6) October 1989, for Solar Particle Events (SPE) spectra.

- **Calculate**

This is the main menu item in **MacSpace™** which is used for the various calculations. The following sub-menu items are available in this menu:

- **Crew Dose...**

This calculation involves the determination of the crew dose by mission phase and the total dose for the selected mission and for the configured spacecraft.

- **Radiation Risk...**

This calculation involves the determination of the crew radiation risk by mission phase for the selected mission and for the configured spacecraft. The crew dose calculation must be performed first.

A SAMPLE RUN

In this section a sample step-by-step session of MacSpace™ is briefly described along with the entered input and the expected results. In order to perform a MacSpace™ run, the following step should be followed:

(1) Make sure that your Macintosh has an FPU and it is running under System 7.0 or later,

(2) Make sure that Excel 5.0 or later is installed in your system,

(3) Insert the diskette and copy the file named "MacSpace™ v1.0" anywhere into your harddisk,

(4) Double-click on the icon of the file named "MacSpace™ v1.0"; this should start execution of the program,

(5) A start-up dialog will appear; either click the "Credits" button for more information or click the "OK" button to dismiss the start-up dialog box,

(6) Following dismissal of the start-up dialog box, you should be viewing either an empty worksheet or a worksheet filled with calculations from prior runs; you can either delete these prior runs, overwrite the existing numbers or create a new work-sheet,

(7) From the menu "MacSpace™" select the menu item "Mission"; you should be able to view a sub-menu with four sub-menu items,

(8) Select the "Mars" sub-menu item from the "Mission" menu; a Mars mission is the only scenario currently available,

(9) Selection of the "Mars" sub-menu should reveal a dialog box with three available options; select the "NEP" button and click the "OK" button; an NEP Mars mission is the only scenarios currently available in MacSpace™,

(10) You should be viewing the various inputs to an NEP Mars mission scenario, with default values available for each mission phase duration and power level requirements; you will be able to alter mission phase duration, though power level requirements cannot be altered in this version of MacSpace™,

(11) Make any changes to the mission duration and click the "OK" button,

(12) From the menu "MacSpace™" select the menu item "Config Vehicle"; you should be able to view a sub-menu with four sub-menu items,

(13) Select the "Reactors" sub-menu item from the "Config Vehicle" menu,

(14) You should be viewing a dialog box which allows you to set the various reactor options; you will be able to alter the tungsten shield thickness (not the material itself), and the lithium-hydride shield thickness (again, not the material itself),

(15) Make any changes to the reactor options and click the "OK" button,

(16) From the menu "MacSpace™" and menu item "Config Vehicle", select the sub-menu item "Habitat",

(17) You should be viewing a dialog box which allows you to set the various crew habitat options; you will not be able to alter any of the habitat settings at this point, click the "OK" button,

(18) From the menu "MacSpace™" and select the menu item "Options...",

(19) You should be viewing a dialog box which allows you to set the various natural radiation options, such as the GCR flux levels and the solar flare spectra; you can

only select the solar minimum flux level and among three solar flare spectra; make your selections and click the "OK" button,

(20) From the menu "MacSpace™" and menu item "Calculate", select the sub-menu item "Crew Dose...",

(21) You should be viewing a dialog box which allows you to check the various radiation dose sources for the calculations; make your selections and click the "OK" button, this should initiate the calculations with the results written on "Sheet1" of the open workbook,

(22) From the menu "MacSpace™" and menu item "Calculate", select the sub-menu item "Radiation Risk...",

(23) You should be viewing a dialog box which allows you to set the risk factors for the various radiation dose sources involved in the calculations; set the risk factors and click the "OK" button, this should initiate the calculations with the results written, again, on "Sheet1" of the open workbook.

For the default settings in MacSpace™, you should obtain the following results:

Mars NEP Mission
Dose Calculations

Mission Phase	Duration (days)	Cumulative Duration (days)	Power (MWth)
Earth Spiral-Out (from 450 km)	443.0	443.0	75.0
Heliocentric to Mars			
1st Portion: Thrust	253.0	696.0	75.0
2nd Portion: Coast	162.0	858.0	0.6
3rd Portion: Thrust	85.0	943.0	75.0
Mars Spiral-In	86.0	1,029.0	75.0
Mars Operations	150.0	1,179.0	1.2
Mars Spiral-Out	39.0	1,218.0	75.0
Heliocentric to Earth			
1st Portion: Thrust	74.0	1,292.0	75.0
2nd Portion: Coast	211.0	1,503.0	0.6
3rd Portion: Thrust	68.0	1,571.0	75.0
Earth Spiral-In (to 450 km)	239.0	1,810.0	75.0
Earth Orbit Arrival	Variable	Variable	Shutdown
Total NEP Mission Parameters		1,810.0	

GCR Dose (Sv)	SPE Dose (Sv)	Neutron Dose (Sv)	Photon Dose (Sv)
0.00E+00	0.00E+00	0.00E+00	0.00E+00
3.17E-01	3.45E-01	3.40E-02	1.25E-04
2.03E-01	0.00E+00	2.17E-02	8.02E-05
1.06E-01	0.00E+00	1.14E-02	4.21E-05
1.08E-01	0.00E+00	1.15E-02	4.26E-05
1.88E-01	0.00E+00	2.01E-02	7.43E-05
4.88E-02	0.00E+00	5.23E-03	1.93E-05
9.27E-02	0.00E+00	9.93E-03	3.67E-05
2.64E-01	0.00E+00	2.83E-02	1.05E-04
8.51E-02	0.00E+00	9.13E-03	3.37E-05
0.00E+00	0.00E+00	0.00E+00	0.00E+00
0.00E+00	0.00E+00	0.00E+00	0.00E+00
1.4	0.3	0.2	0.0

Total Mission Phase Dose (Sv)	GCR Risk (% Increase in Lifetime)	SPE Risk (% Increase in Lifetime)	Neutron Risk (% Increase in Lifetime)	Photon Risk (% Increase in Lifetime)
0.00E+00	0.0	0.0	0.0	0.0
6.96E-01	0.6	0.5	0.0	0.0
2.25E-01	0.4	0.0	0.0	0.0
1.18E-01	0.2	0.0	0.0	0.0
1.19E-01	0.2	0.0	0.0	0.0
2.08E-01	0.4	0.0	0.0	0.0
5.41E-02	0.1	0.0	0.0	0.0

1.03E-01	0.2	0.0	0.0	0.0
2.93E-01	0.5	0.0	0.0	0.0
9.43E-02	0.2	0.0	0.0	0.0
0.00E+00	0.0	0.0	0.0	0.0
0.00E+00	0.0	0.0	0.0	0.0
1.9	2.8	0.5	0.2	0.0

Key Reactor Parameters

Man-made Radiation Shields
 Gamma Shield
 Material   Tungsten
 Thickness (m)   0.2
 Neutron Shield
 Material   Lithium Hydride
 Thickness (m)   0.4

Key Habitat Parameters

Natural Radiation Shield
 Material   Aluminum
 Thickness (gm/cm^2)   10.0

CHAPTER VII

CONCLUSIONS AND RECOMMENDATIONS

SUMMARY

The study of man-made radiation dose to the crew of a nuclear-powered space vehicle was performed utilizing the MCNP radiation transport code. In addition, natural radiation dose was incorporated using estimates previously made at the NASA Langley Research Center. In Chapter I, the Mars mission project and its historical context were introduced. Furthermore, the dose limits, which control any activity involved in a nuclear radiation environment, were discussed. Chapter II provided background information on previous dose estimates for natural space radiation, a description of the NEP vehicle, and estimates of radiation doses for man-made sources in space missions. Chapter III presented an overview of the methods used to assess the man-made radiation source term used in this project. In particular, brief descriptions of TWODANT and ORIGEN2 codes were presented, followed by the operating and post-shutdown fluxes of the scaled SP-100 reactor. Chapter IV described the computational methods used in this project. Particularly, the Monte Carlo method was introduced, the MCNP code was described, and the input file of the project was analyzed. In Chapter V, the project results were presented and discussed. Finally, in Chapter VI, a brief user's guide was presented for the skeletal version of the computational tool developed in this project.

The literature review highlighted some of the advantages of nuclear propulsion for deep space missions, such as a Mars mission. It emphasized that space natural radiation sources create a hostile environment. Consequently, the time spent in space should be minimized and this can be done by shortening the travel time. There is currently no comprehensive dose estimate for the NEP vehicle in the literature. In this work, the dose variations as a function of two parameters, namely the tungsten and the lithium hydride layer thickness of the shadow shield, were assessed.

CONCLUSIONS

The shield thickness required to reduce the reactor dose to the crew below the 0.05 Sv y^{-1} limit is summarized in Table 7.1. The data indicate that a 30-cm thick tungsten layer followed by a 55-cm thick lithium hydride layer would serve as an adequate shield considering only the photon and neutron source terms from the reactor and its shield. Photon production by neutron interactions in the shield have not been considered, yet the LiH layer would probably have to be increased to further attenuate this photon component of the crew dose.

Table 7.1 Summary of tungsten and lithium hydride thickness requirements to lower the dose rate inside the crew compartment for the source particles below the 1.67 10^{-2} Sv y^{-1} limit.

W Thickness (cm)	LiH Thickness (cm)		
	Neutron Component	Photon Component	Total
10	52	140	140
20	40	No requirement	40
30	30	No requirement	30

Because of MCNP deep penetration limitations, the dosimetry results had to be interpolated. The study identified that photons generated by the reactor neutrons interacting with the shield material were the main dosimetric concern. In general, the neutron source is the major shield design concern for the SP-100 reactor. Photons from the reactor are easily shielded and contribute in a negligible way to the total dose as long as the tungsten layer exceeds 15 cm in thickness.

RECOMMENDATIONS

This study attempted to use MCNP variance reduction techniques in the most effective manner according to the knowledge of the author. Nevertheless, these techniques might be improved by a more experienced MCNP user. The MCNP manual indicates that successful use of MCNP variance reduction techniques is often difficult, tending to be more of an art than a science.

This research did not model the three reactors simultaneously, and no run following the particles from the bottom of the reactor to the crew compartment in one straight run was performed. This was not executed because of the computer and code limitation. MCNP limits the user to a maximum of 99999 surfaces and 99999 cells. The maximum number of surfaces is easily reached when the model is complex. Nevertheless, it would be interesting to know whether the presence of the beam truss structures could modify in any significant way the dose rates estimated in the current model. This task would require some model simplifications. A good example would be to model only one of the three reactors.

This work was performed with the photon and neutron source terms for an operating SP-100 reactor at beginning of life. The next step would be to complete the dose assessment by performing a similar study, as the one in this report, using the post-shutdown reactor fluxes presented in previous chapters. In these cases, the only concern would be photon sources from the decay of the fission product inventory.

The neutron cross-section libraries for tungsten available at the time the study was performed appear to substantially overestimate the production of neutron-generated photons. It would be highly recommended to perform the same calculations with more recent neutron cross-sections.

Furthermore, it should be interesting to study the effects of dose rate with an added second tungsten layer at the bottom of the shield. The purpose of this added layer would be to attenuate all the photons generated by the neutrons inside the shield if this indeed appears to be a concern. However, this added layer may generate additional photons in further neutron reactions which would not be attenuated at all. Moreover, the

material characteristics, and the weight limits are other factors which influence the shield design and these items would also have to be considered in any final shielding analysis.

Finally, a four-layer-design of beryllium, depleted lithium hydride, tungsten, and natural lithium hydride should be considered. This shadow shield option has been considered by NASA Lewis researchers but it has not been adopted for this project. As a result of the research outcomes presented in this report, it seems necessary to attenuate the neutron flux before the tungsten layer in order to decrease the number of photons generated by neutron interactions with tungsten.

REFERENCES

Briesmeister, J. F. MCNP - A general monte carlo code for neutron and photon transport. Version 3A. Los Alamos, NM: Los Alamos National Laboratory; LA-7396-M, Rev.2; 1986.

Briesmeister, J. F.; Hendricks, J. S. MCNP4 Newsletter. Los Alamos, NM: Los Alamos National Laboratory; X-6:JFB-91-177; 1991.

Badhwar, G. D.; O'Neill P. M. An improved model of GCR for space exploration missions. Nucl. Tracks Radiat. Meas. 20:403-410; 1992.

Badhwar, G. D.; Cucinotta F. A.; O'Neill P. M. Depth-dose equivalent relationship for cosmic rays at various solar minima. Rad. Res. 134:9-15; 1993

Bolch, W. E.; Thomas, J. K.; Peddicord, K. L.; Nelson, P.; Marshall, D. T.; Busche, D. M. A radiological assessment of nuclear power and propulsion operations near the Space Station Freedom. College Station, TX: Texas A&M University; NASA Contractor Report 185185; 1990.

Cashwell, E. D.; Neergaard, J. R.; Taylor, W. M.; Turner, G. D. MCN: A neutron Monte Carlo code. Los Alamos, NM: Los Alamos Scientific Laboratory; LA-5157-MS; 1972.

Cashwell, E. D.; Neergaard, J. R.; Everett, C. J.; Schrandt, R. G.; Taylor, W. M.; Turner, G. D. Monte Carlo photon codes: MCG and MCP. Los Alamos, NM: Los Alamos Scientific Laboratory; LA-4751; 1973.

Croff, A. G. ORIGEN2: A Versatile Computer Code for Calculating the Nuclide Compositions and Characteristics of Nuclear Materials, Nuclear Technology, Vol. 62, pp. 335-352, September 1983.

George, J. A. Integrated shielding systems for manned interplanetary spaceflight. Symposium on Space Nuclear Power and Propulsion; Albuquerque, NM; 1992a.

George, J. A. Personal Communication. Cleveland, OH: NASA Lewis Research Center; 1992b.

Halbleib, J. A.; Mehlhorn, T. A. ITS: the integrated TIGER Series of coupled electron/photon Monte Carlo transport codes. Nucl. Sci. Eng. 92:338; 1986.

International Commission on Radiological Protection. Recommendations of the International Commission on Radiological Protection. Oxford: Pergamon Press; ICRP Publication 26; 1977.

International Commission on Radiological Protection. Data for use in protection against external radiation. Oxford: Pergamon Press; ICRP Publication 51; 1987.

R-1

International Commission on Radiological Protection. 1990 recommendations of the International Commission on Radiological Protection. Oxford: Pergamon Press; ICRP Publication 60; 1990.

Kinsey, R. Data formats and procedures for the Evaluated Nuclear Data File, ENDF. Brookhaven, NY: Brookhaven National Laboratory; BNL-NCS-50496; 1979.

Lehmer, D. H. Mathematical methods in large-scale computing units. Ann. Comput. Lab., Harvard Univ. 26:141-146; 1951.

McCracken, D. D. The Monte Carlo Method. Sci. Am. 192(5):90-96; 1955.

McKissock, B. I.; Bloomfield, H. S. Space nuclear reactor shields for manned and unmanned applications. Cleveland, OH: NASA Lewis Research Center; TM-102064, 1989.

National Aeronautics and Space Administration, Office of Aeronautics and Exploration Technology. Nuclear thermal and nuclear electric propulsion Workshop; 1990.

National Council on Radiation Protection and Measurements. Guidance on radiation received in space activities. Recommendations of the National Council on Radiation Protection and Measurements. NCRP REPORT No. 98; 1989.

O'Dell, R. D.; Brinkley, F. W.; Marr, D. R; Alcouffe, R. E Revised User's Manual for ONEDANT: A Code Package for One-Dimensional, Diffusion-Accelerated, Neutral-Particle Transport; Los Alamos, NM: Los Alamos National Laboratory; LA-9184-M, Rev., December 1989.

Occupational Safety and Health Administration. Radiation Protection Guidance to Federal Agencies for Occupational Exposure; Recommendations Approved by the President. Federal Register; 52 (17); 1987.

Sager, P. H. Radiation shield requirements for manned nuclear propulsion space vehicles. Symposium on Space Nuclear Power and Propulsion; Albuquerque, NM; 1992.

Schnitzler, B. G.; Borowski, S. K. Radiation dose estimates for typical piloted NTR lunar and Mars engine operations. AIAA 91-3407; AIAA/NASA/OAI Conference on Advanced SEI Technologies; 1991.

Simonsen, L. C.; Cucinotta, F. A.; Atwell, W.; Nealy, J. E. Temporal analysis of the October 1989 proton flare using computerized anatomical models. Rad. Res. 133:1-11; 1993.

Townsend, L. W.; Nealy, J. E.; Wilson, J. W. Preliminary estimates of radiation exposures for manned interplanetary missions from anomalously large solar flare events. NASA Technical Memorandum 100620; 1988.

Townsend, L. W.; Nealy, J. E.; Wilson, J. W.; Simonsen, L. C. Estimates of galactic cosmic ray shielding requirements during solar minimum. NASA Technical Memorandum 4167; 1990.

Townsend, L. W.; Shinn, J. L.; Wilson, J. W. Interplanetary crew exposure estimates for the August 1972 and October 1989 solar particle events. Rad. Res. 126: 108-110; 1991.

Townsend, L. W.; Cucinotta, F. A.; Wilson, J. W. Interplanetary crew exposure estimates for galactic cosmic rays. Rad. Res. 129: 48-52; 1992.

APPENDIX A

LIST OF ACRONYMS

AL	Anomalously Large
ALARA	As Low As Reasonably Achievable
ALSPE	Anomalously Large Solar Particle Events
BFO	Blood Forming Organs
BRYNTRN	Baryon Transport Computer Code
CAM	Computerized Anatomical Man
DCF	Fluence-to-Dose Equivalent Conversion Factors
ECCV	Earth Crew Capture Vehicle
GCR	Galactic Cosmic Rays
HZE	High atomic number (Z) and Energy particles
ICRP	International Commission on Radiological Protection
IMLEO	Initial Mass at Low Earth's Orbit
ITS	Integrated Tiger Series
LANL	Los Alamos National Laboratory
LEO	Low Earth Orbit
LET	Linear Energy Transfer
MCG	Monte Carlo Code for Gamma Transport
MCN	Monte Carlo Code for Neutron Transport
MCNP	General Monte Carlo Code for Neutron and Photon Transport
MeV	Mega Electron Volt, unit of energy $1\ MeV = 1.6\ 10^{-19}$ Joules
MT	Metric Ton
NASA	National Aeronautics and Space Administration
NCRP	National Council on Radiation Protection and Measurements
NEP	Nuclear Electric Propulsion
NTP	Nuclear Thermal Propulsion
NTR	Nuclear Thermal Rocket
OSHA	Occupational Safety and Health Administration

SAA	South Atlantic Anomaly
SEI	Space Exploration Initiative
SPE	Solar Particle Event
SP-100	The reactor system employed for the NEP vehicle
SSF	Space Station Freedom
Sv	Sievert, dose Equivalent unit
	$1 \text{ Sv} = 1 \text{ J kg}^{-1}$

APPENDIX B

MCNP INPUT FILES

Appendix B.1   **MCNP Neutron Runs Through the Shield.**
Input File for neutron runs through the shield geometry.


```
HPM1 -- NEP 25 MWTH REACTOR 1 IS MODELED -- REFLECTOR, SHIELD
C   Cell Card
C   Shield
1    6 -.479   -1 -2 3   IMP:N=10 IMP:P=1   $6 Li coolant
2    5 -1.85   -4 -5 1  IMP:N=25 IMP:P=4   $5 Be reflector
4    3 -19.3   -4 -7 5  IMP:N=150 IMP:P=100   $3 W photon shield
5    3 -19.3   -4 -8 7  IMP:N=1000 IMP:P=100   $3 W photon shield
10    3 -19.3   -4 8 -12  IMP:N=10000 IMP:P=100   $3 W photon shield
16   2 -.775   12 -4 -13 IMP:N=500000 IMP:P=400   $2 Natural LiH
17   2 -.775   13 -4 -14 IMP:N=5000000 IMP:P=500   $2 Natural LiH
18   2 -.775   14 -4 -15 IMP:N=50000000 IMP:P=600   $2 Natural LiH
19   2 -.775   15 -4 -16 IMP:N=500000000 IMP:P=700   $2 Natural LiH
20   2 -.775   16 -4 -17 IMP:N=5000000000 IMP:P=800   $2 Natural LiH
6    0 (1:2:-3) (-1:4:17) -9 IMP:N=1 IMP:P=1
7    0  9 IMP:N=0 IMP:P=0

C   Surface Card
1    PZ  22.25
2    CZ  28.00   $29.13
3    PZ  0
4    CZ  108
5    PZ  31.79
7    PZ  41.79
8    PZ  51.79
12   PZ  61.79
9    SZ  100 250
13   PZ  70
14   PZ  80
15   PZ  90
16   PZ  100
17   PZ  110

C   Data Card
C   MODE Card. In this case neutron and photon modes
MODE N P
C   Material Card
C   declares materials for
C     2. Natural Lithium Hydride d=0.775 g/cm3
C     3. Tungsten d=19.3 g/cm3
C     5. Beryllium d=1.85 g/cm3
C     6. Liquid Lithium d=0.479 g/cm3
```

```
M2      3006.10C 0.0375  3007.05C 0.4625   1001.35C 0.5
M3      74000.01C 1
M5      4009.03C 1
M6      3006.10C 0.075  3007.05C 0.925
C       Source Card
SDEF   ERG=D1 SUR=3 PAR=1 VEC=0 0 1 DIR=1 POS=0 0 0 RAD=D2
       WGT=7.721134239E14
SI1     0.00 1.39E-10 4.14E-7 1.67E-4 5.53E-3 4.09E-2 1.11E-1 3.02E-1 4.98E-1
       8.21E-1 1.35 2.23
SP1     0 5.1359069E12 2.7980892E13 6.6769457E13 1.3500502E14 1.2020317E14
       1.6045523E14 6.9785371E13 7.6679939E13 4.665485E13 3.4134922E13
       2.9308666E13
SI2     0 28
C     Tally Card
F2:N   1 2 3 4 5 7 8 9 12 13 14 15 16
E2     5.00E-2 2.52E-1 1 4.5 10
F12:P  1 2 4 5 7 8 9 12 13 14 15 16 17
E12    .01 .015 .025 .05 .06 .07 .08 .1 .15 .2 .3 .5 1 3 6 10
NPS    500000
PRINT  -40 -150 -198
```

Appendix B.2   Photon Runs Through the Shield.
MCNP Input File for photon runs through the shield geometry.

PHOTONS -- NEP 25 MWTH REACTOR 1 IS MODELED -- REFLECTOR, SHIELD
```
C    Cell Card
C    Shield
1    6 -.479   1 -2 -3    IMP:P=1    $6 Li coolant 22.25cm
2    5 -1.85   -4 -5 3   IMP:P=2   $5 Be reflector 9.54 cm
3    3 -19.3   -4 -6 5   IMP:P=3    $3 W photon shield 33.5cm
4    3 -19.3   -4 -10 6  IMP:P=10   $3 W
5    3 -19.3   -4 -11 10 IMP:P=50   $3
6    3 -19.3   -4 -12 11 IMP:P=200   $3
7    3 -19.3   -4 -13 12 IMP:P=1000   $3
8    3 -19.3   -4 -14 13 IMP:P=5000   $3
9    3 -19.3   -4 -15 14 IMP:P=20000   $3
10   3 -19.3   -4 -16 15 IMP:P=100000   $3
11   3 -19.3   -4 -17 16 IMP:P=500000   $3
12   3 -19.3   -4 -18 17 IMP:P=2000000   $3
18   2 -.775   18 -4 -20 IMP:P=16000000   $2 N LiH
20   0    (-1:2:3) (-3:4:20) -9 IMP:P=1
21   0    9 IMP:P=0

C    Surface Card
1    PZ 0
2    CZ 28.00    $ 29.13
3    PZ 22.25
4    CZ 108
5    PZ 31.79
6    PZ 33
9    SZ 100 250
10   PZ 35
11   PZ 37
12   PZ 39
13   PZ 41
14   PZ 43
15   PZ 45
16   PZ 47
17   PZ 49
18   PZ 51.79
20   PZ 61.79

C    Data Card
C    MODE Card. In this case photon mode
MODE P
C    Material Card
C    declares materials for
C       2. Natural Lithium Hydride d=0.775 g/cm3
C       3. Tungsten d=19.3 g/cm3
C       5. Beryllium d=1.85 g/cm3
C       6. Liquid Lithium d=0.479 g/cm3
M2    3000.01P 0.5   1000.01P 0.5
```

```
M3     74000.01P 1
M5     4000.01P 1
M6     3000.01P 1
C      Source Card
SDEF   ERG=D1 SUR=5 PAR=2 VEC=0 0 1  POS=0 0 0 RAD=D2
WGT=6.41443811E13
SI1    0 .01 .3 .75 2.5 30
SP1    0 0 1.2231396E13 2.1653101E13 2.1722869E13 8.5370151E12
SI2    0 28
C    Tally Card
F12:P  5 6 9 10 11 12 13 14 15 16 17 18 20
E12    .01 .015 .025 .05 .06 .07 .08 .1 .15 .2 .3 .5 1 3 6 10
NPS    200000
PRINT  -40 -150 -198
```

Appendix B.3   **Neutron Runs Through the Crew Compartment.**
MCNP Input File for neutron runs through the crew compartment
geometry.

CREW4 -- CREW COMPARTMENT ARGON TANKS ION THRUSTERS --
```
C    data from ntn2.4 surface 17 (W-30cm LiH-50cm)
C    Cell Card
C    Crew Compartment
C    Small cylinders (// to y axis)
10   7 -2.7   -26 27 -28 #110    IMP:P=100      $7 aluminum
110  0    -526 527 -528     IMP:P=100          $void inside
C    Big cylinders (coordinate transform)
11   7 -2.7   -29 401 -402 #111     IMP:P=100      $7
111  0    -529 501 -502     IMP:P=100
12   7 -2.7   -30 403 -404 #112   IMP:P=100
112  0    -530 503 -504   IMP:P=100
13   7 -2.7   -31 405 -406 #113   IMP:P=100
113  0    -531 505 -506     IMP:P=100
C    Ion thrusters
14   8 -4.5   -32 33 34 -35 36 -37  IMP:P=10
C    Mars Excursion Vehicle
15   7 -2.7   -38 -39            IMP:P=50    $7 aluminum
C    Argon tanks (same rotation angles as big cylinders)
16   7 -2.7   -40 41  IMP:P=10
17   9 -1.4   -41    IMP:P=20
18   7 -2.7   -42 43   IMP:P=10
19   9 -1.4   -43    IMP:P=20
20   7 -2.7   -44 45   IMP:P=10
21   9 -1.4   -45   IMP:P=20
22   7 -2.7   -46 47   IMP:P=10
23   9 -1.4   -47   IMP:P=20
24   7 -2.7   -48 49   IMP:P=10
25   9 -1.4   -49   IMP:P=20
26   7 -2.7   -50 51   IMP:P=10
27   9 -1.4   -51   IMP:P=20
C    Second Crew Compartment
C    Small cylinders (// to y axis)
39   7 -2.7   -226 27 -28  #139    IMP:P=100  $8 aluminum
139  0    -626 527 -528     IMP:P=100
C    Second Ion thrusters
40   8 -4.5   -32 33 234 -235 -236 237  IMP:P=10
C    Third Crew Compartment
C    Small cylinders (// to y axis)
50   7 -2.7   -326 27 -28  #150   IMP:P=100  $8 aluminum
150  0   -726 527 -528     IMP:P=100
C    Third Ion thrusters
51   8 -4.5   -32 33 334 -335 336 -337  IMP:P=10
C    Outside world,void
52   0    -60 61 -62 #14 #15 #40 #51 40 42 44 46 48 50 (26:-27:28)
     (29:-401:402) (30:-403:404) (31:-405:406) (226:-27:28)
     (326:-27:28) IMP:P=1
```

53   0   60:-61:62 IMP:P=0

C   Surface Card
C   First Small Cylinder
C   A cylinder of radius 200, //y, x'=0, z'=9.22m
26   C/Y 0 1022 200
526 C/Y 0 1022 196.3
C   A plane at y = 500
27   PY   500
527   PY   503.7
C   A plane at y = 900
28   PY   900
528   PY   896.3
C   Big Cylinders (Crew compartment)
C   A cylinder of radius 200, //z',TRANSLATION, rotation (zz'0=150, TR1)
29   1 CZ 200
529   1 CZ 196.3
401 1 PZ 451
402 1 PZ 1701
501 1 PZ 454.7
502 1 PZ 1697.3
C   A cylinder of radius 200, //x, axis at z=-561
30   C/X   700 -600 200
530   C/X   700 -600 196.3
403 PX -625
404 PX 625
503 PX -621.3
504 PX 621.3
C   A cylinder of radius 200, /Z,translation, rotation (30, TR6)
31   6 CZ 200
531   6 CZ 196.3
405 6 PZ -1701
406 6 PZ -451
505 6 PZ -1697.3
506 6 PZ -454.7
C   Ion Thrusters
C   A plane at y = -750
32   PY -750
C   A plane at y = -800
33   PY -800
C   A plane at x = -250
34   PX -250
C   A plane at x = 250
35   PX   250
C   A plane at z = 300
36   PZ 300
C   A plane at z = 400
37   PZ 400
C   ECCV
C   A cone: y axis, origin (0,700,0), angle 30, 6.5m tall
38   KY 700 0.333 1
C   A plane at y = 1350

B-6

```
39   PY   1350
C                        Argon Tanks
C    A sphere 4.0064m in diam
40   3 SZ  850 200.32
C    Inside sphere 3.8m in diam
41   3 SZ  850 190
C    A sphere 4.0064m in diam
42   3 SZ  1290 200.32
C    Inside sphere 3.8m in diam
43   3 SZ  1290 190
C    A sphere 4.0064m in diam
44   7 SX  -220 200.32
C    Inside sphere 3.8m in diam
45   7 SX  -220 190
C    A sphere 4.0064m in diam
46   7 SX  220 200.32
C    Inside sphere 3.8m in diam
47   7 SX  220 190
C    A sphere 4.0064m in diam
48   4 SZ  -850 200.32
C    Inside sphere 3.8m in diam
49   4 SZ  -850 190
C    A sphere 4.0064m in diam
50   4 SZ  -1290 200.32
C    Inside sphere 3.8m in diam
51   4 SZ  -1290 190
C    A Cylinder defining the outside world
60   CZ  1500
61   PZ  -3000
62   PZ  12500
C
226  5 C/Y  0 -1150 200
626  5 C/Y  0 -1150 196.3
234  5 PX   -250
235  5 PX   250
236  5 PZ   -300
237  5 PZ   -400
326  2 C/Y  0 1150 200
726  2 C/Y  0 1150 196.3
334  2 PX   -250
335  2 PX   250
336  2 PZ   300
337  2 PZ   400

C   Data Card
C   MODE Card. In this case neutron and photon modes
MODE N P
C   Transformations
TR1   0 700 1200  3J 0 1 0 0.5 0 -0.866 $ 150# translation (big cylind)
TR2   0 0 0    3J 0 1 0 0.866 0 -0.5 $ 120#
TR3   0 0 1252  3J 0 1 0 0.5 0 -0.866 $ 150# and transl (Ar tanks 40-43)
TR4   0 0 1252  0.866 0 -0.5 0 1 0   $ 30# and translation (Ar tank 48-50)
```

```
TR5    0 0 0   .5 0 -.866 0 1 0    $ 60# (3rd beam)
TR6    0 700 1200 0.866 0 -0.5 0 1 0     $ 30# and translation (big cylind)
TR7    0 0 -600
C    Material Card
C    declares materials for
C        7. Aluminum d=2.7 g/cm3
C        8. Titanium d=4.5 g/cm3
C        9. Liquid Argon d=1.4 g/cm3
M7     13027.35C 1
M8     22000.35C 1
M9     18000.01C 1
C    Source Card
SDEF   ERG=D1  PAR=1 VEC=0 0 -1 DIR=D2 POS=0 0 12384.09
          WGT= 9.65097E+00
SI1    0.00 5.00E-2 2.52E-1 1 4.5 10
SP1    0 5.90795E+0 1.25498E+0 1.71952E+0 7.68520E-01  0
SI2    0 .988 1
SP2     0  0 1
 C    Tally Card
F4:N   110 111 112 113 139 150 T
E4    5.00E-2 2.52E-1 1 4.5 10
F14:P 110 111 112 113 139 150 T
E14   .01 .015 .025 .05 .06 .07 .08 .1 .15 .2 .3 .5 1 3 6 10
NPS    500000
PRINT
```

Appendix B.4   **Photon Runs Through the Crew Compartment.**
MCNP Input File for photon runs through the crew compartment geometry.

```
C   CREW1 -- CREW COMPARTMENT ARGON TANKS ION THRUSTERS --
30 cm of W 50 cm of LiH
C    data from ntn2.4 surface 17
C    Cell Card
C    Crew Compartment
C    Small cylinders (// to y axis)
10   7 -2.7   -26 27 -28 #110    IMP:P=100     $7 aluminum
110  0    -526 527 -528     IMP:P=100          $void inside
C    Big cylinders (coordinate transform)
11   7 -2.7   -29 401 -402 #111    IMP:P=100     $7
111  0     -529 501 -502     IMP:P=100
12   7 -2.7   -30 403 -404 #112   IMP:P=100
112  0     -530 503 -504   IMP:P=100
13   7 -2.7   -31 405 -406  #113   IMP:P=100
113  0     -531 505 -506    IMP:P=100
C    Ion thrusters
14   8 -4.5   -32 33 34 -35 36 -37  IMP:P=10
C    Mars Excursion Vehicle
15   7 -2.7   -38 -39           IMP:P=50   $7 aluminum
C    Argon tanks (same rotation angles as big cylinders)
16   7 -2.7   -40 41  IMP:P=10
17   9 -1.4   -41    IMP:P=20
18   7 -2.7   -42 43   IMP:P=10
19   9 -1.4   -43    IMP:P=20
20   7 -2.7   -44 45   IMP:P=10
21   9 -1.4   -45   IMP:P=20
22   7 -2.7   -46 47   IMP:P=10
23   9 -1.4   -47    IMP:P=20
24   7 -2.7   -48 49   IMP:P=10
25   9 -1.4   -49   IMP:P=20
26   7 -2.7   -50 51   IMP:P=10
27   9 -1.4   -51    IMP:P=20
C    Second Crew Compartment
C    Small cylinders (// to y axis)
39    7 -2.7   -226 27 -28  #139    IMP:P=100  $8 aluminum
139  0    -626 527 -528     IMP:P=100
C    Second Ion thrusters
40   8 -4.5   -32 33 234 -235 -236 237  IMP:P=10
C    Third Crew Compartment
C    Small cylinders (// to y axis)
50    7 -2.7   -326 27 -28  #150   IMP:P=100  $8 aluminum
150  0   -726 527 -528    IMP:P=100
C    Third Ion thrusters
51   8 -4.5   -32 33 334 -335 336 -337  IMP:P=10
C    Outside world,void
52   0    -60 61 -62 #14 #15 #40 #51 40 42 44 46 48 50 (26:-27:28)
```

```
        (29:-401:402) (30:-403:404) (31:-405:406) (226:-27:28)
        (326:-27:28) IMP:P=1
53   0    60:-61:62  IMP:P=0

C   Surface Card
C                First Small Cylinder
C    A cylinder of radius 200, //y, x'=0, z'=9.22m
26   C/Y  0 1022 200
526  C/Y  0 1022 196.3
C    A plane at y = 500
27   PY   500
527   PY  503.7
C    A plane at y = 900
28   PY   900
528   PY  896.3
C                Big Cylinders (Crew compartment)
C    A cylinder of radius 200, //z',TRANSLATION, rotation (zz'0=150, TR1)
29   1 CZ  200
529   1 CZ  196.3
401  1 PZ 451
402  1 PZ 1701
501  1 PZ 454.7
502  1 PZ 1697.3
C    A cylinder of radius 200, //x, axis at z=-561
30   C/X   700 -600 200
530   C/X   700 -600 196.3
403  PX -625
404  PX  625
503  PX -621.3
504  PX  621.3
C    A cylinder of radius 200, /Z,translation, rotation (30, TR6)
31   6 CZ 200
531   6 CZ 196.3
405  6 PZ -1701
406  6 PZ -451
505  6 PZ -1697.3
506  6 PZ -454.7
C                Ion Thrusters
C    A plane at y = -750
32   PY  -750
C    A plane at y = -800
33   PY  -800
C    A plane at x = -250
34   PX  -250
C    A plane at x = 250
35   PX  250
C    A plane at z = 300
36   PZ  300
C    A plane at z = 400
37   PZ  400
C                ECCV
C    A cone: y axis, origin (0,700,0), angle 30, 6.5m tall
```

```
38    KY   700 0.333 1
C     A plane at y = 1350
39    PY   1350
C                        Argon Tanks
C     A sphere 4.0064m in diam
40    3 SZ  850 200.32
C     Inside sphere 3.8m in diam
41    3 SZ  850 190
C     A sphere 4.0064m in diam
42    3 SZ  1290 200.32
C     Inside sphere 3.8m in diam
43    3 SZ  1290 190
C     A sphere 4.0064m in diam
44    7 SX  -220 200.32
C     Inside sphere 3.8m in diam
45    7 SX  -220 190
C     A sphere 4.0064m in diam
46    7 SX  220 200.32
C     Inside sphere 3.8m in diam
47    7 SX  220 190
C     A sphere 4.0064m in diam
48    4 SZ  -850 200.32
C     Inside sphere 3.8m in diam
49    4 SZ  -850 190
C     A sphere 4.0064m in diam
50    4 SZ  -1290 200.32
C     Inside sphere 3.8m in diam
51    4 SZ  -1290 190
C     A Cylinder defining the outside world
60    CZ   1500
61    PZ   -3000
62    PZ   12500
C
226   5 C/Y  0 -1150 200
626   5 C/Y  0 -1150 196.3
234   5 PX   -250
235   5 PX   250
236   5 PZ   -300
237   5 PZ   -400
326   2 C/Y  0 1150 200
726   2 C/Y  0 1150 196.3
334   2 PX   -250
335   2 PX   250
336   2 PZ   300
337   2 PZ   400

C   Data Card
C   MODE Card. In this case photon mode
MODE P
C   Transformations
TR1   0 700 1200   3J 0 1 0 0.5 0 -0.866 $ 150# translation (big cylind)
TR2   0 0 0    3J 0 1 0 0.866 0 -0.5 $ 120#
```

```
TR3    0 0 1252   3J 0 1 0 0.5 0 -0.866  $ 150# and transl (Ar tanks 40-43)
TR4    0 0 1252   0.866 0 -0.5 0 1 0    $ 30# and translation (Ar tank 48-50)
TR5    0 0 0   .5 0 -.866 0 1 0    $ 60# (3rd beam)
TR6    0 700 1200 0.866 0 -0.5 0 1 0     $ 30# and translation (big cylind)
TR7    0 0 -600
C    Material Card
C    declares materials for
C        7. Aluminum d=2.7 g/cm3
C        8. Titanium d=4.5 g/cm3
C        9. Liquid Argon d=1.4 g/cm3
M7     13000.01P 1
M8     22000.01P 1
M9     18000.01P 1
C    Source Card
SDEF   ERG=D1  PAR=2 VEC=0 0 -1 DIR=D2 POS=0 0 12384.09
        WGT=2.08428E+06
SI1    0 .01 .015 .025 .05 .06 .07 .08 .1 .15 .2 .3 .5 1 3 6 10
SP1    0 8.42663E+02 2.07116E+04 1.70104E+05 3.35592E+05 8.15307E+04
        6.51968E+04 5.29651E+04 9.04114E+04 1.41051E+05 9.14781E+04
        1.21780E+05 1.76617E+05 2.19369E+05 3.73527E+05 1.30622E+05
        1.24789E+04
SI2    0 .988 1
SP2    0 0 1
C    Tally Card
F14:P 110 111 112 113 139 150 T
E14    .01 .015 .025 .05 .06 .07 .08 .1 .15 .2 .3 .5 1 3 6 10
NPS    2000000
PRINT
```

MCNP OUTPUT FILES

Appendix C.1. **Example of Neutron Tally**
Surface flux for various energy bins.

```
surface  1
     energy
        5.0000E-02   2.74347E+10 0.0027
        2.5200E-01   1.05833E+10 0.0041
        1.0000E+00   4.68495E+09 0.0063
        4.5000E+00   9.08039E+08 0.0130
        1.0000E+01   0.00000E+00 0.0000
             total    4.36110E+10 0.0021
```

Appendix C.1. Example of Photon Tally

Surface flux for various energy bins.

surface 1

energy

1.0000E-02	4.66268E+05	0.8291
1.5000E-02	1.94170E+07	0.4581
2.5000E-02	1.14973E+08	0.1691
5.0000E-02	6.56650E+08	0.0877
6.0000E-02	2.26439E+08	0.0802
7.0000E-02	2.05652E+08	0.0812
8.0000E-02	1.93850E+08	0.0950
1.0000E-01	3.98321E+08	0.0817
1.5000E-01	6.53421E+08	0.0579
2.0000E-01	4.57823E+08	0.0907
3.0000E-01	6.21146E+08	0.0493
5.0000E-01	8.98456E+08	0.0469
1.0000E+00	8.53329E+08	0.0582
3.0000E+00	1.57062E+09	0.0219
6.0000E+00	5.30791E+08	0.0327
1.0000E+01	9.72476E+07	0.0699
total	7.49860E+09	0.0202
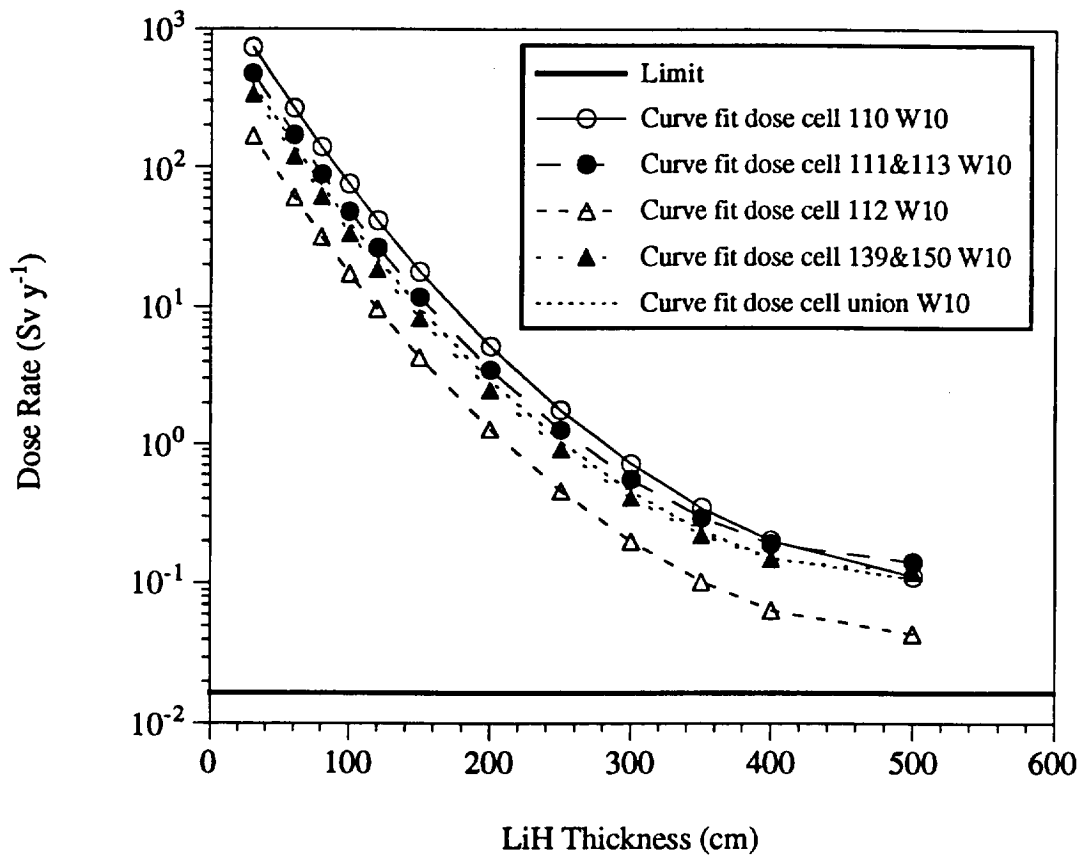
CURVE FITS

Figure D.a Curve fit of the photon dose rates inside the six crew compartments due to one SP-100 reactor neutron interactions through the shield with a 10-cm thick tungsten layer and a variable lithium hydride thickness.
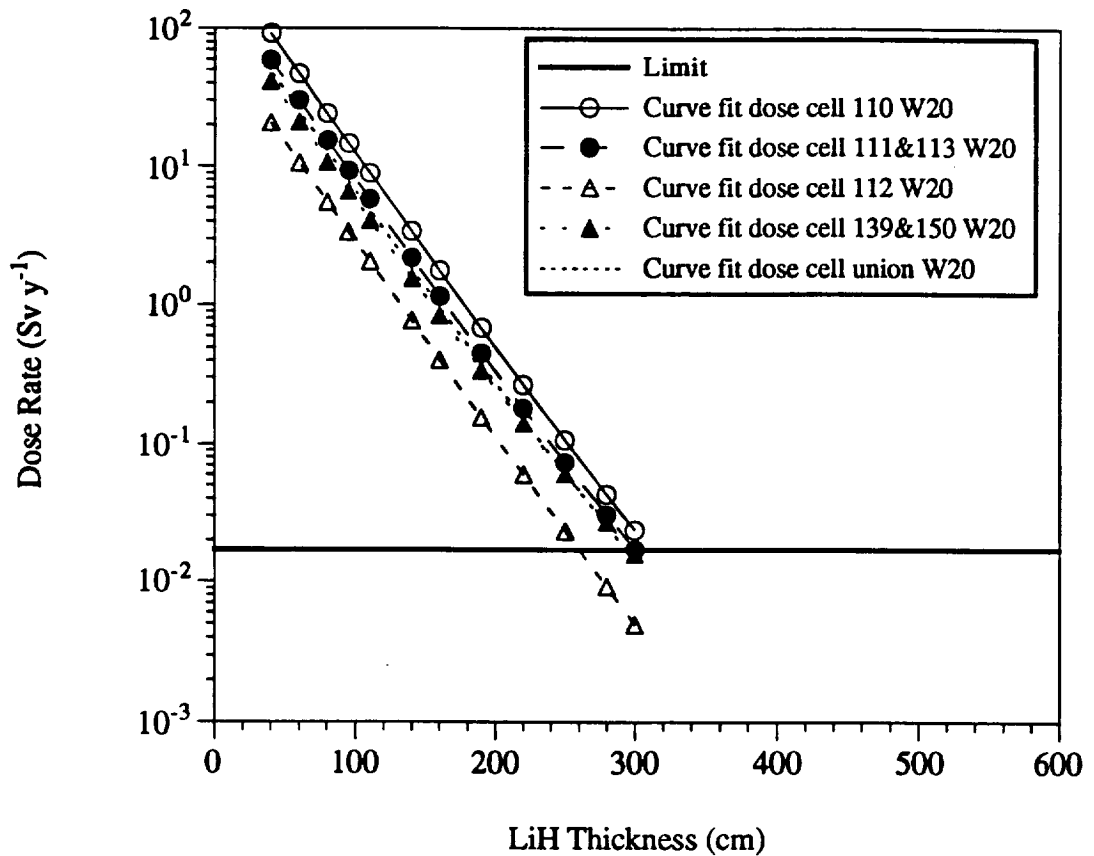
Figure D.b Curve fit of the photon dose rates inside the six crew compartments due to one SP-100 reactor neutron interactions through the shield with a 20-cm thick tungsten layer and a variable lithium hydride thickness.
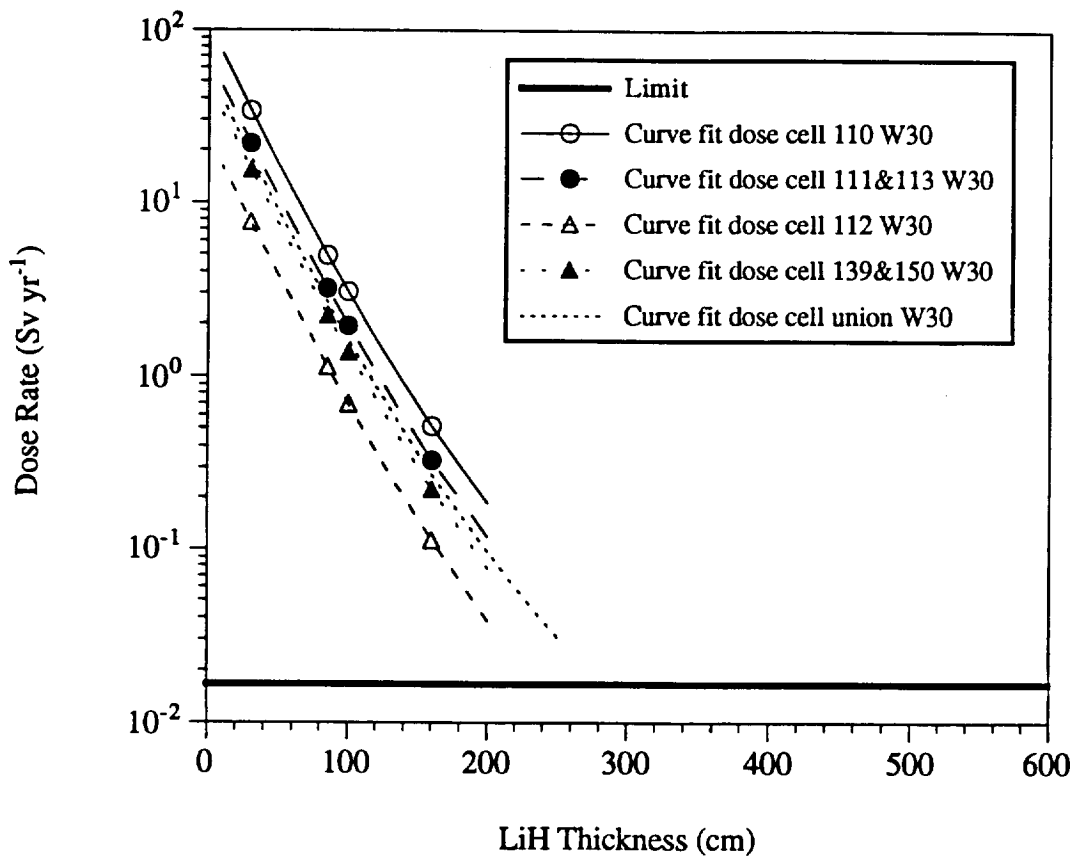
Figure D.c Curve fit of the photon dose rates inside the six crew compartments due to one SP-100 reactor neutron interactions through the shield with a 30-cm thick tungsten layer and a variable lithium hydride thickness.

REPORT DOCUMENTATION PAGE

Form Approved
OMB No. 0704-0188

1. AGENCY USE ONLY (Leave blank)	2. REPORT DATE February 1996	3. REPORT TYPE AND DATES COVERED Final Contractor Report

4. TITLE AND SUBTITLE

Investigation of Natural and Man-Made Radiation Effects on Crews on Long Duration Space Missions

5. FUNDING NUMBERS

WU–506–31–3M
G–NAG3–1326

6. AUTHOR(S)

Wesley E. Bolch and Alexander Parlos

7. PERFORMING ORGANIZATION NAME(S) AND ADDRESS(ES)

Texas A&M University
Department of Nuclear Engineering
College Station, Texas 77843–2124

8. PERFORMING ORGANIZATION REPORT NUMBER

E–9371

9. SPONSORING/MONITORING AGENCY NAME(S) AND ADDRESS(ES)

National Aeronautics and Space Administration
Lewis Research Center
Cleveland, Ohio 44135–3191

10. SPONSORING/MONITORING AGENCY REPORT NUMBER

NASA CR–195424

11. SUPPLEMENTARY NOTES

Project Manager, Steven M. Stevenson, Advanced Space Analysis Office, NASA Lewis Research Center, organization code 6840, (216) 977–7087.

12a. DISTRIBUTION/AVAILABILITY STATEMENT

Unclassified - Unlimited
Subject Categories 52 and 91

This publication is available from the NASA Center for Aerospace Information, (301) 621–0390.

12b. DISTRIBUTION CODE

13. ABSTRACT (Maximum 200 words)

Over the past several years, NASA has studied a variety of mission scenarios designed to establish a permanent human presence on the surface of Mars. Nuclear Electric Propulsion (NEP) is one of the possible designs for this program. During the initial stages of vehicle design work, careful consideration must be given to, not only the shielding requirements of natural space radiations, but to the shielding and configuration requirements of the on-board reactors. In this work, the radiation transport code MCNP has been used to make initial estimates of crew exposures to reactor radiation fields for a specific manned NEP vehicle design. In this design, three 25 MW_t scaled SP–100–class reactor radiations are shielded by three identical shields. Each shield layers beryllium, tungsten, and lithium hydride between the reactor and the crew compartment. Separate calculations are made of both the exiting neutron and gamma fluxes from the reactors during beginning-of-life, full-power operation. This data is then used as the source terms for particle transport in MCNP. The total gamma and neutron fluxes exiting the reactor shields are recorded and separate transport calculations are then performed for a 10 g cm^{-2} crew compartment aluminum thickness. Estimates of crew exposures have been assessed for various thicknesses of the shield tungsten and lithium hydride layers. A minimal tungsten thickness of 20 cm is required to shield the reactor photons below the 0.05 Sv y^{-1} man-made radiation limit. In addition to a 20-cm thick tungsten layer, a 40-cm thick lithium hydride layer is required to shield the reactor neutrons below the annual limit. If the tungsten layer is 30-cm thick, the lithium hydride layer should be at least 30-cm thick. These estimates do not take the photons generated by neutron interactions inside the shield into account because the neutron MCNP cross sections do not as yet allow reliable estimates of photon production in these materials. These results, along with natural space radiation shielding estimates calculated at NASA Langley, have been used to provide preliminary input data into a new MacIntosh-based radiation exposure analysis tool developed at Texas A&M. A skeletal version of the tool now being developed will allow soon rapid radiation exposure and risk analyses to be performed on a variety of Lunar and Mars missions utilizing a nuclear-power vehicles.

14. SUBJECT TERMS

Radiation/space missions; NEP; NTR vehicles

15. NUMBER OF PAGES
134

16. PRICE CODE
A07

17. SECURITY CLASSIFICATION OF REPORT	18. SECURITY CLASSIFICATION OF THIS PAGE	19. SECURITY CLASSIFICATION OF ABSTRACT	20. LIMITATION OF ABSTRACT
Unclassified	Unclassified	Unclassified	